MIT

# Benchmark for Evaluation And Validation of Reactor Simulations

**RELEASE rev. 2.0.2**

*MIT **C**omputational **R**eactor **P**hysics **G**roup*

April 11, 2018

# Authors

Nicholas Horelik
Bryan Herman
Matthew Ellis
Shikhar Kumar
Jingang Liang
Benoit Forget
Kord Smith

# Acknowledgements

We are extremely grateful for the detailed core specifications and measurement data provided to us by the utility, which will remain un-named. Without their generosity this benchmark would not be possible. We are also very grateful for the work of the Advanced Simulation and Design Integration team at the Knolls Atomic Power Laboratory, who contributed significantly to the development of this document by reviewing, beta-testing, and making important suggestions from the very beginning. We would also like to acknowledge the contributions of Koroush Shirvan for his extensive reviewing and quality assurance work, as well as Paul Romano for his help developing and debugging the OpenMC model of this benchmark. Finally, we would like to thank Andrew Godfrey and Benjamin Collins at Oak Ridge National Laboratory, who provided significant feedback for the second major version of this document.

Partial funding for the development of this benchmark was provided by the Center for Exascale Simulation of Advanced Reactors, one of three exascale codesign centers funded by the Department of Energy's Office of Advanced Scientific Computing Research.

# Citation

N. Horelik, B. Herman, B. Forget, and K. Smith. Benchmark for Evaluation and Validation of Reactor Simulations (BEAVRS), v1.0.1. *Proc. Int. Conf. Mathematics and Computational Methods Applied to Nuc. Sci. & Eng.*, 2013. Sun Valley, Idaho

# Changelog

## 10/30/17 - 2.0.2

- Update Cycle 2 Power History plot to include correct End of Cycle
- Re-calculated all material compositions using latest isotopic natural abundances data, IUPAC 2013

## 10/26/16 - 2.0.1

- Corrected the critical Boron concentration from 1237 to 1273 ppm in Cycle 2
- Improved re-alignment algorithm in processing measurement data

## 09/06/16 - 2.0

- Slight shifts to all axial planes
- Added B4C control rod material and updated the control rod specification
- Updated the grid spacer specifications with more accurate heights
- Updated the control rod 0% withdrawn axial location
- Updated the burnable poison insertion axial location
- Added upper plenum and end plugs to burnable poison rods
- Added upper plenum, end plugs, and spacer region to control rods
- Changed from air to helium for control rod and control rod gaps
- Updated neutron shield panel specification
- Updated RPV geometry and material specification
- Added the core liner
- Added water gap between fuel assemblies and baffle
- Added new materials for nozzle and support plate structure to conserve mass and volume fractions
- Added inlet coolant temperature measurements
- Added tilt-corrected data

## 10/16/13 - 1.1.1

- Added new bare instrument thimble figure and additional clarification regarding instrument tubes below the dashpot.

## 10/16/13 - 1.1

- Added cycle 2 information: shuffling pattern, burnable absorbers, fresh assembly materials specification, zero power physics test data. For differences and additions see Tables 1, 4-8, and 23, Sources 52, 53 and 71, Sections 2.2.2.1, 2.2.3.1, 3.2 and 3.3, and Figures 15, 17, 19, and 29.
- Added note in Section 3.3 regarding quality of detector trace data
- Added new materials for cycle 2 enrichments
- Added detailed assembly loadings (fresh fuel only) for cycle 2
- All mass densities (and number densities) of fuel have been changed to agree with exact fuel pin dimensions reported in specification

## 2/21/13 - 1.0.1

- Inconel was misreported as the grid material in Figure 24, changed to Zircaloy
- Grid thickness reported in the caption of Figure 23 did not match figure
- Grid thickness reported in the caption of Figure 24 did not match figure
- Grid strap thickness reported in the caption of Figure 25 did not match figure

## 1/31/13 - 1.0

- Changed Mass density and composition of SS304

## 1/18/13 - 0.2.5

- Updated RPV thickness to accurate source
- Updated inconel spring mass and dimension to approximate source

- Changed top/bottom egg-crate dimensions to properly conserve inconel mass. Top/bottom grids now have different radial dimensions vs. intermediate grids for the egg-crate.
- Hot Zero Power temperature was changed from 560 K to 560 F.
- All Fuel material mass and number densities have been changed to reflect actual core-averaged Uranium assembly loading for each enrichment.
- Burnable absorber specification was changed so that the active poison extends from the top of the active fuel to 2 in. above the bottom of the active fuel. The blank pin above burnable absorbers was also changed from Zircaloy to Stainless Steel.
- Added air gap to control rods
- Changed Ag-In-Cd cladding material to SS304
- Changed water density to reflect boron in it (changed boron num dens)
- Fixed Air mass density, factor of 10 lower
- Changed RPV inner and outer radii

## 12/17/12 - 0.2.4

- Revised instrument tube and burnable absorber tube pincell details above active fuel regions.

## 12/4/12 - 0.2.3

- Changed instrument tube and guide tube pincell details above and below active fuel regions.

# ABSTRACT

Advances in parallel computing have made possible the development of high-fidelity tools for the design and analysis of nuclear reactor cores, and such tools require extensive verification and validation. This document describes BEAVRS, a new multi-cycle full-core Pressurized Water Reactor (PWR) depletion benchmark based on two operational cycles of a commercial nuclear power plant that provides a detailed description of fuel assemblies, burnable absorbers, in-core fission detectors, core loading patterns, and numerous in-vessel components. This benchmark enables analysts to develop extremely detailed reactor core models that can be used for testing and validation of coupled neutron transport, thermal-hydraulics, and fuel isotopic depletion. The benchmark also provides measured reactor data for Hot Zero Power (HZP) physics tests, boron letdown curves, and three-dimensional in-core flux maps from fifty-eight instrumented assemblies. It should be noted however, that not all the necessary data are presented in this document. It will be necessary for analysts to make appropriate judgements and assumptions depending on methods employed.

This document and its associated data package is hosted online at the MIT Computational Reactor Physics Group website `http://crpg.mit.edu/`, where future revisions and refinements to the benchmark specification will be made publicly available.

# Contents

# List of Figures

# List of Tables

# List of Source References

# Definitions and Acronyms

| | |
|---|---|
| **ARO** | All Rods Out |
| **BAF** | Bottom of Active Fuel |
| **BP** | Burnable Poison |
| **BOC** | Beginning of Cycle |
| **CASL** | Consortium for Advanced Simulation of Light Water Reactors (LWRs) |
| **CESAR** | Center for Exascale Simulation of Advanced Reactors |
| **EFPD** | Effective Full Power Days |
| **EPRI** | Electric Power Research Institute |
| **FFTF** | Fast Flux Test Factility |
| **HZP** | Hot Zero Power |
| **IR** | Inner Radius |
| **LMFR** | Liquid Metal Fast Reactor |
| **LWR** | Light Water Reactor |
| **MOX** | Mixed Oxide |
| **OR** | Outer Radius |
| **pcm** | per cent mille |
| **ppm** | parts per million |
| **PWR** | Pressurized Water Reactor |
| **SS304** | Stainless Steel 304 |
| **TAF** | Top of Active Fuel |

# 1 Introduction

Advances in computing capabilities are further improving the feasibility of fast-running high-fidelity simulations of nuclear cores. Where current core simulations require a series of homogenization procedures to model reactors on a coarse-mesh in order to overcome memory and computer processing limitations [2], modern techniques aspire to provide solutions using fully-detailed geometries with far fewer approximations. For instance, recent research efforts improving the scalability and efficiency of Monte Carlo neutron transport algorithms have resulted in very accurate solutions to the well-known Hoogenboom-Martin problem [3] with the MC21 Monte Carlo code [4] [5], with statistical uncertainties approaching the 1% pin-power accuracy criterion proposed by Smith [6] for full-core Monte Carlo analysis. Likewise, modern deterministic approaches are targeting similar accuracy on some of the world's largest supercomputers [7]. Indeed, the development of such high-fidelity full-core modelling capabilities for LWRs is the stated goal of several DOE projects such as CASL (Consortium for Advanced Simulation of LWRs) [8] and CESAR (Center for Exascale Simulation of Advanced Reactors) [9]. However, there is a lack of detailed and relevant benchmarks needed to validate these methods, and a more complete benchmark that includes measured reactor data is presented here.

Nearly all non-proprietary benchmarks do not capture the detail of LWRs needed to validate high-fidelity methods being developed today. For instance, the OECD LWR and Pressurized Water Reactor (PWR) reactor benchmark specifications [10] mostly refer to simple lattice experiments, limited physics testing configurations, and small test reactors. Whereas several full-core LMFR models are available (FFTF, JOYO, etc.), LWRs are markedly under represented. This is particularly true for full-core benchmarks of most interest to the methods development and regulatory community: production reactors similar to operating and planned commercial units. Some recent publications come close to satisfying this need, but they ultimately fall short either in scope or applicability. For instance, a 2011 EPRI report [11] provides reactivity and depletion data with several benchmark specifications for PWR assembly lattices. These benchmarks, while using full-core simulations and measured data, take the approach of reducing the benchmark to single-assembly calculations and do not provide detailed full-core tests or measured reactor data.

A distinction should be noted between the kind of data-backed benchmark being pursued here and the code-comparison benchmarks often used to evaluate methods. For instance, several newer and widely-used LWR benchmarking suites are not backed by measured data, such as the C5G7 MOX benchmarks [12], the Hoogenboom-Martin LWR Monte Carlo benchmark [4], and the approximate PWR specification by Douglas et al. [13]. Instead, comparisons are based on results submitted by many different parties using a variety of codes. Measured reactor data is required for a credible validation.

This document introduces a new benchmark that addresses many of the shortcomings of previous LWR benchmarks by providing a highly-detailed PWR specification with two cycles of measured operational data that can be used to validate high-fidelity core analysis methods.

# 2 Benchmark Specifications

## 2.1 Overview

The core geometry specifications are described in 3 levels of increasing scope, detailing each of the hierarchical elements of the model. First the radial geometry is described, followed by a section detailing the axial parameters.

At the lowest level, the radial geometry of each of the pincell types used throughout the core is described. Next, the fuel assembly design is detailed, including the possible configurations of burnable absorbers and the radial specification of the grid spacers. Finally, the greater core geometry is described, including the fuel assembly enrichment locations, the positions of burnable absorbers, instrument tubes, control rod banks, and shutdown banks, as well as the baffle that surrounds the fuel assemblies, the core barrel, four neutron shield panels, and the reactor pressure vessel and liner.

After the radial and axial geometry descriptions, a material specifications section lists the details of each of the materials referred to. Table 1 provides a summary of key model parameters that will be specified in greater detail in subsequent sections, and Figure 1 shows a core cross section indicating the radial structures and assembly loading pattern.

Table 1: Summary of key model parameters.

| Core Lattice | | Source |
|---|---|---|
| No. Fuel Assemblies | 193 | 1 |
| Loading Pattern | w/o U235 | |
| Region 1 (cycle 1) | 1.60† | 1 |
| Region 2 (cycle 1) | 2.40† | 1 |
| Region 3 (cycle 1) | 3.10† | 1 |
| Region 4A (cycle 2) | 3.20†† | 1 |
| Region 4B (cycle 2) | 3.40†† | 1 |
| Cycle 1 Heavy Metal Loading | 81.8 MT | 3 |
| **Fuel Assemblies** | | |
| Pin Lattice Configuration | 17 × 17 | 4 |
| Active Fuel Length | 365.76 cm | 5 |
| No. Fuel Rods | 264 | 4 |
| No. Grid Spacers | 8 | 4 |
| **Control** | | |
| Control Rod Material (Upper Region) | B4C | 57 |
| Control Rod Material (Lower Region) | Ag-In-Cd | 56 |
| No. Control Rod Banks | 57 | 1 |
| No. Burnable Poison Rods in Core | 1266 | 1 |
| Burnable Poison Material | Borosilicate Glass, 12.5 w/o $B_2O_3$ | 4 |
| **Performance** | | |
| Core Power | 3411 MWth | 6 |
| Operating Pressure | 2250 psia | 6 |
| Core Flow Rate | $61.5 \times 10^6$ kg/hr (5% bypass‡) | 7 |

† Cycle 1Actual core-averaged enrichments calculated from detailed assembly loadings, see Source 70.
†† Cycle 2 Actual core-averaged enrichments calculated from detailed assembly loadings, see Source 71.
‡ It is assumed that 5% of core flow rate goes core into bypass region. A fraction of this flow rate passes through guide tubes. The flow rate should be estimated so that no boiling occurs in these regions.

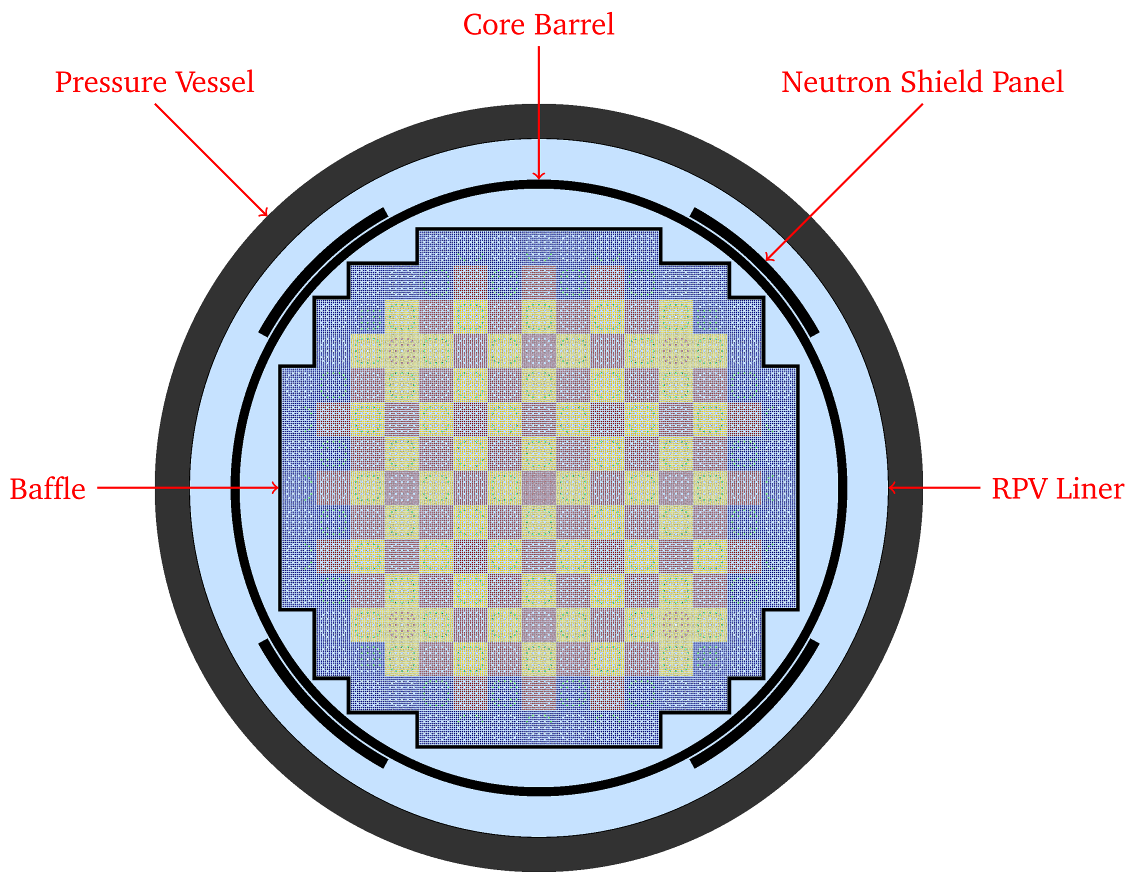


Figure 1: Core cross-section indicating radial structures and enrichment loading pattern (cycle 1). Black denote stainless steel, dark gray denotes carbon steel, light blue denotes water, and red, yellow, and dark blue denote the 1.6, 2.4, and 3.1 w/o U235 regions, respectively.

## 2.2 Radial Geometry

### 2.2.1 Pin Types

In this section the radial parameters of each of the pincell types used in the fuel assemblies are detailed. Each of these describes a complete pincell surrounded by the main coolant - in other words, the outer guide tube shell that surrounds instrument tubes, control rods, and burnable absorber rods is presented here as part of those pincells.

While the following radial parameters are constant throughout the axial extent of the core of most pins, a distinction is made for the pins that have components below the control rod stop at the bottom of the core. This region, referred to as the “dashpot,” consists of a tapering of the guide tubes to a thinner radius that causes the constriction of flow to naturally prevent control rods from extending too far into the core. In this model, this is approximated by a region of thinner guide tubes (described further in later sections). Thus radial parameters are provided for pins for both regions where appropriate. Note that the central guide tubes of each assembly (the "instrument tubes") do not shrink for the dashpot.

For all figures in this section, dimensions and materials are specified in order starting from the inner region, through the outer rings. No thermal expansion is considered.

**Figure 2 — Fuel Pin**

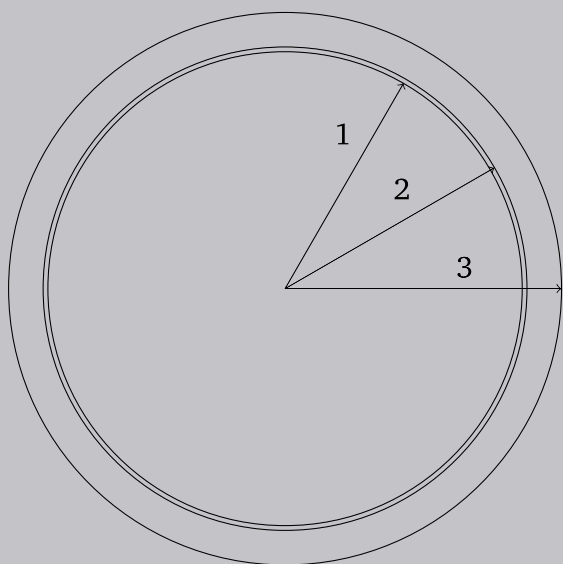


| Arrow | Radius (cm) | Material | Source |
|---|---|---|---|
| 1 | 0.39218 | Fuel | 8 |
| 2 | 0.40005 | Helium | 9 |
| 3 | 0.45720 | Zircaloy | 10 |

## Figure 3 — Upper Fuel Pin Plenum

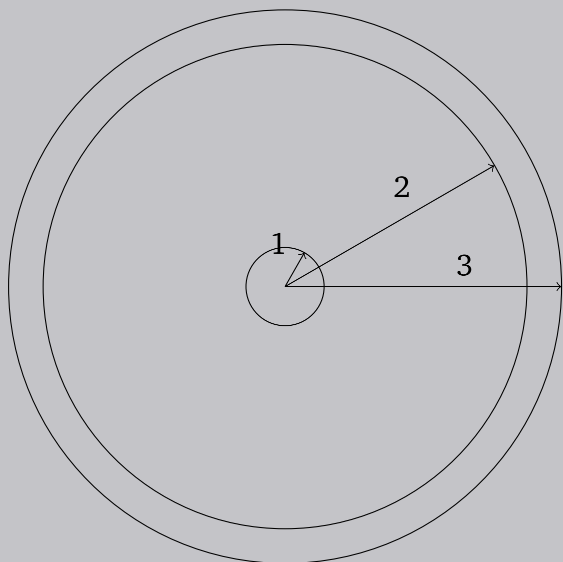


| Arrow | Radius (cm) | Material | Source |
|---|---|---|---|
| 1 | 0.06459 | Inconel | 11 |
| 2 | 0.40005 | Helium | 9 |
| 3 | 0.45720 | Zircaloy | 10 |

This shows the radial geometry used in the upper plenum region of the fuel pins, with a small mass of Inconel to approximate the spring.

## Figure 4 — Empty Guide Tube Geometry above Dashpot

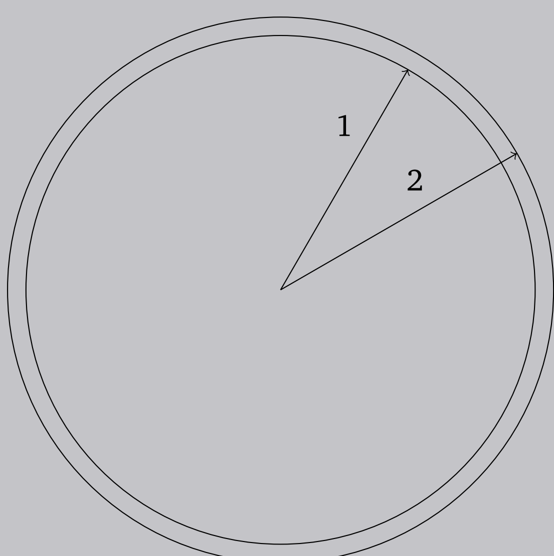


| Arrow | Radius (cm) | Material | Source |
|---|---|---|---|
| 1 | 0.56134 | Water | 13 |
| 2 | 0.60198 | Zircaloy | 14 |

## Figure 5 — Empty Guide Tube Geometry at Dashpot

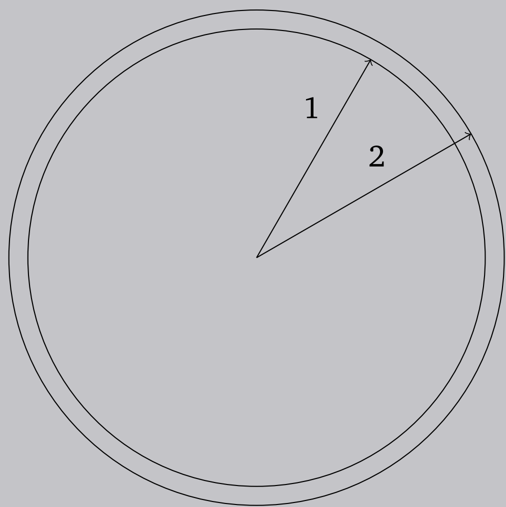


| Arrow | Radius (cm) | Material | Source |
|---|---|---|---|
| 1 | 0.50419 | Water | 15 |
| 2 | 0.54610 | Zircaloy | 16 |

## Figure 6 — Instrument Tube Pin Geometry

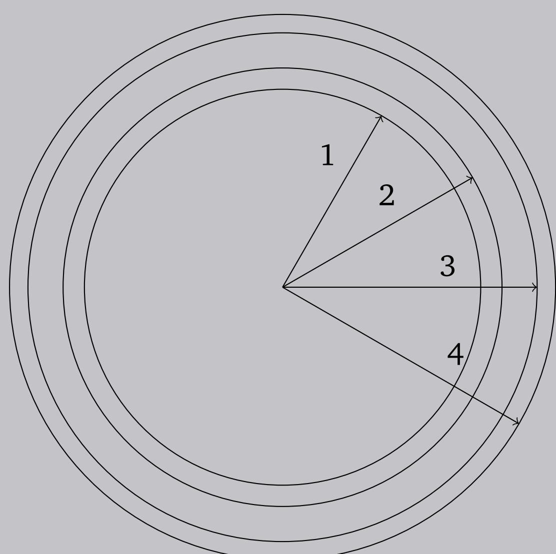


| Arrow | Radius (cm) | Material | Source |
|---|---|---|---|
| 1 | 0.43688 | Air | 17 |
| 2 | 0.48387 | Zircaloy | 18 |
| 3 | 0.56134 | Water | 13 |
| 4 | 0.60198 | Zircaloy | 14 |

The thimble radii were chosen to be equivalent to the outer thimble radii of control rods and burnable absorber rods by assumption. Note that not all instrument tube positions contain the thimble defined by the first 2 radii in the diagram above, as discussed in Section 2.2.3.3. This pincell does not change at the dashpot.

## Figure 7 — Bare Instrument Thimble Pin Geometry

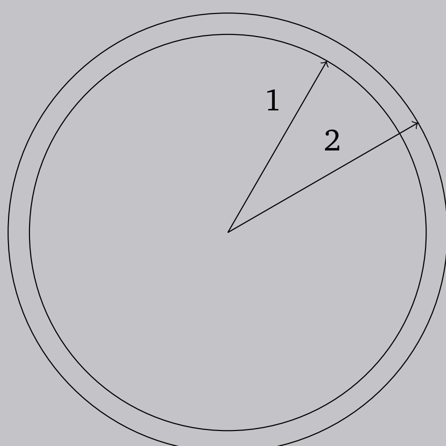


| Arrow | Radius (cm) | Material | Source |
|---|---|---|---|
| 1 | 0.43688 | Air | 17 |
| 2 | 0.48387 | Zircaloy | 18 |

The bare instrument thimble for regions below the instrument tube.

## Figure 8 — BP Geometry above Dashpot

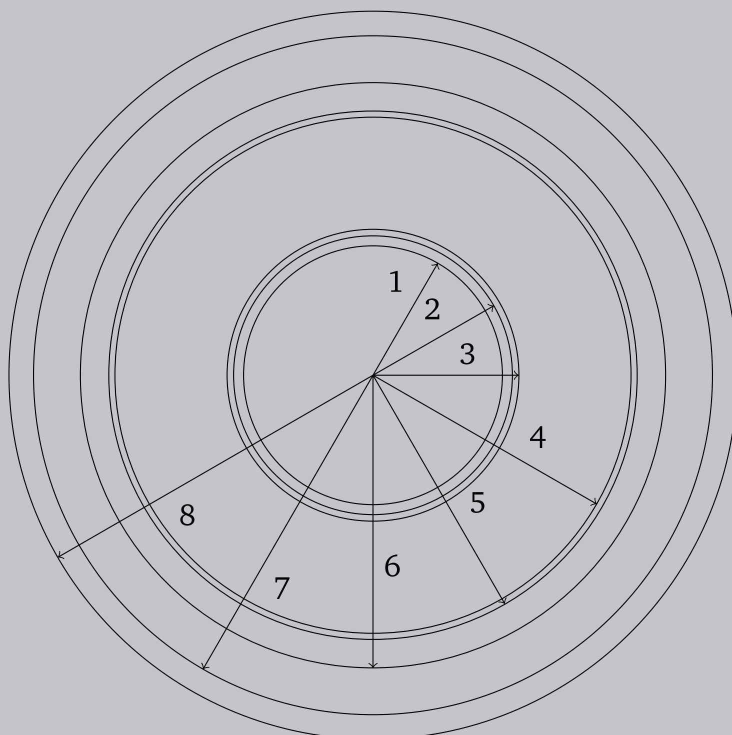


| Arrow | Radius (cm) | Material | Source |
|---|---|---|---|
| 1 | 0.21400 | Air | 19 |
| 2 | 0.23051 | SS304 | 20 |
| 3 | 0.24130 | Helium | 21 |
| 4 | 0.42672 | Borosilicate Glass | 22 |
| 5 | 0.43688 | Helium | 23 |
| 6 | 0.48387 | SS304 | 24 |
| 7 | 0.56134 | Water | 13 |
| 8 | 0.60198 | Zircaloy | 14 |

## Figure 9 — BP Plenum Geometry

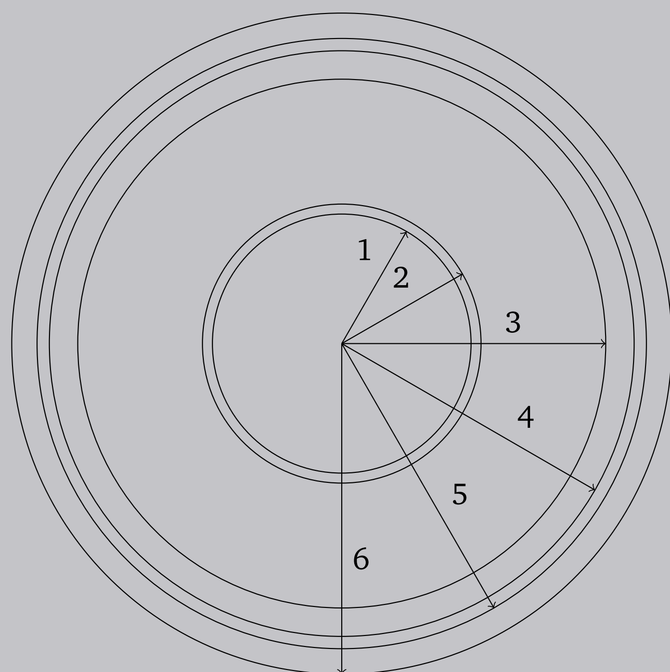


| Arrow | Radius (cm) | Material | Source |
|---|---|---|---|
| 1 | 0.21400 | Air | 19 |
| 2 | 0.23051 | SS304 | 20 |
| 3 | 0.43688 | Helium | 23 |
| 4 | 0.48387 | SS304 | 24 |
| 5 | 0.50419 | Water | 15 |
| 6 | 0.54610 | Zircaloy | 16 |

## Figure 10 — Control Rod Pin Upper Geometry

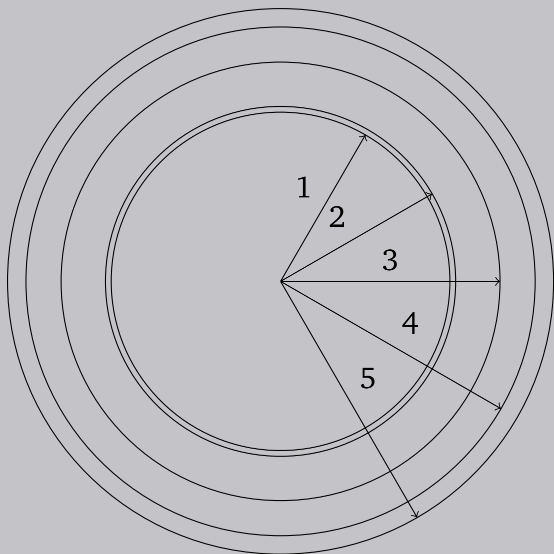


| Arrow | Radius (cm) | Material | Source |
|---|---|---|---|
| 1 | 0.37338 | B4C | 28 |
| 2 | 0.38608 | Helium | 25 |
| 3 | 0.48387 | SS304 | 26 |
| 4 | 0.56134 | Water | 13 |
| 5 | 0.60198 | Zircaloy | 14 |

## Figure 11 — Control Rod Pin Lower Geometry

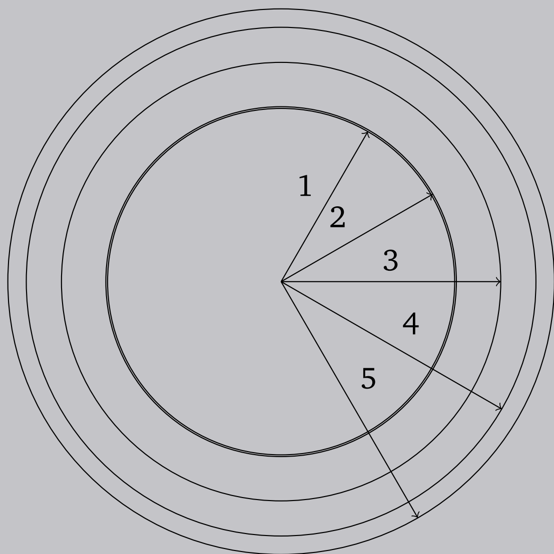


| Arrow | Radius (cm) | Material | Source |
|---|---|---|---|
| 1 | 0.38227 | Ag-In-Cd | 27 |
| 2 | 0.38608 | Helium | 25 |
| 3 | 0.48387 | SS304 | 26 |
| 4 | 0.56134 | Water | 13 |
| 5 | 0.60198 | Zircaloy | 14 |

## Figure 12 — Control Rod Pin Spacer Geometry

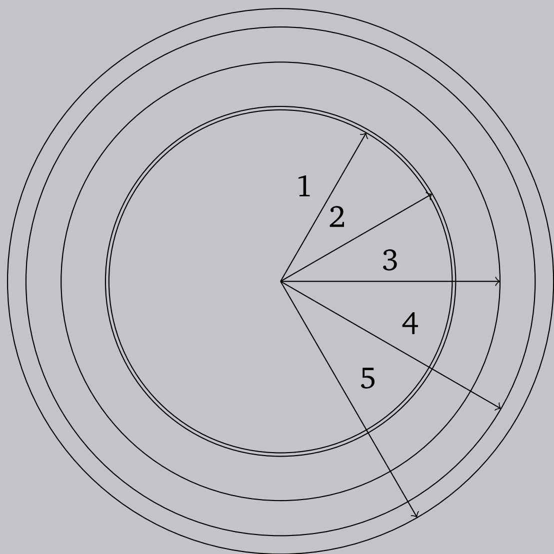


| Arrow | Radius (cm) | Material | Source |
|---|---|---|---|
| 1 | 0.37845 | SS304 | 29 |
| 2 | 0.38608 | Helium | 25 |
| 3 | 0.48387 | SS304 | 26 |
| 4 | 0.56134 | Water | 13 |
| 5 | 0.60198 | Zircaloy | 14 |

## Figure 13 — Control Rod Pin Plenum Geometry

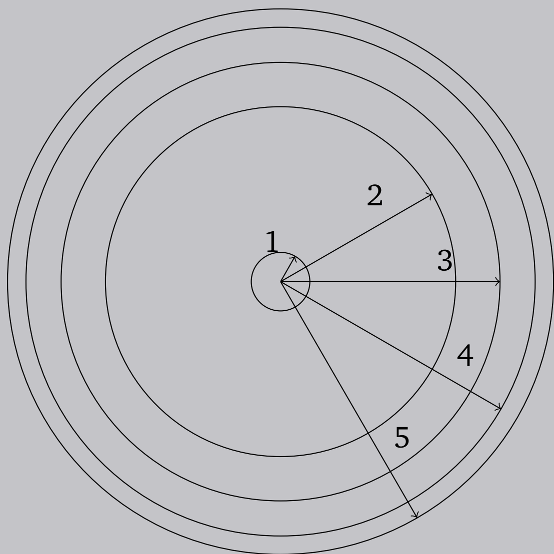


| Arrow | Radius (cm) | Material | Source |
|---|---|---|---|
| 1 | 0.06459 | Inconel | 12 |
| 2 | 0.38608 | Helium | 25 |
| 3 | 0.48387 | SS304 | 26 |
| 4 | 0.56134 | Water | 13 |
| 5 | 0.60198 | Zircaloy | 14 |

### 2.2.2 Fuel Assemblies

Each of the assemblies in the core is made up of a 17 × 17 array of pins described in Section 2.2.1. Table 2 outlines the important parameters of each, and the positions of the guide tubes are shown in Figure 14.

Assemblies are made up of one of three different enrichment fuel pins, and the guide tube positions can be filled with one of several different burnable absorber configurations described in Section 2.2.2.1. For any configuration, the center guide tube may contain an instrument tube. The details of the layout of these features throughout the core are described in Section 2.2.3.

Table 2: Fuel assembly parameters.

| | | Source |
|---|---|---|
| Fuel Assembly Lattice Pitch | 21.50364 cm | 30 |
| Pin Lattice Pitch | 1.25984 cm | 31 |
| Pin Lattice Configuration | 17 × 17 | 4 |
| No. Fuel Rods | 264 | 4 |
| No. Guide Tube Positions | 24 | 4 |
| No. Instrument Tube Positions | 1 | 4 |
| | | |
| No. Grid Spacers | 8 | 4 |
| Top/Bottom Grid Spacer Material | Inconel 718 | 4 |
| Top/Bottom Grid Sleeve Material | Stainless Steel 304 | 4 |
| Intermediate Grid Spacer and Sleeve Material | Zircaloy | 4 |
| Weight of Inconcel per Top/Bottom Grid | 390.136 g | 32 |
| Weight of Stainless Steel per Top/Bottom Grid | 91.0329 g | 34 |
| Weight of Zircaloy per intermediate Grid | 1,169.23 g | 33 |

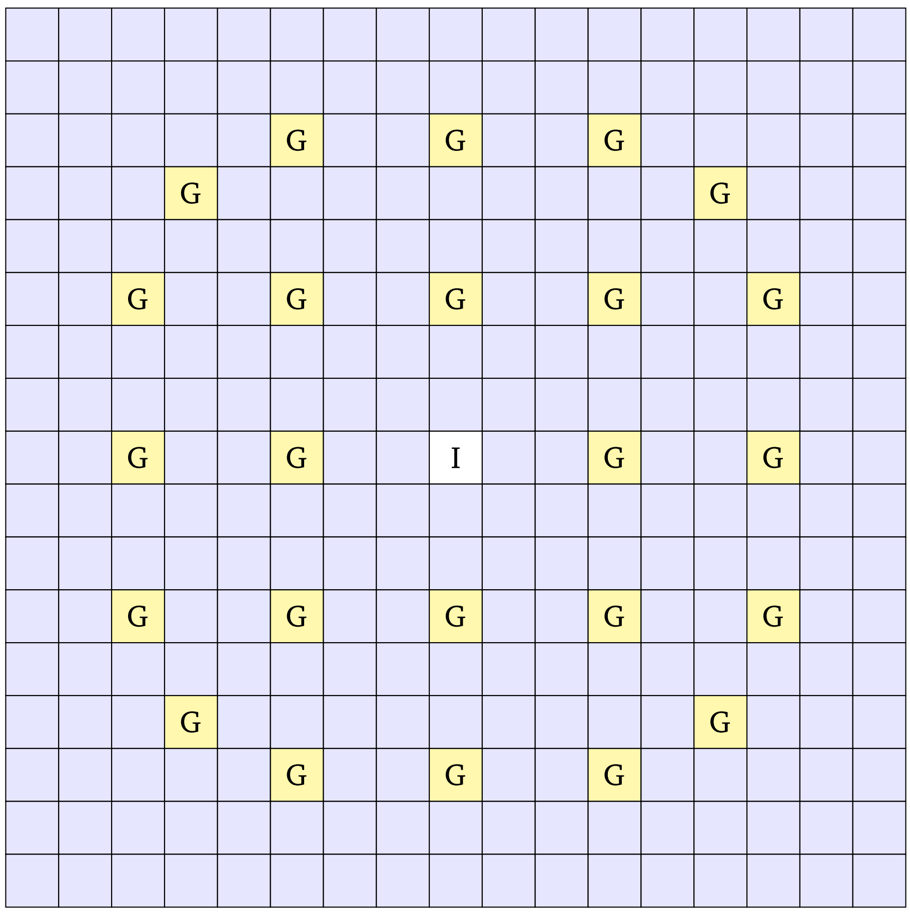


Figure 14: Fuel assembly guide tube locations. Blank locations denote fuel rods, **G** denotes a guide tube location, and **I** denotes a guide tube position that might contain an instrument tube. Source: 35

#### 2.2.2.1 Burnable Absorber Configurations

Assemblies in the core that do not contain control rods may posses one of 5 burnable absorber configurations, or have none at all. Figures 15 through 22 depict these configurations. Each configuration appears in all four quadrants of the core, and thus the 6BA and 5BA configurations need to be rotated as indicated. Note that the 12BA configuration is different between cycle 1 and cycle 2.

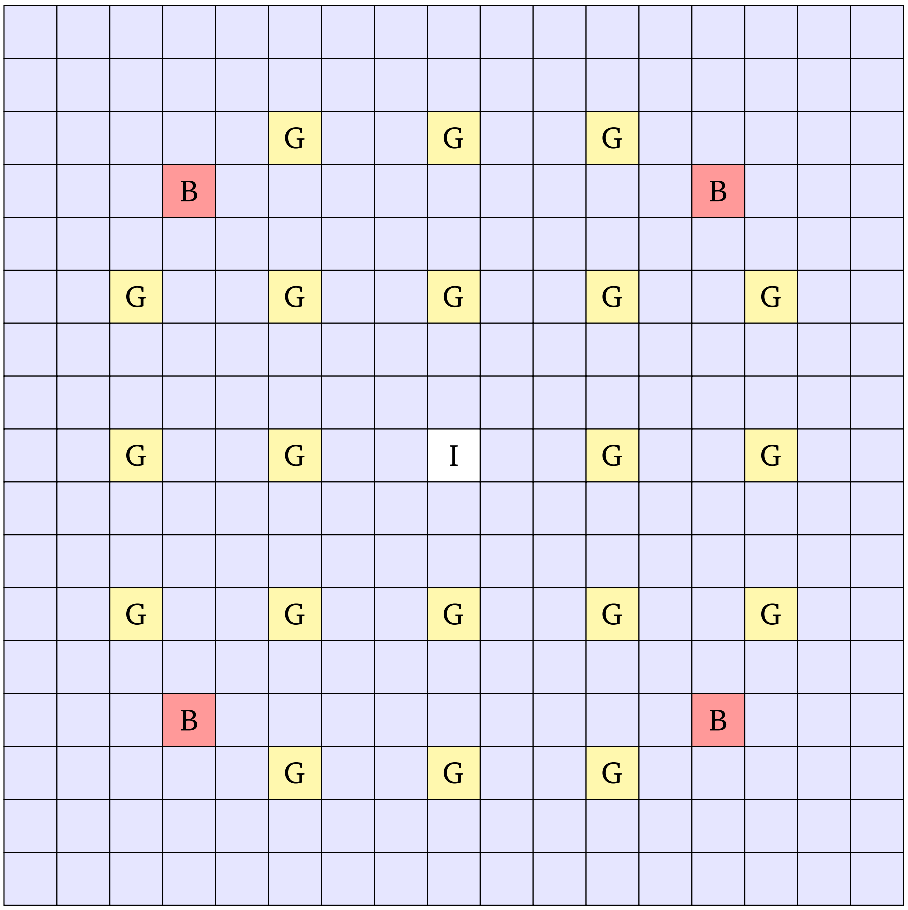


Figure 15: The 4BA burnable absorber configuration. Blank locations denote fuel rods, **G** denotes a guide tube location, **B** denotes a burnable absorber rod, and **I** denotes a guide tube position that might contain an instrument tube. Source: 35

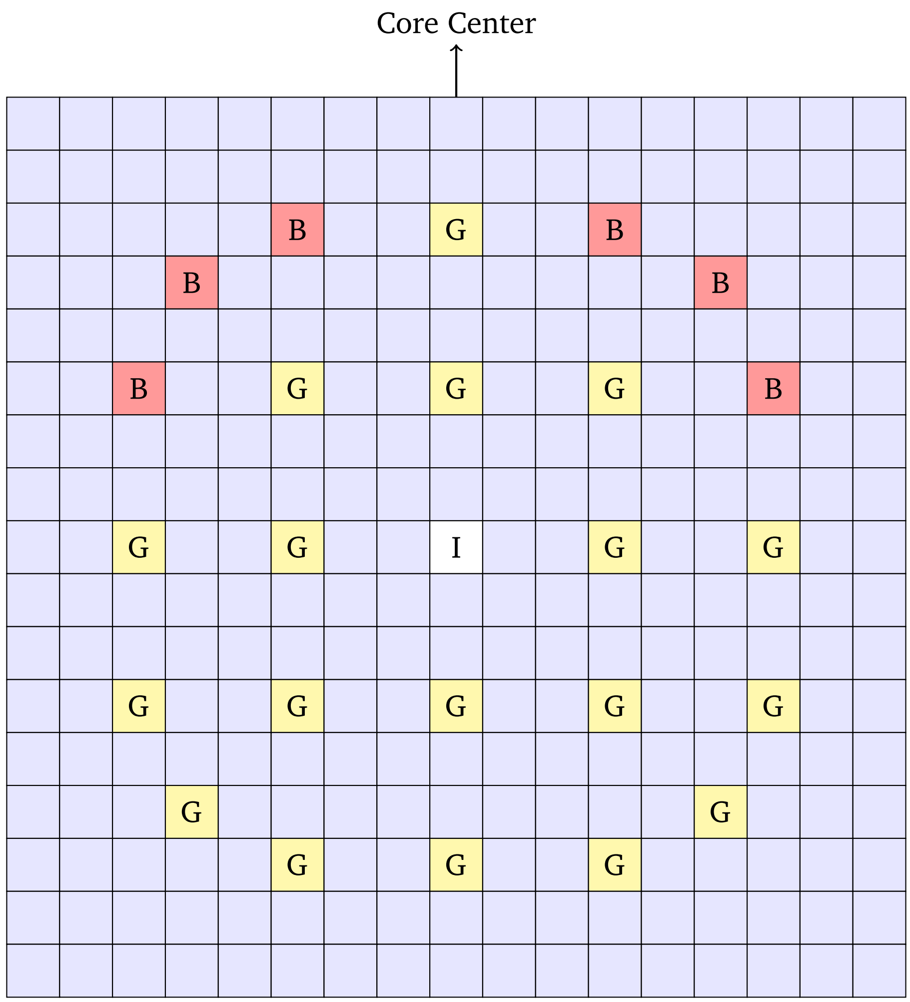


Figure 16: The 6BA burnable absorber configuration. Blank locations denote fuel rods, **G** denotes a guide tube location, **B** denotes a burnable absorber rod, and **I** denotes a guide tube position that might contain an instrument tube. Source: 35

| | | | | | | | | | | | | | | | | |
|---|---|---|---|---|---|---|---|---|---|---|---|---|---|---|---|---|
| | | | | | | | | | | | | | | | | |
| | | | | | | | | | | | | | | | | |
| | | | | | G | | | G | | | G | | | | | |
| | | | B | | | | | | | | | | B | | | |
| | | | | | | | | | | | | | | | | |
| | | G | | | G | | | B | | | G | | | G | | |
| | | | | | | | | | | | | | | | | |
| | | | | | | | | | | | | | | | | |
| | | G | | | B | | | I | | | B | | | G | | |
| | | | | | | | | | | | | | | | | |
| | | | | | | | | | | | | | | | | |
| | | G | | | G | | | B | | | G | | | G | | |
| | | | | | | | | | | | | | | | | |
| | | | B | | | | | | | | | | B | | | |
| | | | | | G | | | G | | | G | | | | | |
| | | | | | | | | | | | | | | | | |
| | | | | | | | | | | | | | | | | |

Figure 17: The 8BA burnable absorber configuration. Blank locations denote fuel rods, **G** denotes a guide tube location, **B** denotes a burnable absorber rod, and **I** denotes a guide tube position that might contain an instrument tube. Source: 35

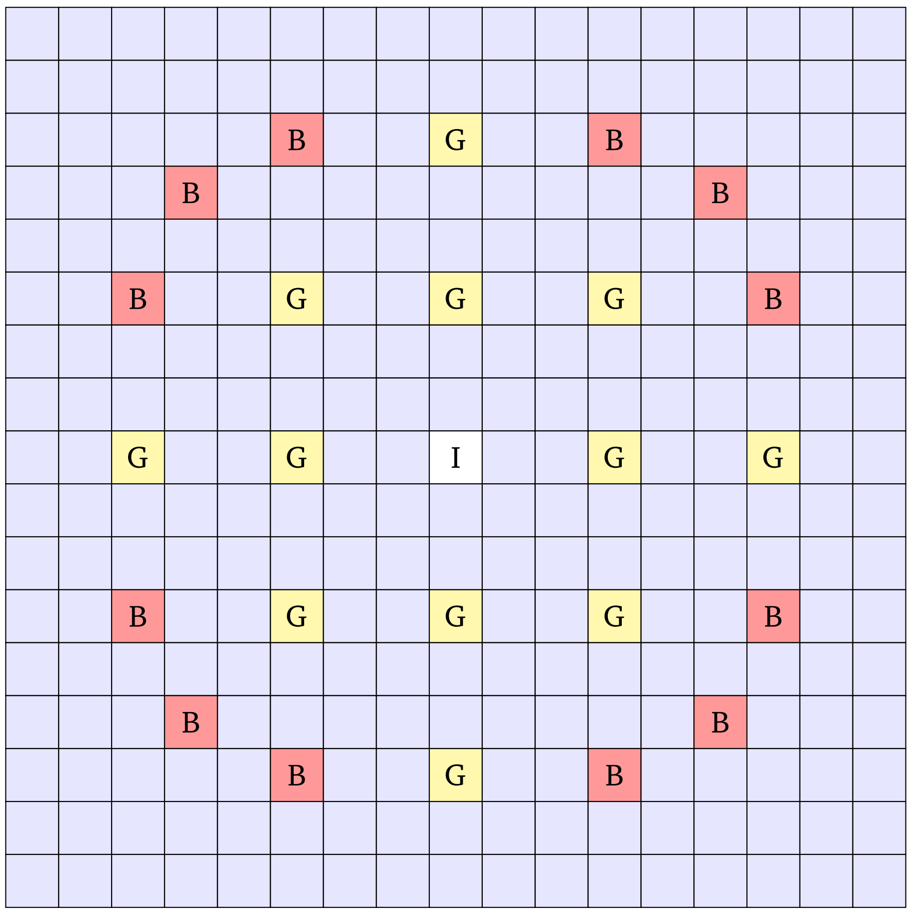


Figure 18: The 12BA burnable absorber configuration for cycle 1. Blank locations denote fuel rods, **G** denotes a guide tube location, **B** denotes a burnable absorber rod, and **I** denotes a guide tube position that might contain an instrument tube. Source: 35

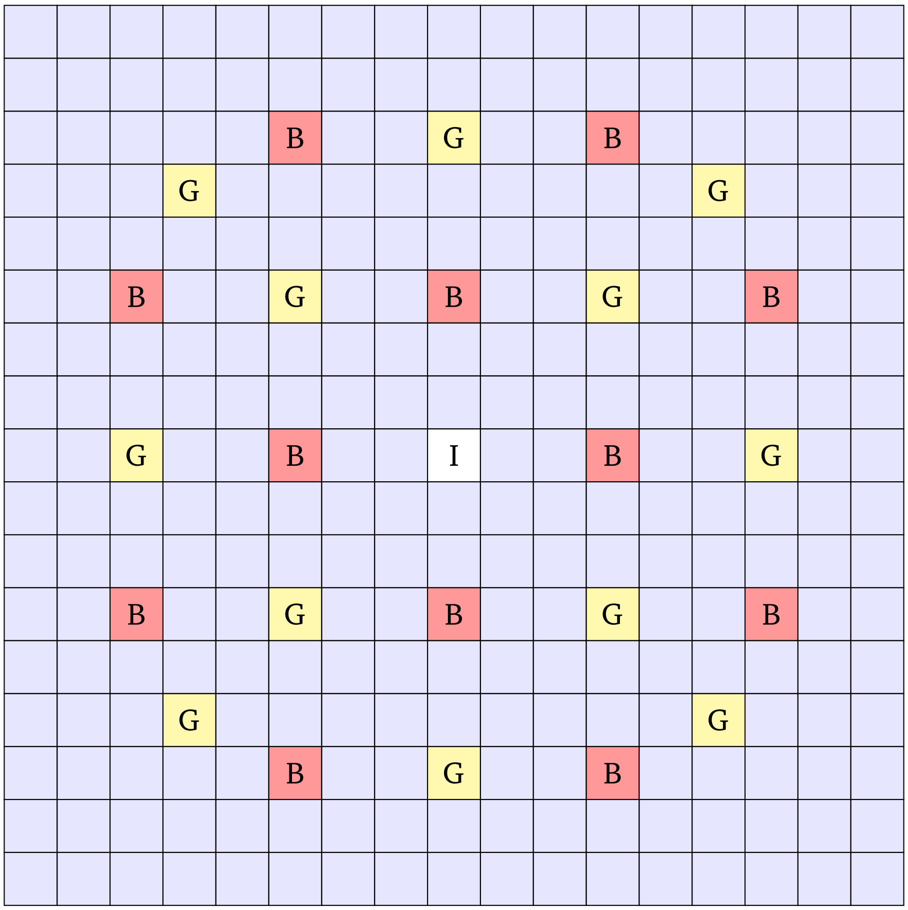


Figure 19: The 12BA burnable absorber configuration for cycle 2. Blank locations denote fuel rods, **G** denotes a guide tube location, **B** denotes a burnable absorber rod, and **I** denotes a guide tube position that might contain an instrument tube. Source: 35

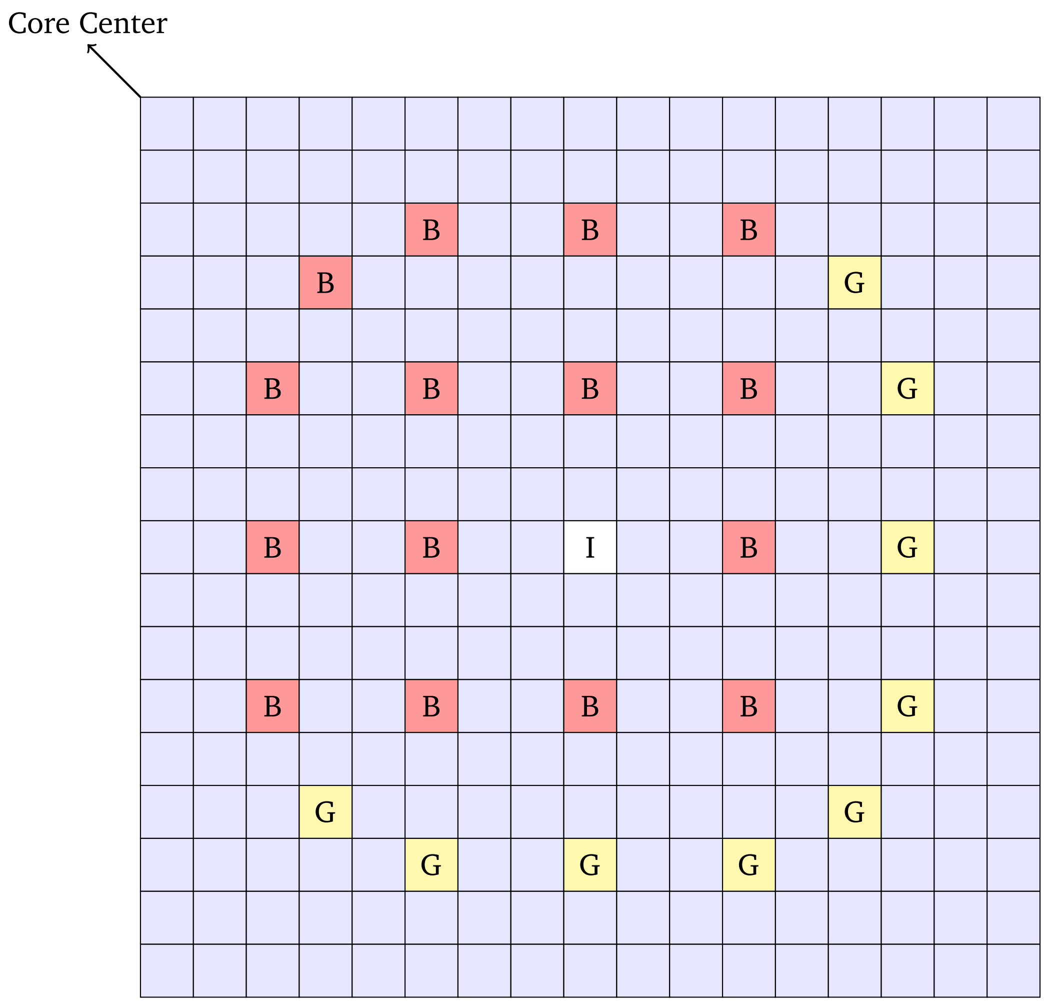


Figure 20: The 15BA burnable absorber configuration. Blank locations denote fuel rods, **G** denotes a guide tube location, **B** denotes a burnable absorber rod, and **I** denotes a guide tube position that might contain an instrument tube. Source: 35

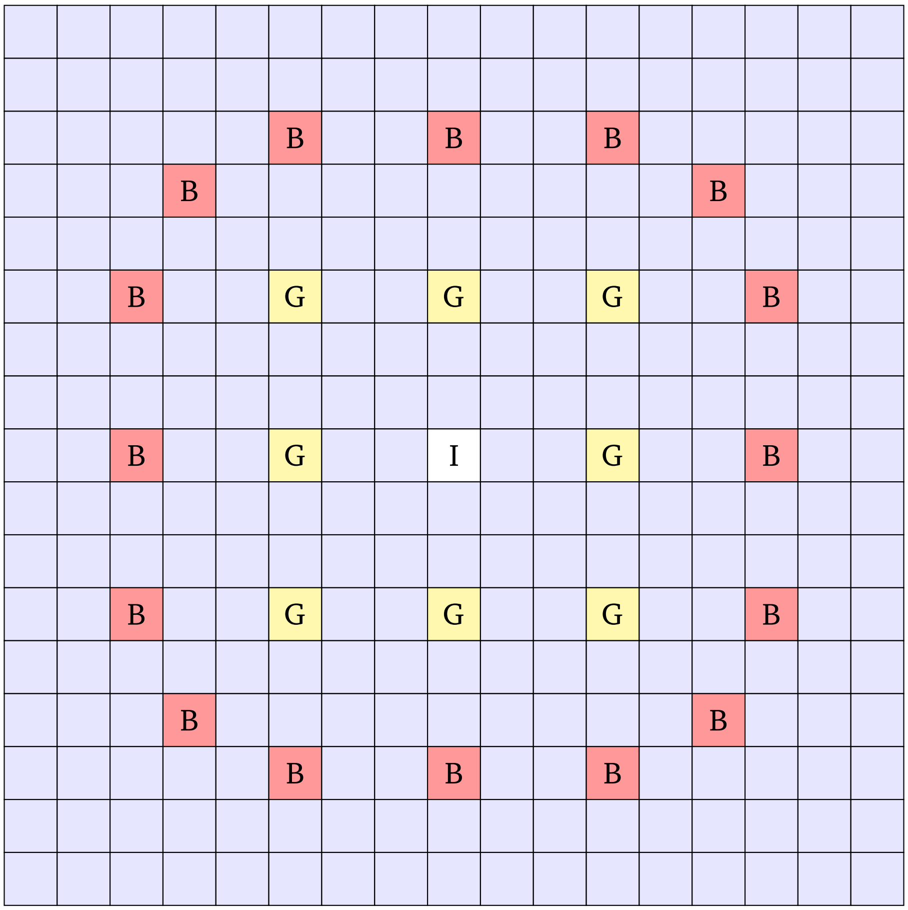


Figure 21: The 16BA burnable absorber configuration. Blank locations denote fuel rods, **G** denotes a guide tube location, **B** denotes a burnable absorber rod, and **I** denotes a guide tube position that might contain an instrument tube. Source: 35

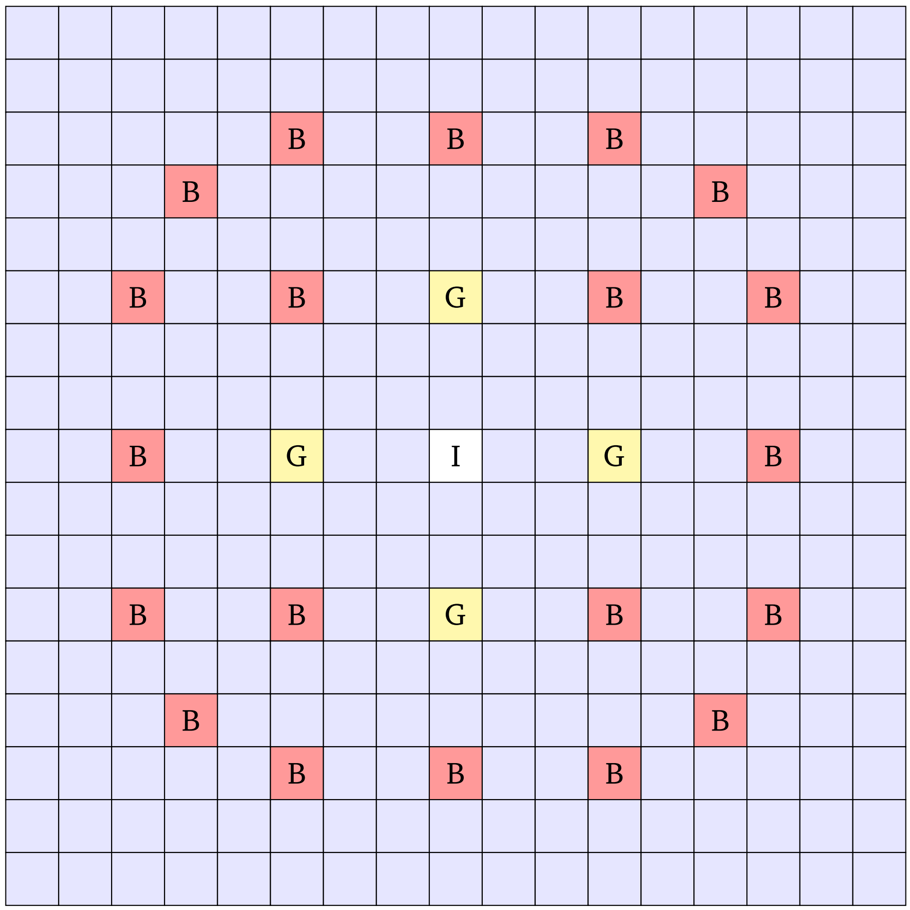


Figure 22: The 20BA burnable absorber configuration. Blank locations denote fuel rods, **G** denotes a guide tube location, **B** denotes a burnable absorber rod, and **I** denotes a guide tube position that might contain an instrument tube. Source: 35

#### 2.2.2.2 Radial Grid Spacer Specifications

In axial regions containing spacers, dimensions are chosen to conserve the total weight of Inconel, Zircaloy, and stainless steel in each grid, as listed in Table 2. The present model creates an egg-crate structure around each pincell as well as a sleeve around assemblies.

The middle six grid spacers consist entirely of Zircaloy while the top and bottom spacers consist of a Stainless Steel 304 (SS304) sleeve with Inconel internal structures. As described in Source 36, for the top/bottom grids the entire mass of the Inconel was distributed evenly among each of the 289 pincells in box of appropriate thickness inside the outer edges of the pincells. Additionally, the stainless steel mass of the grid sleeve was placed in a box of appropriate thickness around the outside of the assembly, fitting inside the region between assemblies. The 6 intermediate grids also consist of both these regions (outer grid sleeve and inner egg-crate), filled with Zircaloy. This was done for a top/bottom grid height of 1.322in and an intermediate grid height of 2.25in, with the same grid sleeve dimensions for each grid type. The inner egg-crate dimensions differ between each grid type.

Figures 23 and 24 show the modified pincell geometry used for the inner grid structure around a fuel pin for each grid type, where the box thicknesses are chosen to conserve mass in the total grid. The same box is also placed around the guide tube pincells for each grid type.

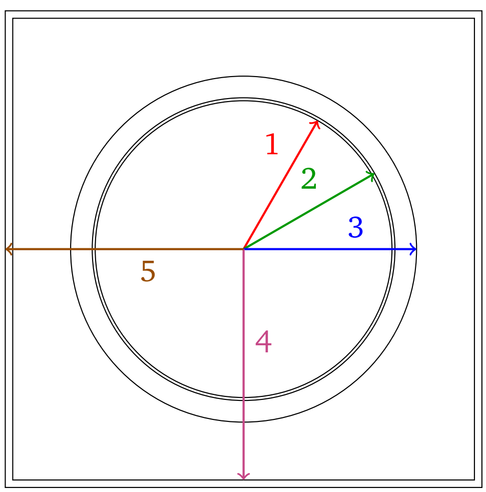


| Arrow | Length (cm) | Material | Source |
|---|---|---|---|
| 1 | 0.39218 | Fuel | 8 |
| 2 | 0.40005 | Helium | 9 |
| 3 | 0.45720 | Zircaloy | 10 |
| 4 | 0.61015 | Water | 36 |
| 5 | 0.62992 | Inconel | 36 |

Figure 23: Fuel pincell geometry for the Inconel 718 top/bottom grid spacer inner egg-crate, chosen to have a thickness of 0.0198cm. Source: 36

Figure 25 shows the dimensions of the grid sleeve assemblies in all grid spacer regions. To see what this looks like in combination with the inner structural component in the pincells see Figure 26, which shows an image of what the aggregate grid spacer model looks like to scale.

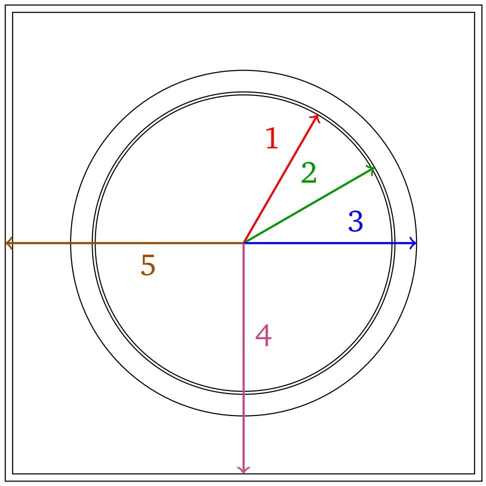


| Arrow | Length (cm) | Material | Source |
|---|---|---|---|
| 1 | 0.39218 | Fuel | 8 |
| 2 | 0.40005 | Helium | 9 |
| 3 | 0.45720 | Zircaloy | 10 |
| 4 | 0.61049 | Water | 36 |
| 5 | 0.62992 | Zircaloy | 36 |

Figure 24: Fuel pincell geometry for the Zircaloy intermediate grid spacer inner egg-crate, chosen to have a thickness of 0.0194cm. Source: 36

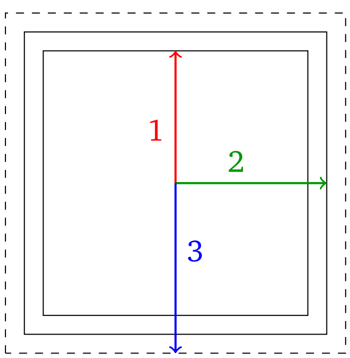


| Arrow | Length (cm) | Material | Source |
|---|---|---|---|
| 1 | 10.70864 | (Assembly) | 36 |
| 2 | 10.74798 | (Grid Sleeve) | 36 |
| 3 | 10.75182 | Water | 30 |

Figure 25: Schematic dimensions of stainless steel grid sleeve. Arrow 1 is the half-width of 17 times the pin lattice pitch; arrow 2 is the outer grid sleeve box half-width; arrow 3 is the outer boundary of the assembly pitch in the overall fuel assembly layout. The grid sleeve thickness was chosen as 0.00384cm to conserve the estimated stainless steel mass. Source: 36

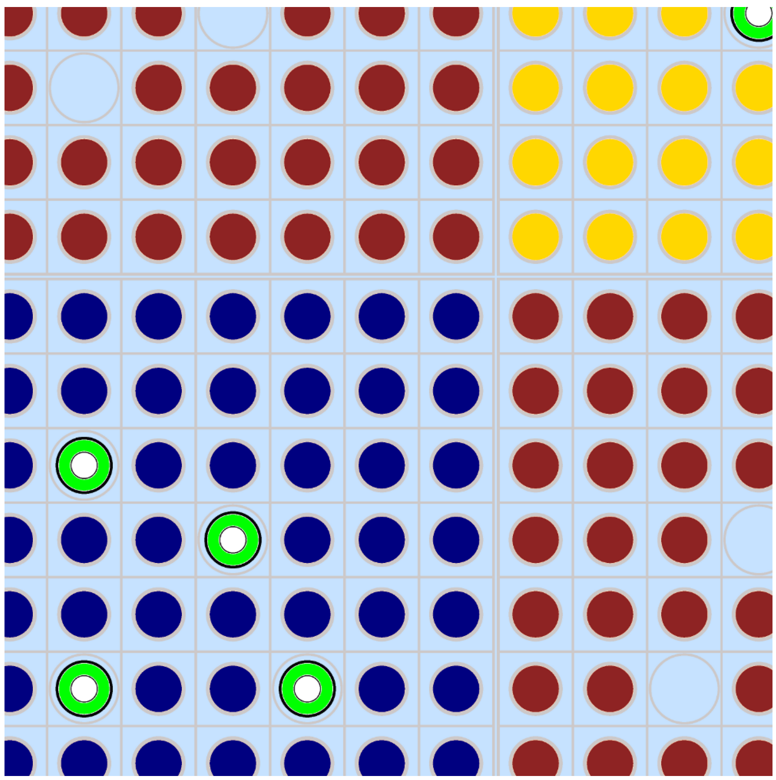

Figure 26: Scale view of an intermediate grid spacer showing inter-assembly spacing at a corner of position J14. Grey is Zircaloy, black is stainless steel, light blue is water, green is burnable absorber, white is air, and dark blue, red and yellow are the three different fuel enrichments.

### 2.2.3 Core Specification

The remainder of the radial specification is made up of the building blocks defined in the previous sections. Specifically, the main core lattice of fuel assemblies is made up of the previously described fuel assemblies, separated by the fuel assembly lattice pitch specified in Table 2. In addition, specifications for the structural components surrounding the fuel assembly lattice are given in Table 3.

Table 3: Structural component specifications.

| | | Source |
|---|---|---|
| Baffle Width | 2.22250 cm | 37 |
| Baffle Water Gap | 0.1627 cm | 41 |
| Baffle Material | Stainless Steel 304 | 41 |
| | | |
| Core Barrel IR | 187.960 cm | 38 |
| Core Barrel OR | 193.675 cm | 39 |
| Core Barrel Material | Stainless Steel 304 | 40 |
| | | |
| Neutron Shield Panel IR | 194.840 cm | 41 |
| Neutron Shield Panel OR | 201.630 cm | 41 |
| Neutron Shield Panel Material | Stainless Steel 304 | 41 |
| Neutron Shield Panel Width | 32° at the 45° marks | 41 |
| | | |
| Pressure Vessel Liner IR | 219.150 cm | 41 |
| Pressure Vessel Liner OR | 219.710 cm | 41 |
| Pressure Vessel Liner Material | Stainless Steel 304 | 47 |
| | | |
| Pressure Vessel IR | 219.710 cm | 41 |
| Pressure Vessel OR | 241.300 cm | 41 |
| Pressure Vessel Material | Carbon Steel 508 | 47 |

#### 2.2.3.1 Enrichment Zones and Burnable Absorber Positions

The initial cycle 1 fuel assembly loading pattern is shown in Figure 27, including the distribution of enrichments as well as burnable absorber locations. The burnable absorber configurations here are described in Section 2.2.2.1, rotated as appropriate for core symmetry. A scale view of burnable absorber pins depicting these rotations is shown in Figure 28.

Figure 29 shows the shuffling pattern for cycle 2, which includes 64 fresh assemblies and a different burnable absorber pattern.

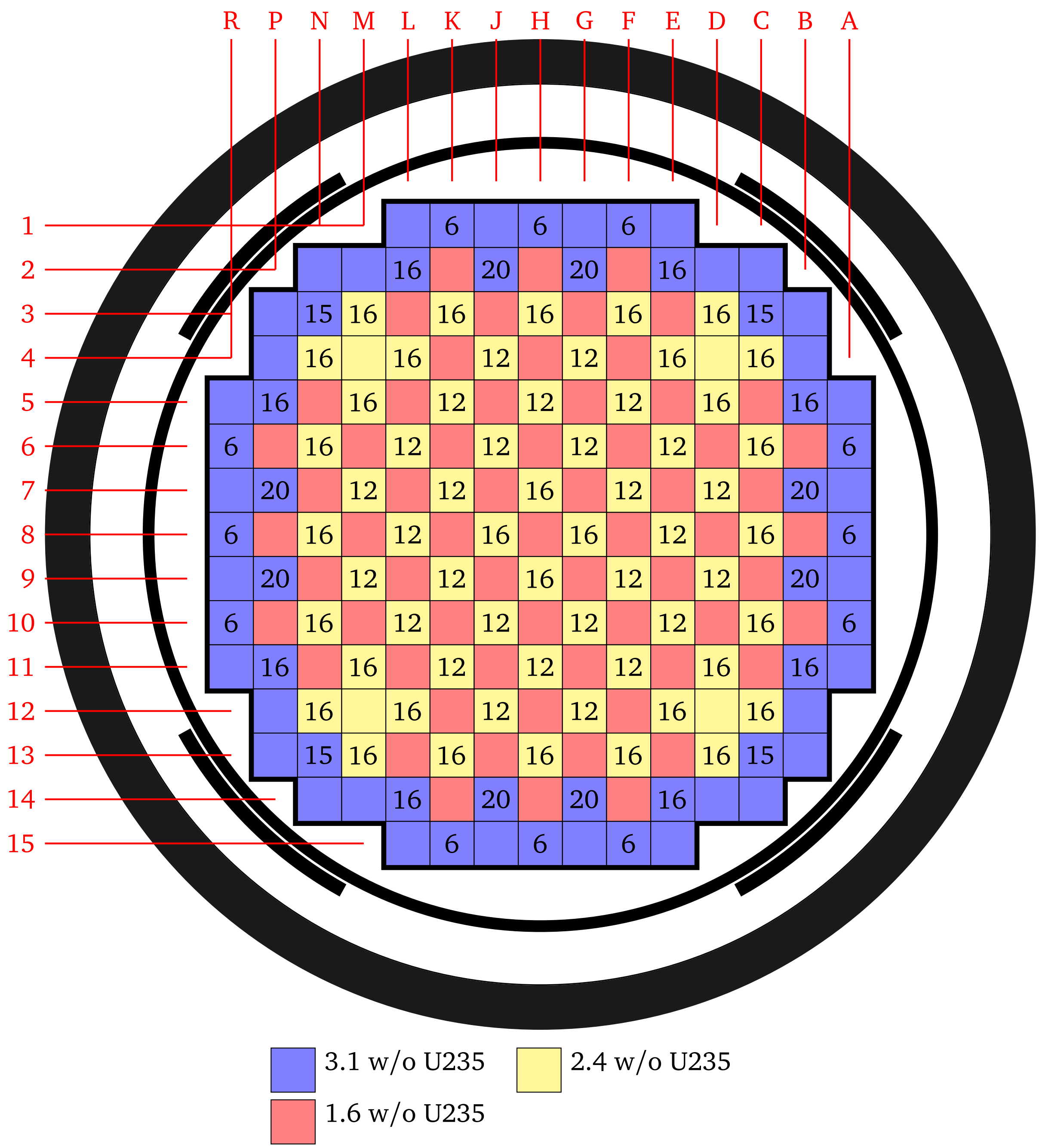


Figure 27: Layout of fuel assemblies showing enrichment loading pattern and burnable absorber positions in cycle 1. Source: 1

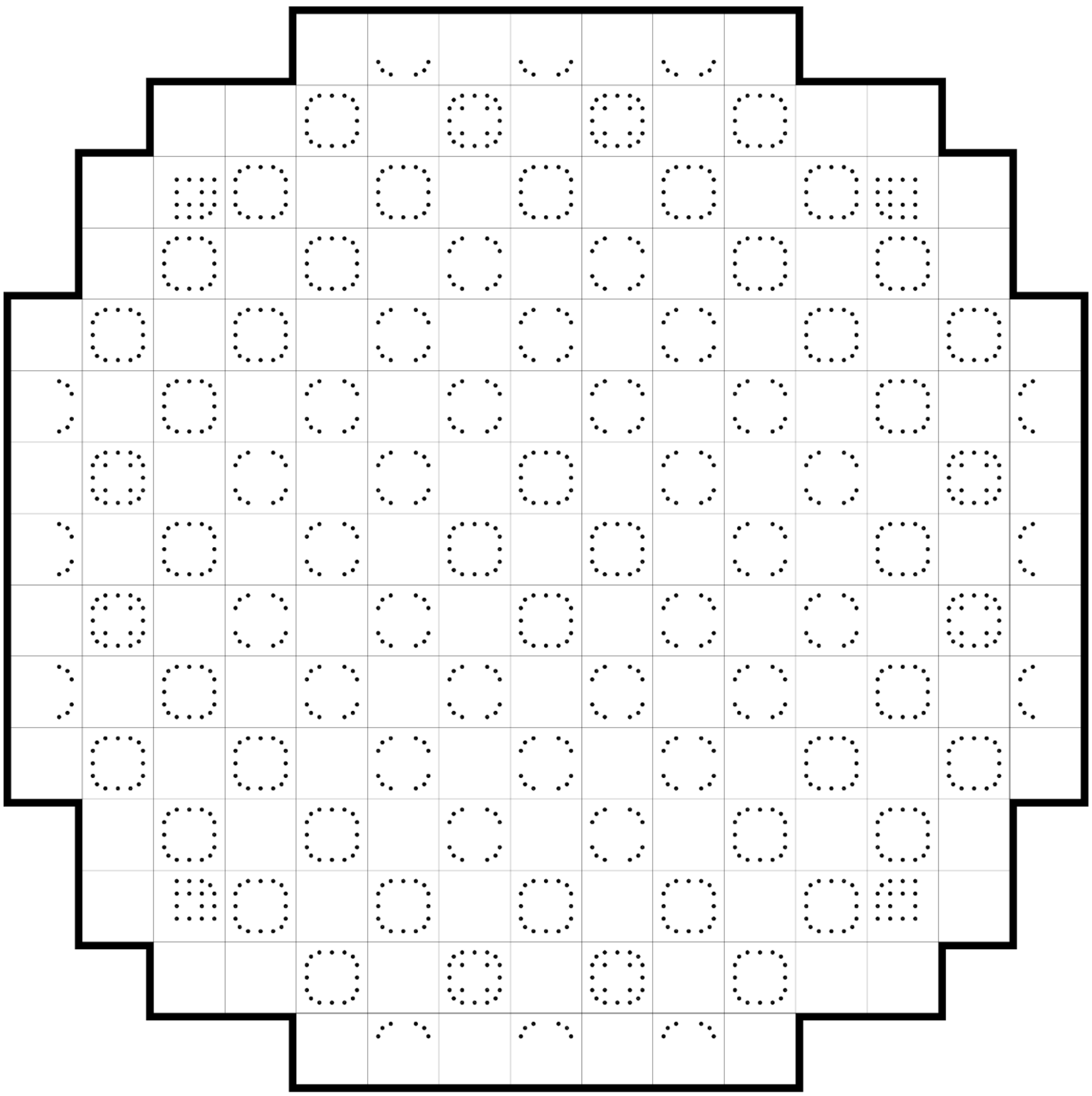

Figure 28: Detailed scale view of burnable absorber pins in cycle 1, showing proper rotations.

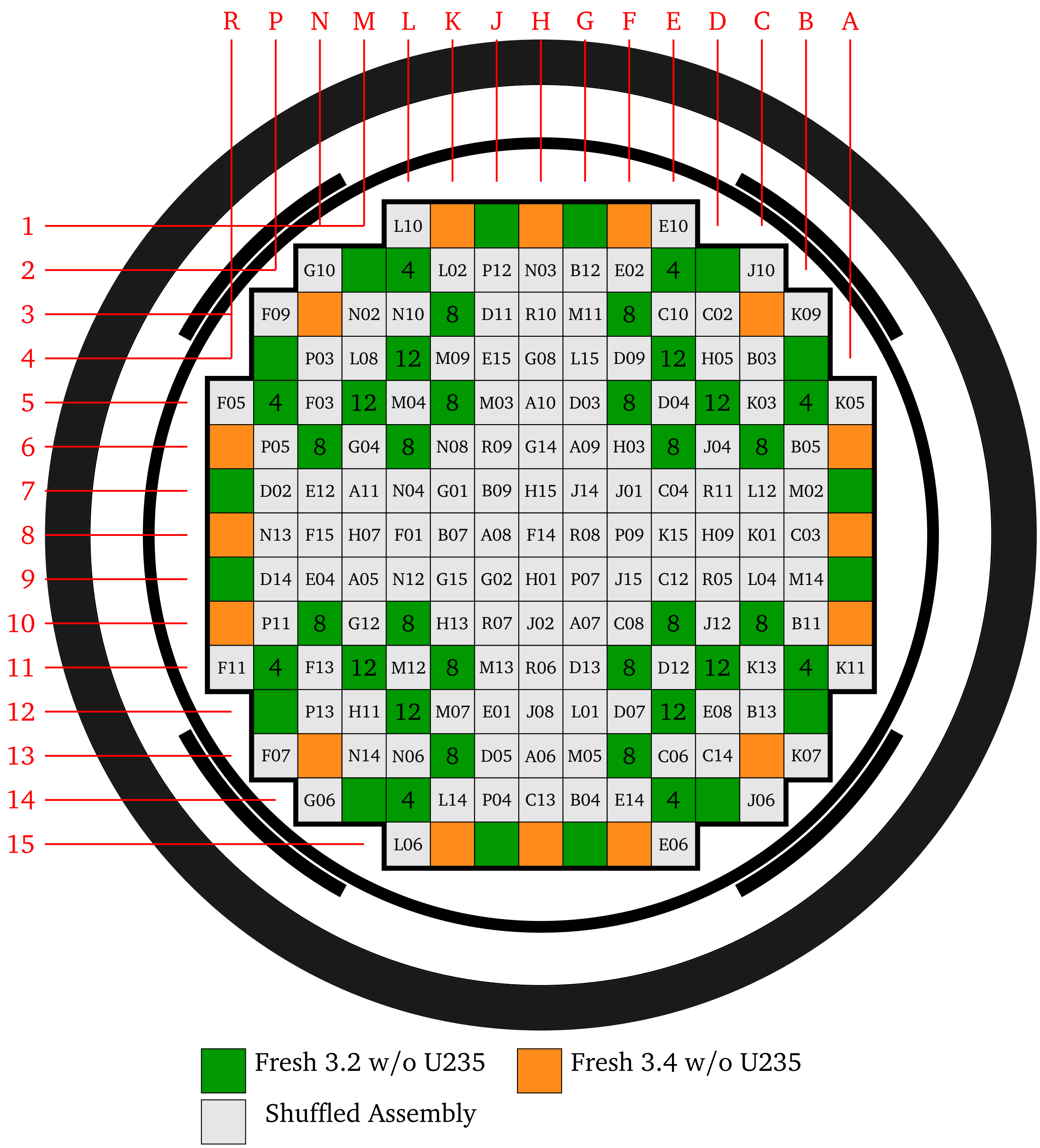


Figure 29: Cycle 2 shuffling pattern, burnable absorber positions, and enrichment loading pattern of fresh assemblies. Sources: 1, 2

#### 2.2.3.2 Control Rod Bank Positions

Each of the four control rod banks - specified by the identifiers A, B, C, and D - are made up of several control rod clusters in multiple fuel assemblies. In control rod clusters, every guide tube is filled with the control rod pincell described in section 2.2.1, with the exception of the center tube. Each of the clusters in a given control rod bank move together.

In addition to the control rod banks, 5 shutdown banks of control rod clusters are included above the core - specified by $S_A$, $S_B$, $S_C$, $S_D$, and $S_E$. These clusters are not used in normal operation, however, their reactivity worth was measured and reported in Table 22.

Figure 30 shows the radial locations of control rod clusters belonging to each control rod and shutdown bank. The axial specifications of each are described later in Section 2.3.5.

The positions of control rod banks do not change between cycle 1 and cycle 2.

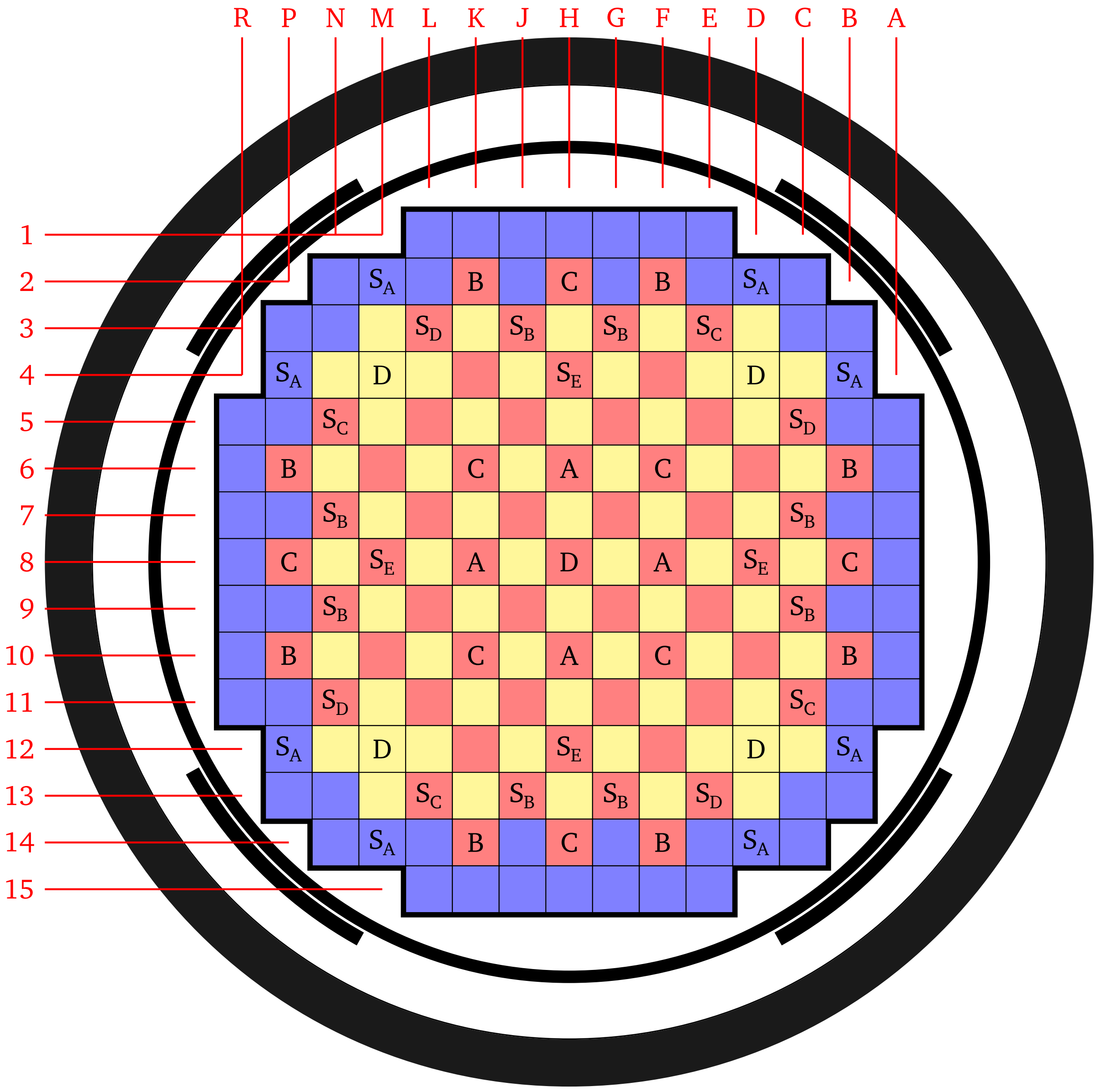


Figure 30: Control rod and shutdown bank positions. Source: 1

#### 2.2.3.3 Instrument Tube Positions

The central guide tube for many fuel assemblies in the core is filled by an instrument tube, as described in Section 2.2.1. Figure 31 shows these positions. Where not indicated, the central guide tube is filled with water, as described in section 2.2.1.

The positions of instrument tubes do not change between cycle 1 and cycle 2.

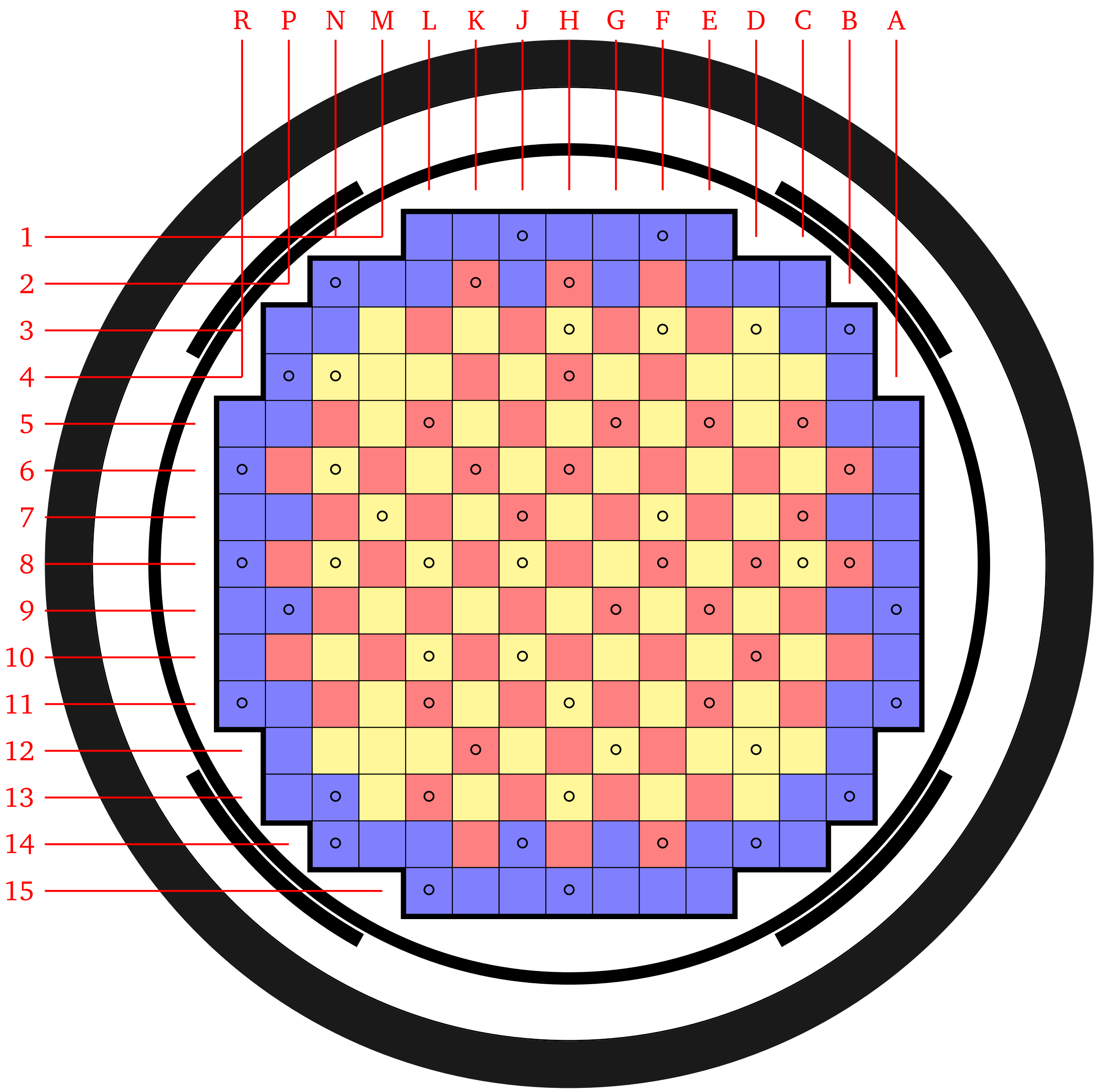


Figure 31: Instrument tube positions. Source: 48

## 2.3 Axial Geometry

While some of the previously-described radial features are uniform along the entire height of the model, many have several different axial zones. For instance, the models of the baffle, core barrel, neutron shield panels, and reactor pressure vessel do not change axially, in contrast to the pincells that make up the fuel assemblies. As presented in the following sections, the axial zones are treated at the pincell level to faciliate easier modelling, since the boundaries for the axial zones for each pincell type are not all at the same planes. With this type of definition, the final aggregate geometry inside the core barrel need only consist of the fuel assemblies, which are made up of only the inter-assembly gridstraps and the pincells that are defined for the entire axial extent.

### 2.3.1 Fuel Rods

Figure 32 shows all different axial sections used in the fuel rod pincell occupying each fuel position in the assemblies. In most places the pincells described in Section 2.2.1 are used, however where indicated the pincell is filled either entirely with water, or with solid pins of either stainless steel or Zircaloy. These solid pins use the outer-most radius of the regular fuel rod pincell.

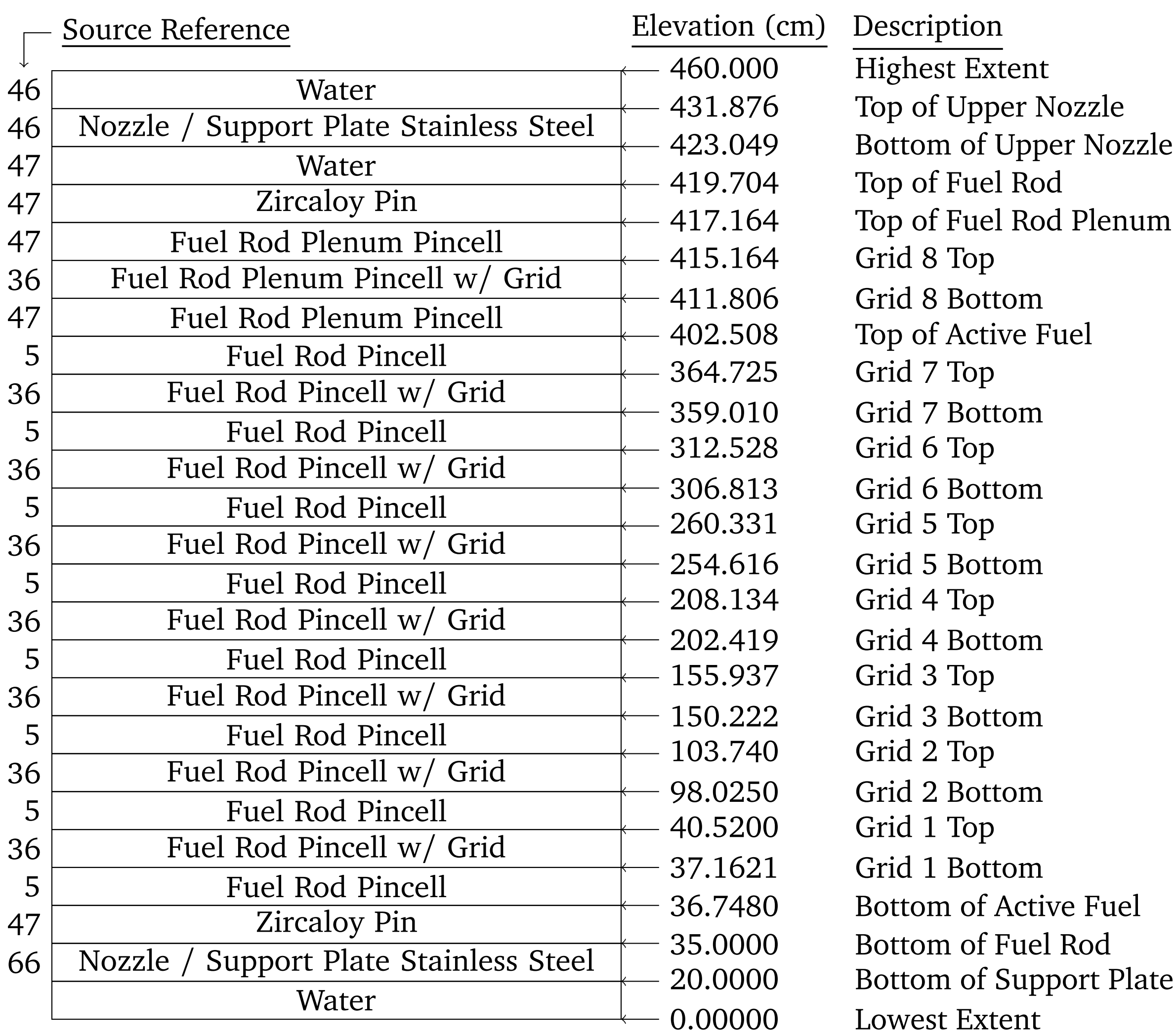


Figure 32: Fuel rod pincell axial specification.

### 2.3.2 Guide Tubes

Figure 33 shows the empty guide tube axial differentiation, referring to the pincells described in Section 2.2.1. As with the fuel rods, the pincell is replaced by water below the fuel region.

| Source Reference | Region |
|---|---|
| 46 | Water |
| 46 | Nozzle / Support Plate Borated Water |
| 44 | Guide Tube Pincell |
| 36 | Guide Tube Pincell w/ Grid |
| 44 | Guide Tube Pincell |
| 36 | Guide Tube Pincell w/ Grid |
| 44 | Guide Tube Pincell |
| 36 | Guide Tube Pincell w/ Grid |
| 44 | Guide Tube Pincell |
| 36 | Guide Tube Pincell w/ Grid |
| 44 | Guide Tube Pincell |
| 36 | Guide Tube Pincell w/ Grid |
| 44 | Guide Tube Pincell |
| 36 | Guide Tube Pincell w/ Grid |
| 44 | Guide Tube Pincell |
| 36 | Guide Tube Pincell w/ Grid |
| 44 | Dashpot Guide Tube |
| 44 | Guide Tube Pincell |
| 36 | Dashpot Guide Tube w/ Grid |
| 44 | Dashpot Guide Tube |
| 66 | Nozzle / Support Plate Borated Water |
| | Water |

| Elevation (cm) | Description |
|---|---|
| 431.876 | Top of Upper Nozzle |
| 423.049 | Bottom of Upper Nozzle |
| 415.164 | Grid 8 Top |
| 411.806 | Grid 8 Bottom |
| 364.725 | Grid 7 Top |
| 359.010 | Grid 7 Bottom |
| 312.528 | Grid 6 Top |
| 306.813 | Grid 6 Bottom |
| 260.331 | Grid 5 Top |
| 254.616 | Grid 5 Bottom |
| 208.134 | Grid 4 Top |
| 202.419 | Grid 4 Bottom |
| 155.937 | Grid 3 Top |
| 150.222 | Grid 3 Bottom |
| 103.740 | Grid 2 Top |
| 98.0250 | Grid 2 Bottom |
| 40.5200 | Grid 1 Top |
| 39.9580 | Control Rod Step 0 |
| 37.1621 | Grid 1 Bottom |
| 35.0000 | Bottom of Fuel Rod |
| 20.0000 | Bottom of Support Plate |
| 0.00000 | Lowest Extent |

Figure 33: Empty guide tube pincell axial specification.

### 2.3.3 Instrument Tubes

Figure 34 shows the instrument tube axial differentiation, referring to the pincells described in Section 2.2.1. This follows the same pattern as the guide tube axial specification, with the caveat that below the fuel region the inner section of the instrument tubes (that is, without the surrounding guide tube) is used through the lowest extent of the geometry. Also note that regardless of whether or not the central instrument tube contains the inner instrument thimble, the outer guide tube does not shrink for the dashpot.

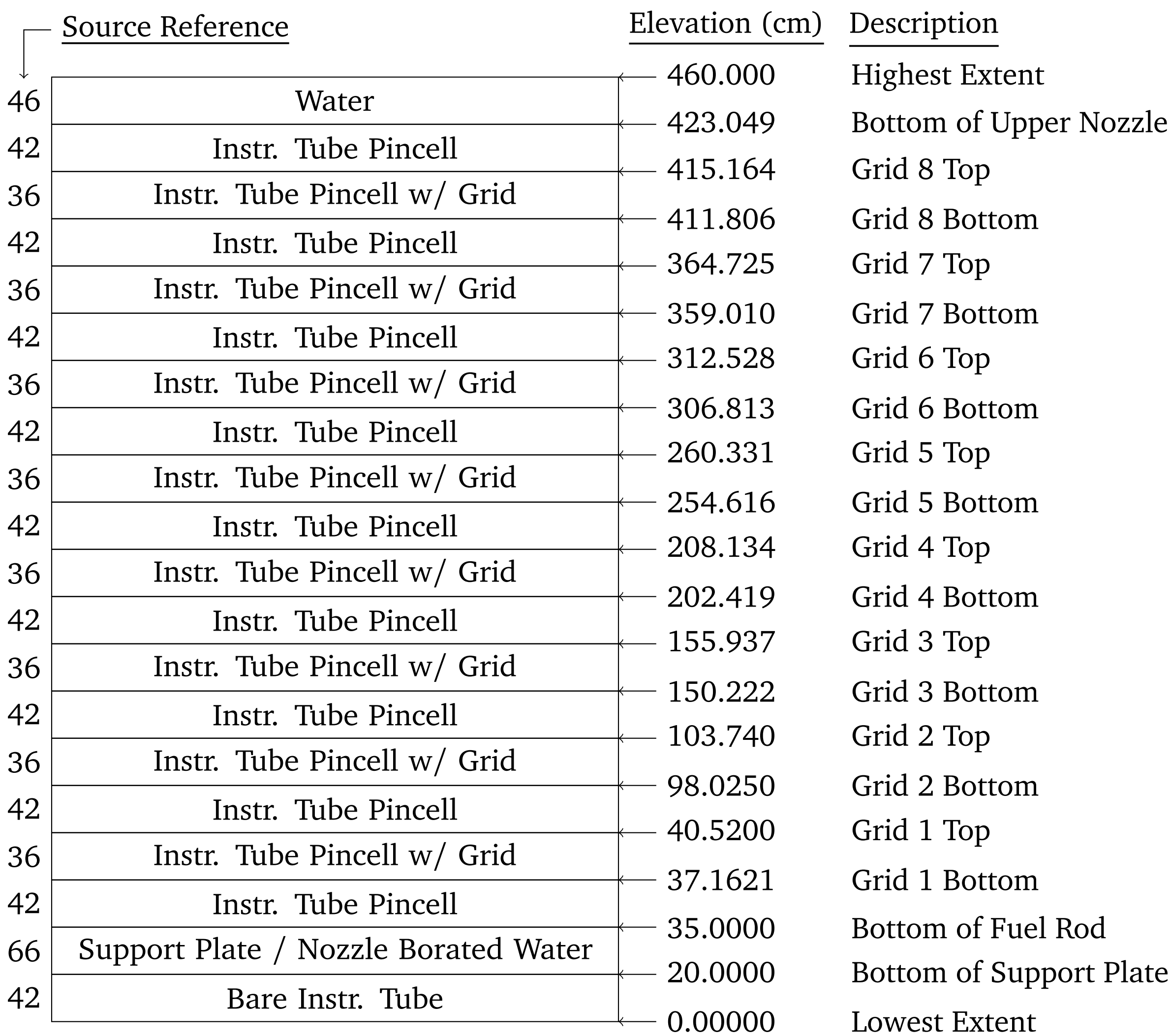


Figure 34: Instrument tube pincell axial specification.

### 2.3.4 Burnable Absorbers

Figure 35 shows the axial regions of the burnable absorber pincells. Here, the active region of burnable absorber rods as presented in Section 2.2.1 extend from a plane a few inches above the bottom of the active fuel to a plane just below the top of the active fuel region. Above there, the outermost inner radius of the burnable absorber rods (or arrow 6 in Figure 8) is used to create a solid stainless steel pin tube through the top of the upper nozzle, inside the guide tube where appropriate.

| Source Reference | Region | Elevation (cm) | Description |
|---|---|---|---|
| | | 460.000 | Highest Extent |
| 46 | Water | | |
| | | 431.876 | Top of Upper Nozzle |
| 43 | Stainless Steel Pin | | |
| | | 423.049 | Bottom of Upper Nozzle |
| 43 | Stainless Steel Pin in GT | | |
| | | 421.532 | Top of BPRA Rod Plenum |
| 43 | BPRA Rod Upper Plenum Pincell | | |
| | | 415.164 | Grid 8 Top |
| 36 | BPRA Rod Plenum Pincell w/ Grid | | |
| | | 411.806 | Grid 8 Bottom |
| 43 | BPRA Rod Plenum Pincell | | |
| | | 401.238 | Top of Active Absorber |
| 43 | Burnable Absorber Pincell | | |
| | | 364.725 | Grid 7 Top |
| 36 | Burnable Absorber Pincell w/ Grid | | |
| | | 359.010 | Grid 7 Bottom |
| 43 | Burnable Absorber Pincell | | |
| | | 312.528 | Grid 6 Top |
| 36 | Burnable Absorber Pincell w/ Grid | | |
| | | 306.813 | Grid 6 Bottom |
| 43 | Burnable Absorber Pincell | | |
| | | 260.331 | Grid 5 Top |
| 36 | Burnable Absorber Pincell w/ Grid | | |
| | | 254.616 | Grid 5 Bottom |
| 43 | Burnable Absorber Pincell | | |
| | | 208.134 | Grid 4 Top |
| 36 | Burnable Absorber Pincell w/ Grid | | |
| | | 202.419 | Grid 4 Bottom |
| 43 | Burnable Absorber Pincell | | |
| | | 155.937 | Grid 3 Top |
| 36 | Burnable Absorber Pincell w/ Grid | | |
| | | 150.222 | Grid 3 Bottom |
| 43 | Burnable Absorber Pincell | | |
| | | 103.740 | Grid 2 Top |
| 36 | Burnable Absorber Pincell w/ Grid | | |
| | | 98.0250 | Grid 2 Bottom |
| 43 | Burnable Absorber Pincell | | |
| | | 40.5580 | Bottom of Active Absorber |
| 43 | Stainless Steel Pin in GT | | |
| | | 40.5200 | Grid 1 Top |
| 43 | SS Pin in GT w/ Grid | | |
| | | 39.9580 | Control Rod Step 0 |
| 43 | SS Pin in Dashpot GT w/ Grid | | |
| | | 38.6600 | Bot. of BPRA Rod |
| 36 | Dashpot Guide Tube w/ Grid | | |
| | | 37.1621 | Grid 1 Bottom |
| 44 | Dashpot Guide Tube | | |
| | | 35.0000 | Bottom of Fuel Rod |
| 66 | Support Plate / Nozzle Borated Water | | |
| | | 20.0000 | Bottom of Support Plate |
| | Water | | |
| | | 0.00000 | Lowest Extent |

Figure 35: Burnable absorber pincell axial specification.

### 2.3.5 Control Rods

Figure 36 shows the control rod axial layout, which depending on the degree of insertion can either be occupied by the empty guide tube pincell or the control rod pincell described in Section 2.2.1. The details of insertion depend on the radial location of the specific control rod cluster, i.e. which control or shutdown bank it belongs to. Unlike the other axial descriptions in this section, Figure 36 presents the axial sections *only* for the control rod thimble that fits inside the guide tube. It is presented for the fully-inserted position; all intermediate planes should be shifted according to the number of steps withdrawn, and the appropriate axial sections created in combination with the surrounding guide tube and grid spacer pincell.

In this model, when fully-inserted the top of the upper control rod active absorber region should be flush with the top of the active fuel region. Control rods are considered to be withdrawn in 228 "steps" until the active region is drawn completely out of the active fuel region. When withdrawn 228 steps, the bottom of the lower control rod active absorber region should be flush with the top of the active fuel region. The total height of the lower and upper control rod regions is 360.68 cm, meaning the step height is 1.58193 cm.

The actual axial planes used depend on the the number of steps of insertion of the rod, and may be superceded by the highest axial plane when appropriate. In other words, the planes presented in Figure 36 should be shifted upwards by the number of steps withdrawn times the step height.

The control and shutdown banks can have any level of partial insertion, where the bottom tips of the rods can be at any axial step level between step 0 and step 228. While each of these banks move their control rod clusters together, their movement is often staggered with the other control rod banks, described in Figure 37 with an insertion sequence example. However, insertion levels for each individual bank are provided for most of the data presented in this benchmark, so the algorithm in Figure 37 may not be needed.

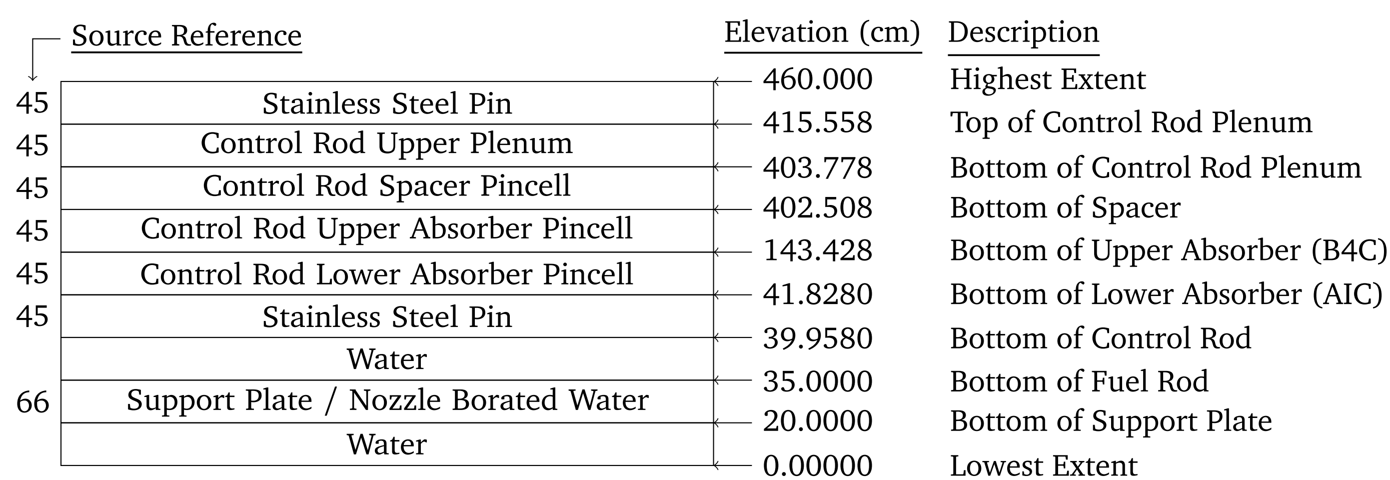


Figure 36: Control rod pincell axial specification when fully-inserted. This only shows axial sections for the control rod itself, which is inside one of the guide tubes.

**Control Rod Insertion Sequence**

Starting from all rods fully withdrawn:

- First D moves in alone, until it gets to 113 steps withdrawn
- Now D and C move together until C gets to 113 steps withdrawn
  (D is all the way in when C is at 115)
- Now C and B move together until B gets to 113 steps withdrawn
  (C is all the way in when B is at 115)
- Now B and A move together until A gets to 0 steps withdrawn
  (B is all the way in when A is at 115)

Assuming only movement of each control rod bank by one step at a time, in total this sequence yields 574 unique positions, which we denote with integer $\mathbb{S}$ steps withdrawn. If $\mathbb{S} = 0$ all control rods are out of the core, and if $\mathbb{S} = 574$ all rods are fully inserted. For example for normal operation with the D bank at the bite position of $\mathbb{S}_D = 213$ steps withdrawn, $\mathbb{S} = 228-213 = 15$. With this notation, the following algorithm provides the elevation of the axial planes of the active region in each control rod bank ($s_i^{\text{bot}}$ and $s_i^{\text{top}}$) for a given $\mathbb{S}$ with the fully inserted elevation $s_0$ and step width $\delta$.

$$
\begin{aligned}
\mathbb{S}_D &= \max(0,\ 228-\mathbb{S}) \\
\mathbb{S}_C &= (\mathbb{S}_D < 113)\ ?\ \max(0,\ 228-\mathbb{S}+113+3)\ :\ 228 \\
\mathbb{S}_B &= (\mathbb{S}_C < 113)\ ?\ \max(0,\ 228-\mathbb{S}+113\times 2+5)\ :\ 228 \\
\mathbb{S}_A &= (\mathbb{S}_B < 113)\ ?\ \max(0,\ 228-\mathbb{S}+113\times 3+7)\ :\ 228
\end{aligned}
$$

$$
\begin{aligned}
s_A^{\text{bot}} &= s_0 + \delta \times \mathbb{S}_A \\
s_B^{\text{bot}} &= s_0 + \delta \times \mathbb{S}_B \\
s_C^{\text{bot}} &= s_0 + \delta \times \mathbb{S}_C \\
s_D^{\text{bot}} &= s_0 + \delta \times \mathbb{S}_D
\end{aligned}
$$

$$
\begin{aligned}
s_A^{\text{top}} &= s_A^{\text{bot}} + \delta \times 228 \\
s_B^{\text{top}} &= s_B^{\text{bot}} + \delta \times 228 \\
s_C^{\text{top}} &= s_C^{\text{bot}} + \delta \times 228 \\
s_D^{\text{top}} &= s_D^{\text{bot}} + \delta \times 228
\end{aligned}
$$

Figure 37: Control rod insertion sequence and axial specification [14].

### 2.3.6 Aggregate

By defining the full extent of the axial geometry in the pincells, several features remain to be described or examined in the final combination of each element of the model. In aggregate it is useful to see an exhaustive list of all axial planes used in the model, as presented in Figure 38. Control rod insertions are treated separately, as discussed in Section 2.3.5.

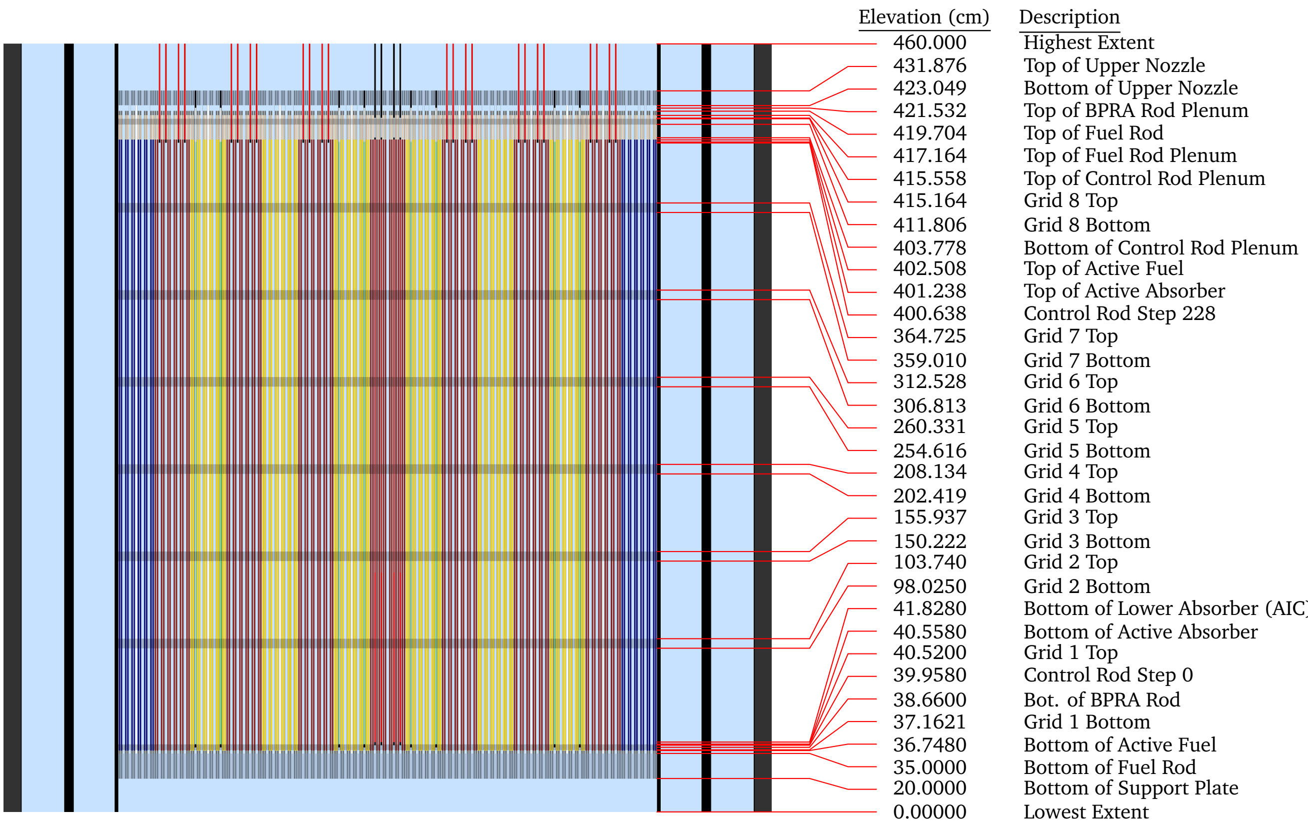


Figure 38: *Left*: Scale view of row 8 axial cross section, with highlighted grid spacers and partial insertion of control rod bank D to the bite position. *Right*: exhaustive list of all axial planes used in the model, excluding partial control rod insertion planes.

#### 2.3.6.1 Grid Spacers

Nearly all axial features of the model are captured in the axial pincell specifications. However, the stainless steel grid sleeve described in Section 2.2.2.2 for each of the 8 grid spacers needs to be defined on the assembly level, as it is not contained within any of the pincell elements. The axial planes used for the grid sleeves are the same as those used for the grids in the pincells, as listed in Figure 38.

#### 2.3.6.2 Nozzles and Support Plate

By defining pincells as solid material pins below and above the fuel rod regions, the model implicitly approximates the nozzle and support plate regions as depicted in Figure 39. While the axial planes used here were taken from Source 46, this does not necessarily represent the true geometry of this portion of the reactor. However, the special densities of water and steel for the nozzle sections were calculated such that the mass and volume fractions of the materials are consistent with [15]. The material compositions of borated water and steel in the nozzle and support plate are in Material 18 and Material 19 respectively. Thus, when modeling, the material "Nozzle / Support Plate Stainless Steel" (19) rather than "Stainless Steel" should be used for all the fuel rods in the upper and lower nozzle / support plate regions as depicted in Figure 32, while the material "Nozzle / Support Plate Borated Water" (19) rather than "Borated Water" should be used for the water in the nozzles and support plate (Figure 33). Figures 32 through 40 illustrate the modeling details with material names and colors that preserve the actual masses of material. Note that since the bottom nozzle and support plate are both stainless steel, no distinction is made between the two regions.

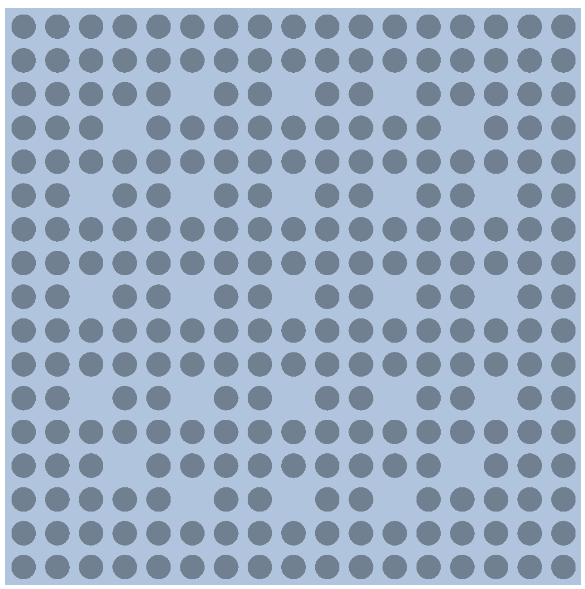

Figure 39: Radial picture of nozzles and support plate in aggregate model

#### 2.3.6.3 Top and Bottom of the Core

For verification, Figure 40 shows scale views close to the bottom and top regions of the core resulting from the aggregate pincell specification as defined previously.

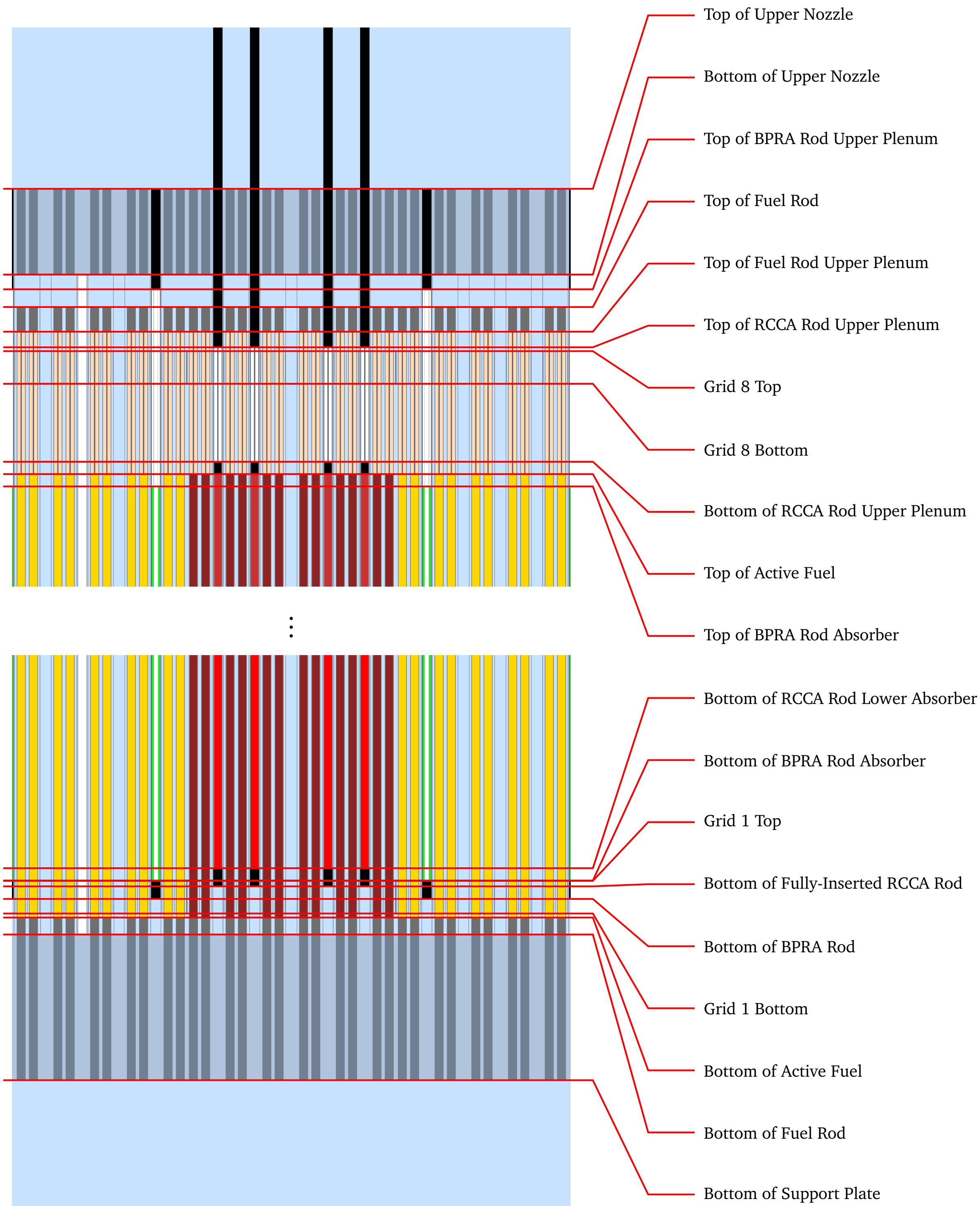


Figure 40: Axial scale view of the model near the top and bottom of the fuel rods in row 8, showing pin plenums, approximated springs, end plugs, and structures. *Blue*: water; *orange*: helium; *black*: stainless steel; *dark gray*: Zircaloy; *dim gray* Inconel; *white*: air; *slate gray*: nozzle / support plate stainless steel; *steel blue*: nozzle / support plate borated water; *green*: borosilicate glass; *yellow*: fuel.

## 2.4 Materials

**Table 4 — Fuel 1.6% Enriched**

| Density (g/cc) | 10.31341 |
|---|---|
| Isotope | Atom Density (atom/b-cm) |
| O16 | 4.5897e-02 |
| O17 | 1.7436e-05 |
| O18 | 9.2032e-05 |
| U234 | 3.0131e-06 |
| U235 | 3.7503e-04 |
| U238 | 2.2625e-02 |

Source: 49

## Table 5 — Fuel 2.4% Enriched

| Density (g/cc) | 10.29748 |
|---|---|
| Isotope | Atom Density (atom/b-cm) |
| O16 | 4.5830e-02 |
| O17 | 1.7411e-05 |
| O18 | 9.1898e-05 |
| U234 | 4.4842e-06 |
| U235 | 5.5814e-04 |
| U238 | 2.2407e-02 |

Source: 50

## Table 6 — Fuel 3.1% Enriched

| Density (g/cc) | 10.30166 |
|---|---|
| Isotope | Atom Density (atom/b-cm) |
| O16 | 4.5853e-02 |
| O17 | 1.7420e-05 |
| O18 | 9.1942e-05 |
| U234 | 5.7987e-06 |
| U235 | 7.2175e-04 |
| U238 | 2.2253e-02 |

Source: 51

## Table 7 — Fuel 3.2% Enriched

| Density (g/cc) | 10.34115 |
|---|---|
| Isotope | Atom Density (atom/b-cm) |
| O16 | 4.6029e-02 |
| O17 | 1.7487e-05 |
| O18 | 9.2296e-05 |
| U234 | 5.9959e-06 |
| U235 | 7.4630e-04 |
| U238 | 2.2317e-02 |

Source: 52

## Table 8 — Fuel 3.4% Enriched

| Density (g/cc) | 10.35917 |
|---|---|
| Isotope | Atom Density (atom/b-cm) |
| O16 | 4.6110e-02 |
| O17 | 1.7517e-05 |
| O18 | 9.2459e-05 |
| U234 | 6.4018e-06 |
| U235 | 7.9681e-04 |
| U238 | 2.2307e-02 |

Source: 53

## Table 9 — Air

| Density (g/cc) | 0.00616 |
|---|---|
| Isotope | Atom Density (atom/b-cm) |
| Ar36 | 7.8730e-09 |
| Ar38 | 1.4844e-09 |
| Ar40 | 2.3506e-06 |
| C12 | 6.7539e-08 |
| C13 | 7.5658e-10 |
| N14 | 1.9680e-04 |
| N15 | 7.2354e-07 |
| O16 | 5.2866e-05 |
| O17 | 2.0084e-08 |
| O18 | 1.0601e-07 |

Source: 54

## Table 10 — Borosilicate Glass

| Density (g/cc) | 2.26 |
|---|---|
| Isotope | Atom Density (atom/b-cm) |
| Al27 | 1.7352e-03 |
| B10 | 9.6506e-04 |
| B11 | 3.9189e-03 |
| O16 | 4.6514e-02 |
| O17 | 1.7671e-05 |
| O18 | 9.3268e-05 |
| Si28 | 1.6926e-02 |
| Si29 | 8.5944e-04 |
| Si30 | 5.6654e-04 |

Source: 55

## Table 11 — Ag-In-Cd Control Rods

| Density (g/cc) | 10.16 |
|---|---|
| Isotope | Atom Density (atom/b-cm) |
| Ag107 | 2.3523e-02 |
| Ag109 | 2.1854e-02 |
| Cd106 | 3.3882e-05 |
| Cd108 | 2.4166e-05 |
| Cd110 | 3.3936e-04 |
| Cd111 | 3.4821e-04 |
| Cd112 | 6.5611e-04 |
| Cd113 | 3.3275e-04 |
| Cd114 | 7.8252e-04 |
| Cd116 | 2.0443e-04 |
| In113 | 3.4219e-04 |
| In115 | 7.6511e-03 |

Source: 56

## Table 12 — B4C Control Rods

| Density (g/cc) | 1.76 |
|---|---|
| Isotope | Atom Density (atom/b-cm) |
| B10 | 1.5206e-02 |
| B11 | 6.1514e-02 |
| C12 | 1.8972e-02 |
| C13 | 2.1252e-04 |

Source: 57

## Table 13 — Helium

| Density (g/cc) | 0.0015981 |
|---|---|
| **Isotope** | **Atom Density (atom/b-cm)** |
| He3 | 4.8089e-10 |
| He4 | 2.4044e-04 |

Source: 58

## Table 14 — Inconel 718

| Density (g/cc) | 8.2 |
|---|---|
| **Isotope** | **Atom Density (atom/b-cm)** |
| Cr50 | 7.8239e-04 |
| Cr52 | 1.5088e-02 |
| Cr53 | 1.7108e-03 |
| Cr54 | 4.2586e-04 |
| Fe54 | 1.4797e-03 |
| Fe56 | 2.3229e-02 |
| Fe57 | 5.3645e-04 |
| Fe58 | 7.1392e-05 |
| Mn55 | 7.8201e-04 |
| Ni58 | 2.9320e-02 |
| Ni60 | 1.1294e-02 |
| Ni61 | 4.9094e-04 |
| Ni62 | 1.5653e-03 |
| Ni64 | 3.9864e-04 |
| Si28 | 5.6757e-04 |
| Si29 | 2.8820e-05 |
| Si30 | 1.8998e-05 |

Source: 59

## Table 15 — Stainless Steel 304

| Density (g/cc) | 8.03 |
|---|---|
| Isotope | Atom Density (atom/b-cm) |
| Cr50 | 7.6778e-04 |
| Cr52 | 1.4806e-02 |
| Cr53 | 1.6789e-03 |
| Cr54 | 4.1791e-04 |
| Fe54 | 3.4620e-03 |
| Fe56 | 5.4345e-02 |
| Fe57 | 1.2551e-03 |
| Fe58 | 1.6703e-04 |
| Mn55 | 1.7604e-03 |
| Ni58 | 5.6089e-03 |
| Ni60 | 2.1605e-03 |
| Ni61 | 9.3917e-05 |
| Ni62 | 2.9945e-04 |
| Ni64 | 7.6261e-05 |
| Si28 | 9.5281e-04 |
| Si29 | 4.8381e-05 |
| Si30 | 3.1893e-05 |

Source: 60

## Table 16 — Zircaloy 4

| Density (g/cc) | 6.55 |
|---|---|
| **Isotope** | **Atom Density (atom/b-cm)** |
| Cr50 | 3.2962e-06 |
| Cr52 | 6.3564e-05 |
| Cr53 | 7.2076e-06 |
| Cr54 | 1.7941e-06 |
| Fe54 | 8.6698e-06 |
| Fe56 | 1.3610e-04 |
| Fe57 | 3.1431e-06 |
| Fe58 | 4.1829e-07 |
| O16 | 3.0744e-04 |
| O17 | 1.1680e-07 |
| O18 | 6.1648e-07 |
| Sn112 | 4.6735e-06 |
| Sn114 | 3.1799e-06 |
| Sn115 | 1.6381e-06 |
| Sn116 | 7.0055e-05 |
| Sn117 | 3.7003e-05 |
| Sn118 | 1.1669e-04 |
| Sn119 | 4.1387e-05 |
| Sn120 | 1.5697e-04 |
| Sn122 | 2.2308e-05 |
| Sn124 | 2.7897e-05 |
| Zr90 | 2.1828e-02 |
| Zr91 | 4.7601e-03 |
| Zr92 | 7.2759e-03 |
| Zr94 | 7.3734e-03 |
| Zr96 | 1.1879e-03 |

Source: 61

## Table 17 — Borated Water

| Density (g/cc) | 0.740582068 |
|---|---|
| Isotope | Atom Density (atom/b-cm) |
| B10 | 7.9714e-06 |
| B11 | 3.2247e-05 |
| H1 | 4.9456e-02 |
| H2 | 7.7035e-06 |
| O16 | 2.4673e-02 |
| O17 | 9.3734e-06 |
| O18 | 4.9474e-05 |

Source: 62

## Table 18 — Nozzle / Support Plate Borated Water

| Density (g/cc) | 0.981002532 |
|---|---|
| Isotope | Atom Density (atom/b-cm) |
| B10 | 1.0559e-05 |
| B11 | 4.2716e-05 |
| H1 | 6.5512e-02 |
| H2 | 1.0204e-05 |
| O16 | 3.2683e-02 |
| O17 | 1.2416e-05 |
| O18 | 6.5535e-05 |

Source: 63

## Table 19 — Nozzle / Support Plate Stainless Steel

| Density (g/cc) | 3.68384807 |
|---|---|
| **Isotope** | **Atom Density (atom/b-cm)** |
| Cr50 | 3.5223e-04 |
| Cr52 | 6.7924e-03 |
| Cr53 | 7.7020e-04 |
| Cr54 | 1.9172e-04 |
| Fe54 | 1.5882e-03 |
| Fe56 | 2.4931e-02 |
| Fe57 | 5.7578e-04 |
| Fe58 | 7.6625e-05 |
| Mn55 | 8.0762e-04 |
| Ni58 | 2.5731e-03 |
| Ni60 | 9.9117e-04 |
| Ni61 | 4.3085e-05 |
| Ni62 | 1.3738e-04 |
| Ni64 | 3.4985e-05 |
| Si28 | 4.3711e-04 |
| Si29 | 2.2195e-05 |
| Si30 | 1.4631e-05 |

Source: 64

## Table 20 — Carbon Steel

| Density (g/cc) | 7.8 | | |
|---|---|---|---|
| Isotope | Atom Density (atom/b-cm) | Isotope | Atom Density (atom/b-cm) |
| Al27 | 4.3523e-05 | B10 | 2.5833e-06 |
| B11 | 1.0450e-05 | C12 | 1.0442e-03 |
| C13 | 1.1697e-05 | Ca40 | 1.7043e-05 |
| Ca42 | 1.1375e-07 | Ca43 | 2.3734e-08 |
| Ca44 | 3.6673e-07 | Ca46 | 7.0322e-10 |
| Ca48 | 3.2875e-08 | Cr50 | 1.3738e-05 |
| Cr52 | 2.6493e-04 | Cr53 | 3.0041e-05 |
| Cr54 | 7.4778e-06 | Cu63 | 1.0223e-04 |
| Cu65 | 4.5608e-05 | Fe54 | 4.7437e-03 |
| Fe56 | 7.4465e-02 | Fe57 | 1.7197e-03 |
| Fe58 | 2.2886e-04 | Mn55 | 6.4126e-04 |
| Mo100 | 2.9814e-05 | Mo92 | 4.4822e-05 |
| Mo94 | 2.8110e-05 | Mo95 | 4.8567e-05 |
| Mo96 | 5.1015e-05 | Mo97 | 2.9319e-05 |
| Mo98 | 7.4327e-05 | Nb93 | 5.0559e-06 |
| Ni58 | 4.0862e-04 | Ni60 | 1.5740e-04 |
| Ni61 | 6.8420e-06 | Ni62 | 2.1815e-05 |
| Ni64 | 5.5557e-06 | P31 | 3.7913e-05 |
| S32 | 3.4808e-05 | S33 | 2.7420e-07 |
| S34 | 1.5368e-06 | S36 | 5.3398e-09 |
| Si28 | 6.1702e-04 | Si29 | 3.1330e-05 |
| Si30 | 2.0653e-05 | Ti46 | 1.2144e-06 |
| Ti47 | 1.0952e-06 | Ti48 | 1.0851e-05 |
| Ti49 | 7.9634e-07 | Ti50 | 7.6249e-07 |
| V50 | 1.1526e-07 | V51 | 4.5989e-05 |
| V51 | 4.5989e-05 | | |

Source: 65

# 3 Operating Data

## 3.1 Processing Measured In-Core Detector Data

In this reactor plant, there are 58 assemblies that contain in-core detectors. This layout of in-core detectors is shown in Figure 31. These detectors are typically U-235 fission chambers varying in mass of U-235. Although there are 58 locations, there are usually only a few detectors (6-10). When measurements are being taken, multiple *passes* are performed to adequately measure all 58 assemblies. Each detector will, however, pass through one common assembly. This becomes important in the normalization process of detector signals.

Before a measurement is taken, detectors are inserted into the core through instrumentation tubes in assemblies until the top of the assembly is hit. Detector measurements are then taken as the detectors are pulled back through the core at a constant speed. Thus, each measurement reported is an integral of the signal over the recording time. Also, axial locations of where data is recorded may be slightly skewed. In these measurements, 61 axial data points were collected and processed with a Python script.

### 3.1.1 Example – Hot Zero Power Measurements

This section will go through the process of filtering measured data for HZP. It should be noted that the algorithm developed to process HZP data was used for all detector data. Therefore, some of the detector maps may show errors in processing. Current work is underway to develop an algorithm that can be applied to all data. Under HZP conditions, the core power for these measurements is approximately 25 MWth. Raw data was processed by first organizing it in Python objects. Each collection of measurements contain detector information for multiple passes through the core in various assemblies. Raw data for HZP is shown in Figure 41. In order to show all detector signals on one plot, each raw data signal was normalized to a sum of unity.

The first step in this process is to remove any detector background signal. This information was supplied with the raw data and can be subtracted from each detector measurement pass. The corrected data for background is shown in Figure 42.

Depending on the strength of the signal being measured, the signal can be amplified by adjusting the gain on the detectors. Gain factors are also reported with the raw data. When processing, these gain factors are multiplied by the measured data. For HZP, all of the gain factors are unity. Figure 43 shows the measured data after gain factors are applied.

In some of the detector signals, zero points exist where the detector failed. These zero points are removed by performing a linear interpolation/extrapolation between/from the nearest two points. The corrected data is shown in Figure 44.

As explained above, there is one common assembly where all detectors will pass. This is needed

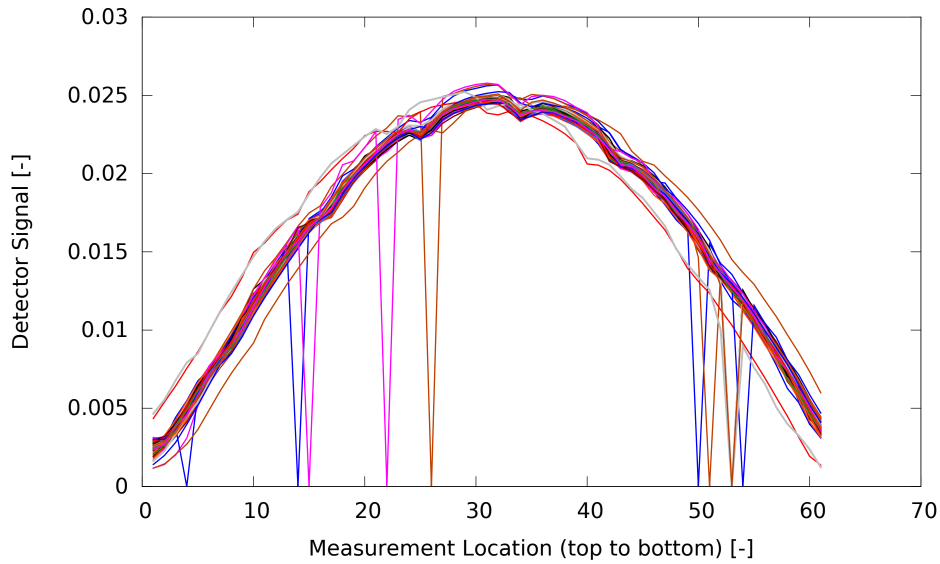


Figure 41: Initial Raw Detector Measurements (top to bottom).

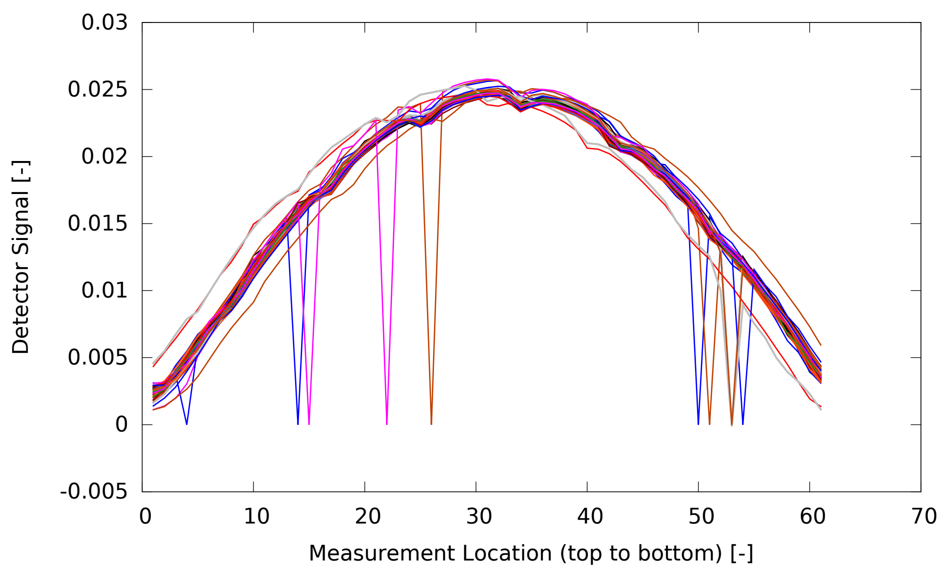


Figure 42: Detector Measurements Corrected for Background (top to bottom).

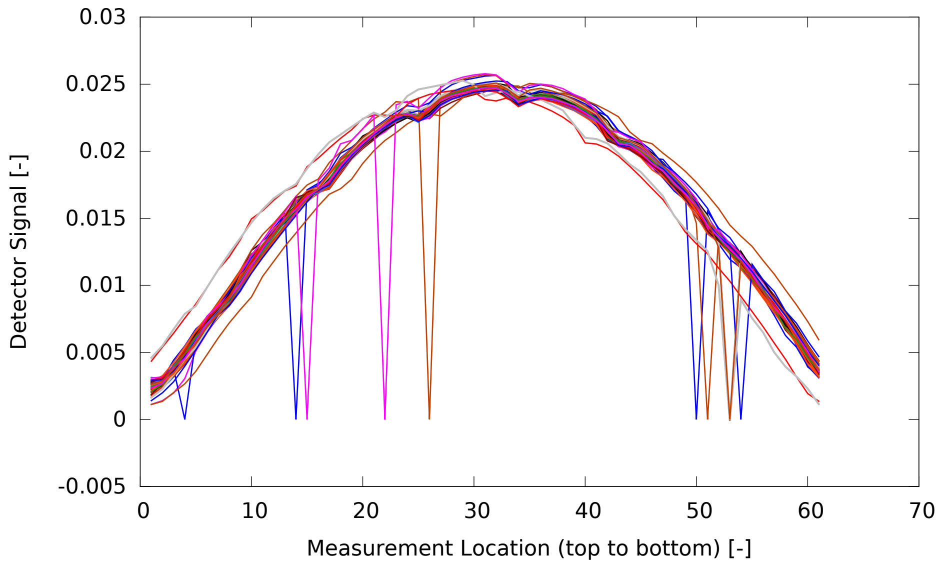


Figure 43: Detector Measurements Gain Factors Applied (top to bottom).

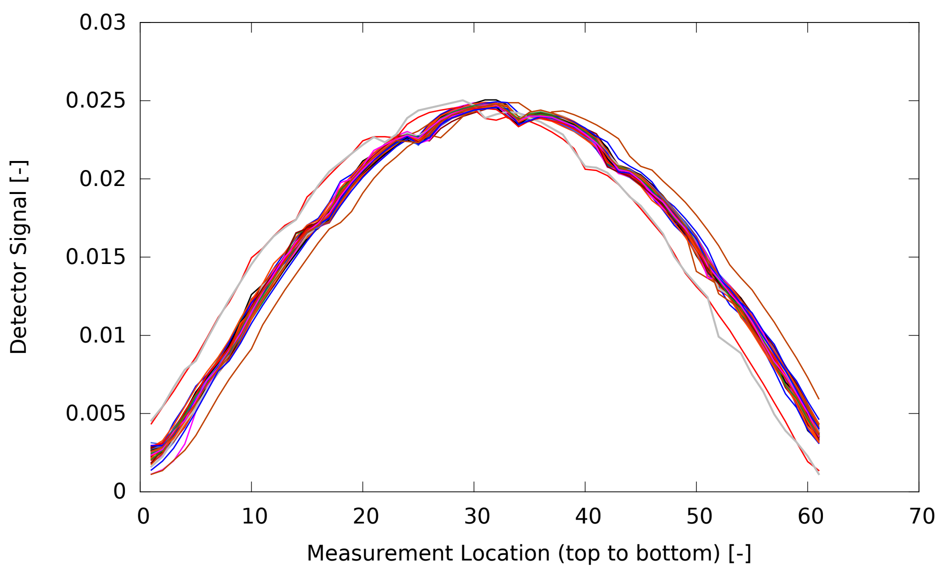


Figure 44: Detector Measurements with Zero Points Removed (top to bottom).

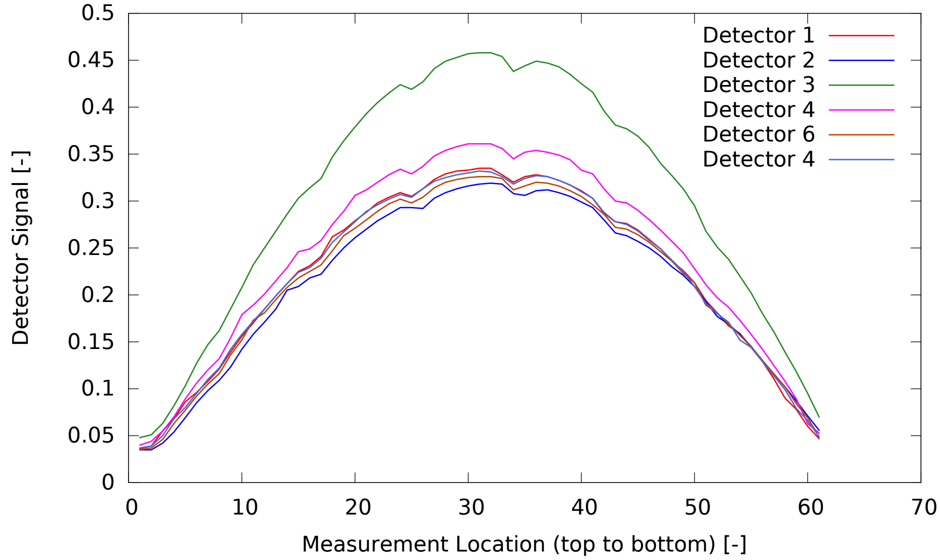


Figure 45: Detector Measurements with in J10 Assembly (top to bottom).

for normalization of detector signals. In this plant, assembly J10 was chosen as the common assembly. Figure 45 shows the measurements taken in assembly J10.

Each detector measurement represents a different measurement pass. The core power during one pass may not be the same as the others. There is typically a small fluctuation present in the core power. To account for this, each signal is divided by the core power reported during that measurement pass. The resulting detector signals are shown in Figure 46 for assembly J10.

The next step in the process is to make sure that all detector signals line up with one another. We can verify this by plotting all 58 detector signals on top of each other. This is the same as plot as Figure 46, except all assemblies are plotted here with signals normalized for shape comparison. This is shown in Figure 47. It is observed that not all of the signals are aligned with each other. Luckily, signals can be aligned to grid depressions. Here, we align to three grid depression positions, 25, 34, and 42, which are located in the centerline of grid 5, grid 4 and grid 3 respectively. The first step in this process is to find the measurement indexes corresponding to the local minimum in three regions, 22 to 28, 31 to 37, and 39 to 45 respectively. Then for each assembly, if the measurement indexes are inconsistent with correct indexes, a shifting length is estimated to make all the measurement indexes best match the correct indexes. All grids are then shifted either left or right. Depending on the shift direction, one end will lose a point and the other will gain one. The data point that is lost is just deleted from the data array, while the point that is gained is determined by a simple linear extrapolation from the nearest two points. The resulting realignment is shown in Figure 48. Results show that all detector signals are more consistently aligned, however still not perfect. The span of these signals can also be attributed to measurement uncertainty as the should all have the same shape once normalized here. There is one signal that is an outlier is observed between measurements 0 and 5. This assembly location corresponds to where control rod bank D is slightly inserted. Therefore, we should expect this depression in the signal toward the top of the core.

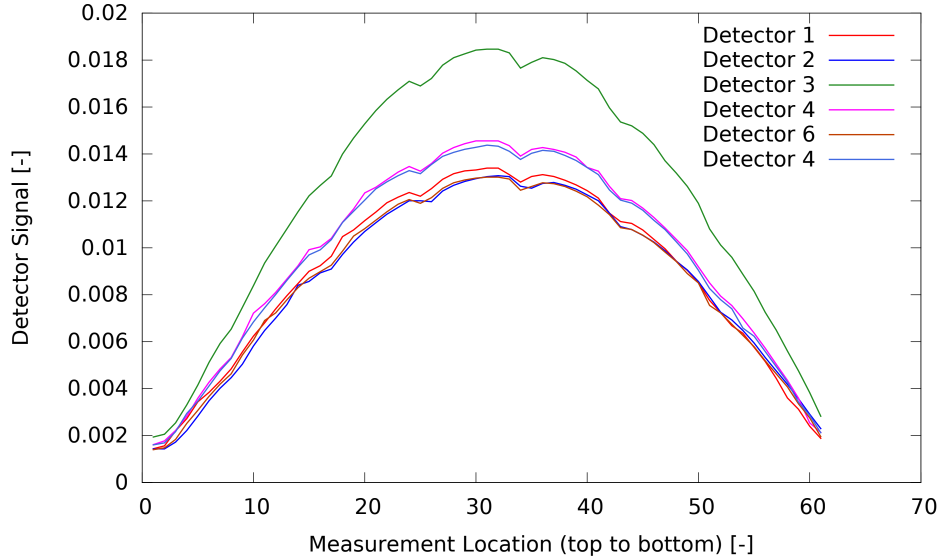


Figure 46: J10 Detector Measurements Divided by Core Power (top to bottom).

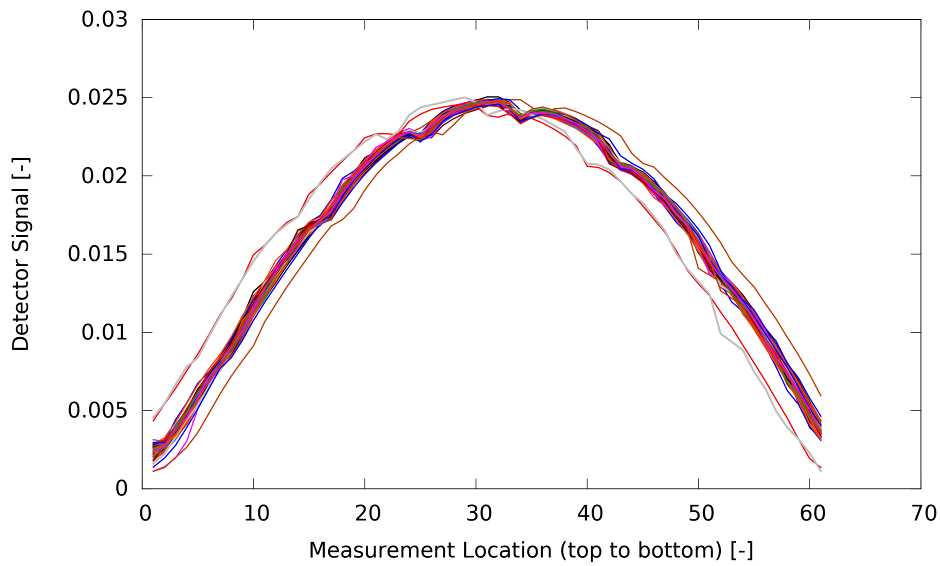


Figure 47: All Detector Signals Before Realignment.

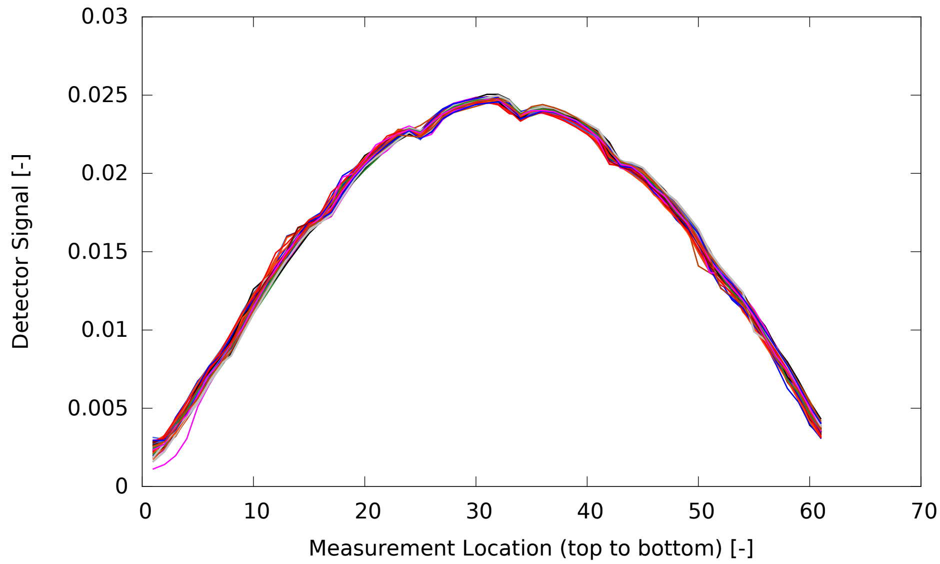


Figure 48: All Detector Signals After Realignment.

The next step in the process is to average detector signals that were measured from the same detector. It is important to look at the raw signals before performing this step since measurements may be poor. If this is observed, the poor measurement is commented out in the data file. In Figure 46 the two signals from detector 4 are close to each other and should be averaged. The resulting signals for assembly J10 are shown in Figure 49.

Each fission chamber detector contains a different amount of U-235. Therefore, some normalization process is needed to account for this mass difference. To get these normalization factors, the average of all detector signals is determined first. Then, normalization factors are computed by taking the ratio of the integral of each individual detector signal to the integral of the mean of all detector signals. For example, for HZP the normalization factors for each detector are:

- Detector 1: 0.922
- Detector 2: 0.901
- Detector 3: 1.272
- Detector 4: 1.002
- Detector 6: 0.903

These normalization factors are then multiplied to each corresponding detector signal in the core. The resulting signals are now very close to each other as shown in Figure 50 for assembly J10.

Lastly, detector signals need to be put on an axial coordinate grid corresponding to points that range from the bottom to top of active fuel. To do this we use the same grid point as before

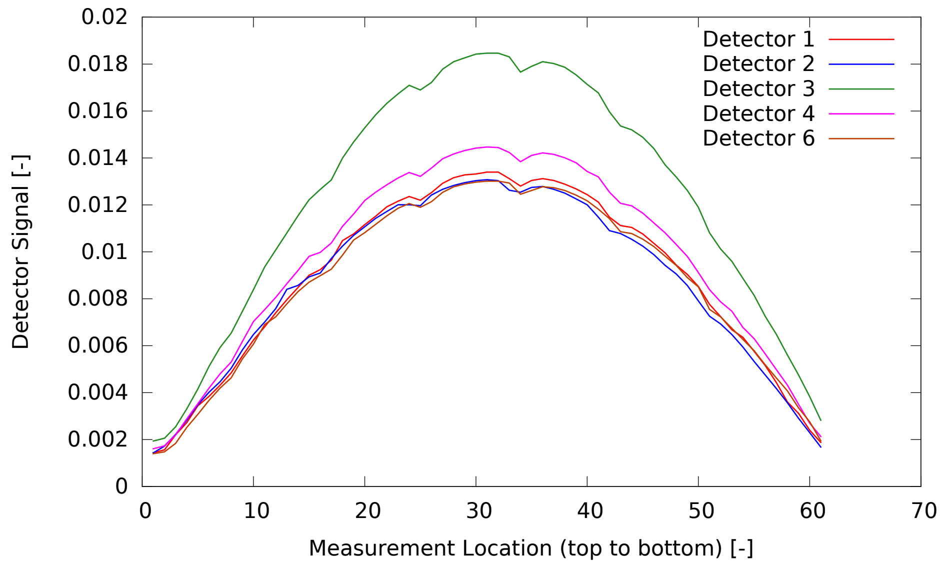


Figure 49: Multiple Detector Signals Averaged in J10 (top to bottom).

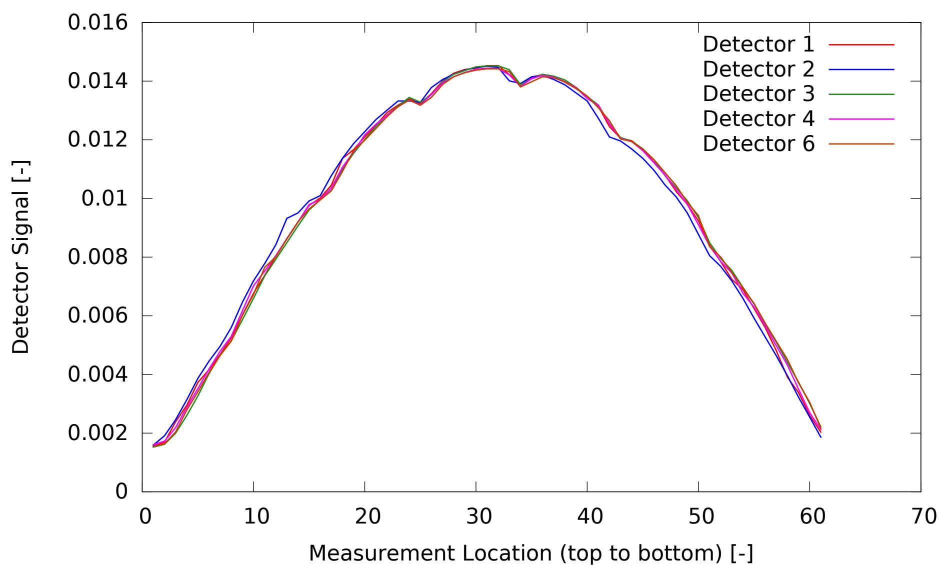


Figure 50: Application of Detector Normalization Factors for J10.

since we know that the centerline location of this grid is at 221.9 cm above bottom of active fuel. The distance between axial measurement locations is assumed uniform and is equal to active core height divided by 60 intervals. A 2nd order spline fit is then used to map from measured data axial locations to a axial map has equal data points exactly at the Top of Active Fuel (TAF) and Bottom of Active Fuel (BAF). A comparison of applying this spline is shown in Figure 51. The spline fit does well for this data, however grid depressions are now less since the

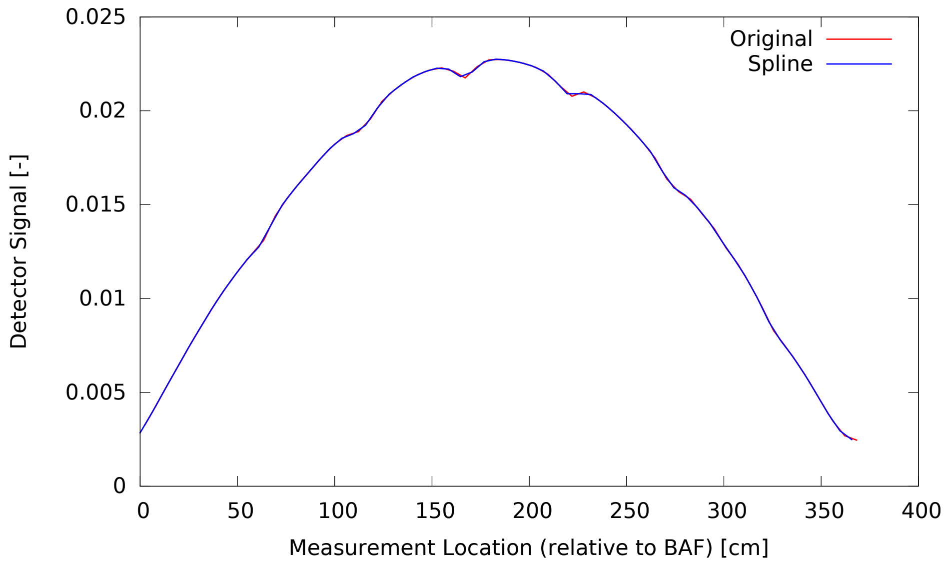


Figure 51: Comparision of Splined Data for Assembly J10.

grid centerline does not match up with the final axial grid. Before the spline, all detector signals were averaged such that there is only one signal per assembly. All splined signals are shown in Figure 52. There is some spread in the data when they are all normalized to one another. There is one detector signal that seems to not follow the same shape at the top of the core. That measurement corresponds to assembly D12 where control rod bank D is slightly inserted and thus there is a depression in the measurement signal. A separate Excel sheet contains all of the processed data organized by measurement data file and by assembly. A plot of the final measurements (not all normalized to sum of unity) is shown in Figure 53.

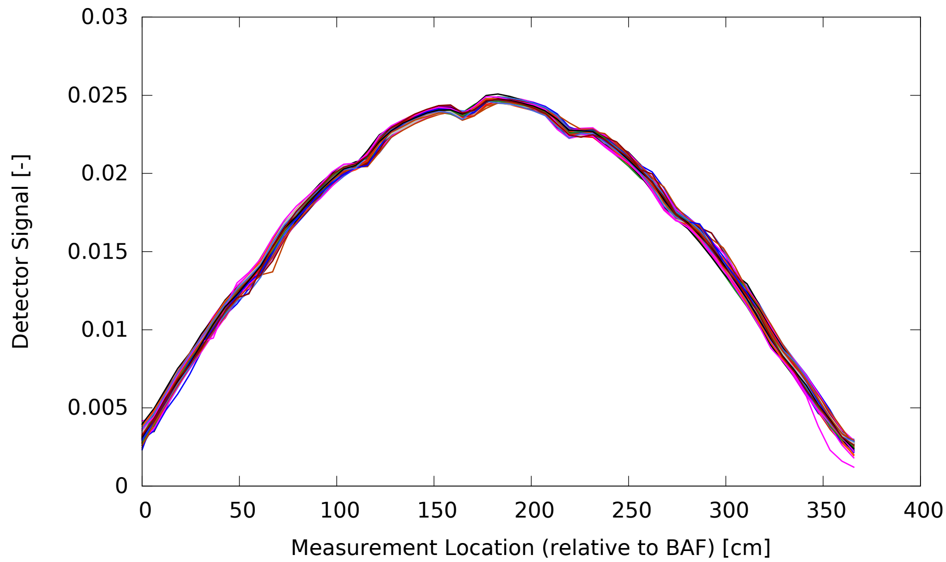


Figure 52: Comparison of All Assemblies after Spline.

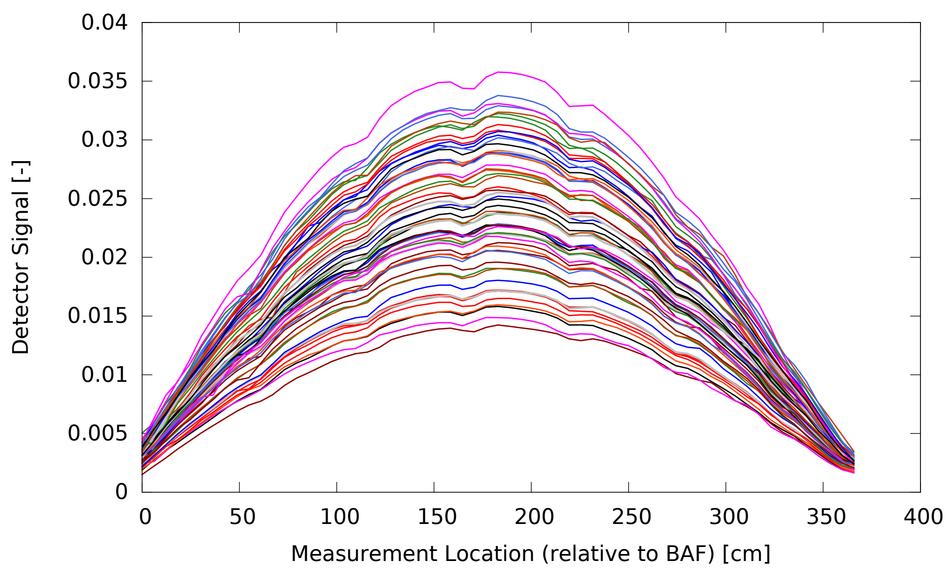


Figure 53: Final Processed HZP Measurement Data.

## 3.2 Hot Zero Power Data Discussion

Table 21 lists the thermal power of the reactor during initial physics testing the first available detector maps. Also included are the rod bank positions and critical boron concentration. This data can be used to evaluate how far off reactor models are from critical at HZP conditions.

Table 21: Cycle 1 hot zero power physics configuration.

| | |
|---|---|
| Core Power | 25 MWth |
| Core Flow Rate | $61.5 \times 10^6$ kg/hr |
| Inlet Coolant Temperature | 560° F |
| Rod Bank A Position | Step 228 |
| Rod Bank B Position | Step 228 |
| Rod Bank C Position | Step 228 |
| Rod Bank D Position | Step 213 |
| Boron Concentration | 975 ppm |

Radial maps were also created to view the average relative power produced per assembly. These were obtained by renormalizing the signals in Figure 53 such that their total sum is the number of detector locations (in this case 58). Each measurement in an assembly was then axially averaged to produce a relative radial peaking factor. In Figure 54, this factor is presented on each assembly where a measurement was taken.

Results show that measurement locations are consistent with the reported instrumentation diagram shown in Figure 31. Since the reactor is quarter-core symmetric (disregarding perturbations from instrument tubes), measurements can be compared. For example, assemblies H13, C8, H3 and N8 are located in symmetric positions. The measured values in these locations should be close. It is observed that the measurements are on the same order, but not all that close. This can happen at low powers and gives us an indication of measurement uncertainty.

Another way to look at the data is to collapse it to quarter core. We can compare rotational quarter core positions. If more than one radial power is available, the mean and standard deviation are reported. Otherwise, the result from Figure 54 is listed without a standard deviation. This is shown in Figure 55. In each assembly, three values are reported. From top to bottom they are: average of radial (axially averaged) signals, standard deviation of average and number of measurements that were averaged. The standard deviations give us some idea on the uncertainty in these measured values. They can range all the way up to 5.4%. A weighted average of the standard deviation was computed to get an idea of the overall measurement uncertainty. This was determined by multiplying each uncertainty by the number of radial powers and then dividing by 58. For HZP, this uncertainty is 3.7%. This is rather high since we really would like to see values below 1%. However, when the power is very low, power tilting can occur which contributes to this high uncertainty.

To compare simulation values to these measured data, axial edits of a tally such as U235 fission

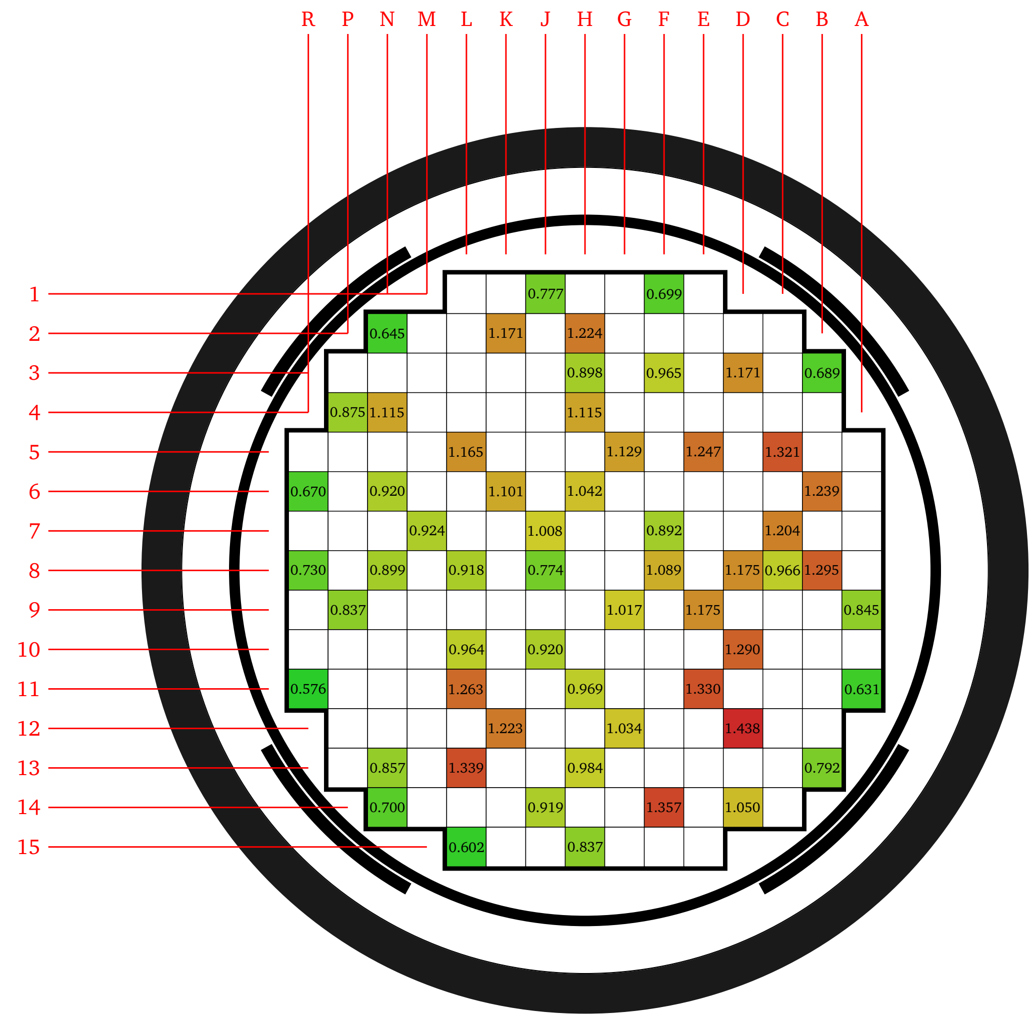


Figure 54: Radial detector measurements (axially integrated).

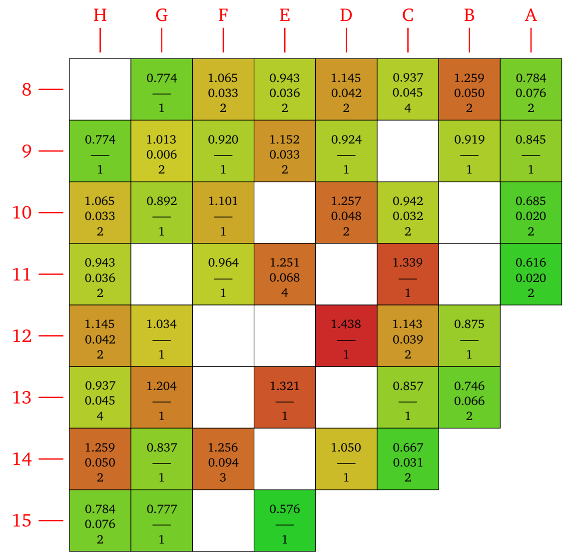


Figure 55: Quarter core (full core folded) radial measurements.

rate must be applied to each instrumented assembly in the core. To be fully consistent with the data a constant width 60 interval mesh (61 points) from bottom of active fuel to top of active fuel should be applied. All signals should be renormalized such that their average is 1.0 (or sum of all signals is 58).

Table 22 presents measured data for control rod bank worths and isothermal temperature coefficients for HZP conditions. Also provided are the critical boron concentrations for each configuration. Likewise, Table 23 presents the same data that is available for cycle 2. In contrast to cycle 1, control rod bank worths in cycle 2 were reported per individual bank.

Table 22: Cycle 1 hot zero power physics data, including critical boron concentrations, control rod bank worths for the full insertion sequence, and isothermal temperature coefficients.

| Crit. Boron Concentrations (ppm) | | Control Rod Bank Worths (pcm) | | Temp. Coeffs. (pcm/°F) | |
|---|---|---|---|---|---|
| All Rods Out (ARO) | 975 | | | ARO | -1.75 |
| D in | 902 | D in | 788 | D in | -2.75 |
| C, D in | 810 | C with D in | 1203 | C, D in | -8.01 |
| | | B with D, C in | 1171 | | |
| A, B, C, D in | 686 | A with D, C, B in | 548 | | |
| | | SE with D, C, B, A in | 461 | | |
| | | SD with D, C, B, A, SE in | 772 | | |
| A, B, C, D, SE, SD, SC in | 508 | SC with D, C, B, A, SE, SD in | 1099 | | |

Table 23: Cycle 2 hot zero power physics data, including critical boron concentrations, control rod bank worths for the full insertion sequence, and isothermal temperature coefficients.

| Crit. Boron Concentrations (ppm) | | Control Rod Bank Worths (pcm) | | Temp. Coeffs. (pcm/°F) | |
|---|---|---|---|---|---|
| ARO | 1405 | | | ARO | -1.71 |
| | | D | 426 | | |
| C in | 1273 | C | 1014 | | |
| | | B | 716 | | |
| | | A | 420 | | |
| | | SE | 438 | | |
| | | SD | 305 | | |
| | | SC | 307 | | |
| | | SB | 781 | | |
| | | SA | 326 | | |
| | | Total | 4733 | | |

## 3.3 Cycle 1 and 2 Available Data

### 3.3.1 Detector Measurement Maps

For Cycle 1 and 2 operation of this reactor, there are detector measurement maps available at various times during operation. For each measurement file, data is given for core power, inlet coolant temperature, core burnup, critical boron concentration and rod bank configuration. Although these are not described here, each measurement file has been processed according to the methodology described in Section 3.1. These are available online at the MIT-CRPG website.

***Important Note:*** Only the first few core power maps were extensively checked for proper treatments by the automated scripts that were developed to process the axial trace data as described in Section 3.1 (i.e. proper treatment of garbage data, wild shifts, etc.). Future releases will include more extensive verification of the remaining core maps.

### 3.3.2 Tilt Corrected Maps

The BEAVRS measured data presents a very large NW-SE (10%) tilt at HZP conditions that cannot be explained by detector measurements alone, since the core loading pattern is known to be symmetric. Simulations of such maps produce symmetric results, thus indicating a phenomenon that has not been accounted for. The leading hypothesis for this tilt is that it is created by a larger water gap in one corner of the core that stems from the core loading. As bundles are inserted and leaning against the baffle, uneven gaps could occur in opposite corners of the core. These gaps even out as the reactor heats up and fuel swells under irradiations. A script is introduced to fit a planar x-y tilt using the available detector data, and adjust the detector measurements so that the resulting radial map is eighth-core symmetric. Figure 56 illustrates a tilt-corrected radial map at HZP conditions that is eighth-core symmetric. Figures 57 and 58 plot the magnitude of the planar tilt over Cycle 1 and 2 respectively, and indeed as predicted, the tilt corrects itself as burnup increases.

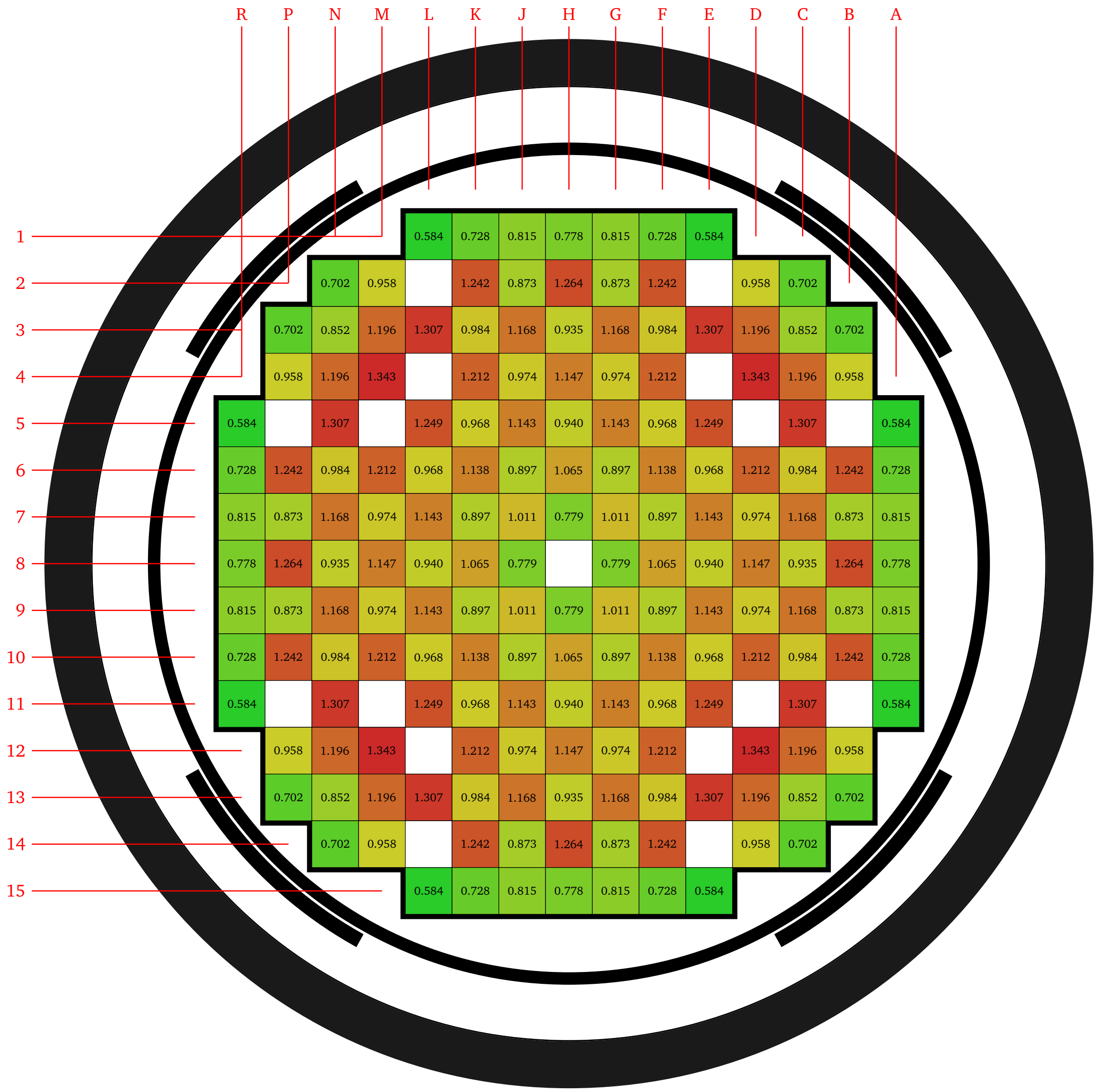


Figure 56: Radial detector measurements (tilt corrected).

For each burnup, tilt-corrected data at each assembly, as well as tilt-corrected radial maps are all available on the MIT-CRPG website. It must be noted that there is no definitive explanation for why this tilt in the data arises or the validity of the planar tilt correction, so this data should be utilized at the user's own discretion.

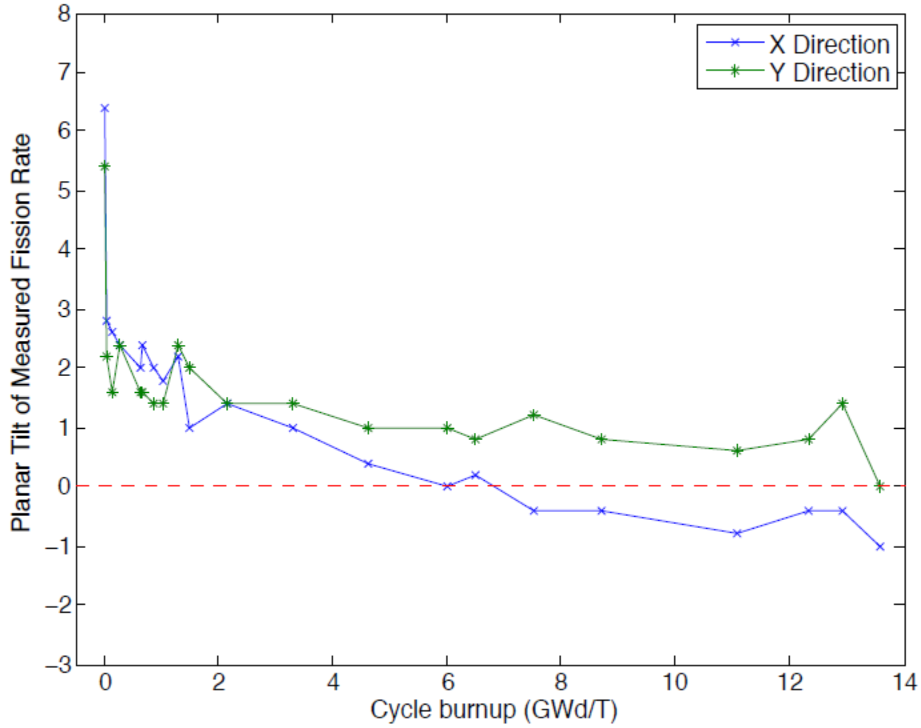


Figure 57: Planar tilt for cycle 1

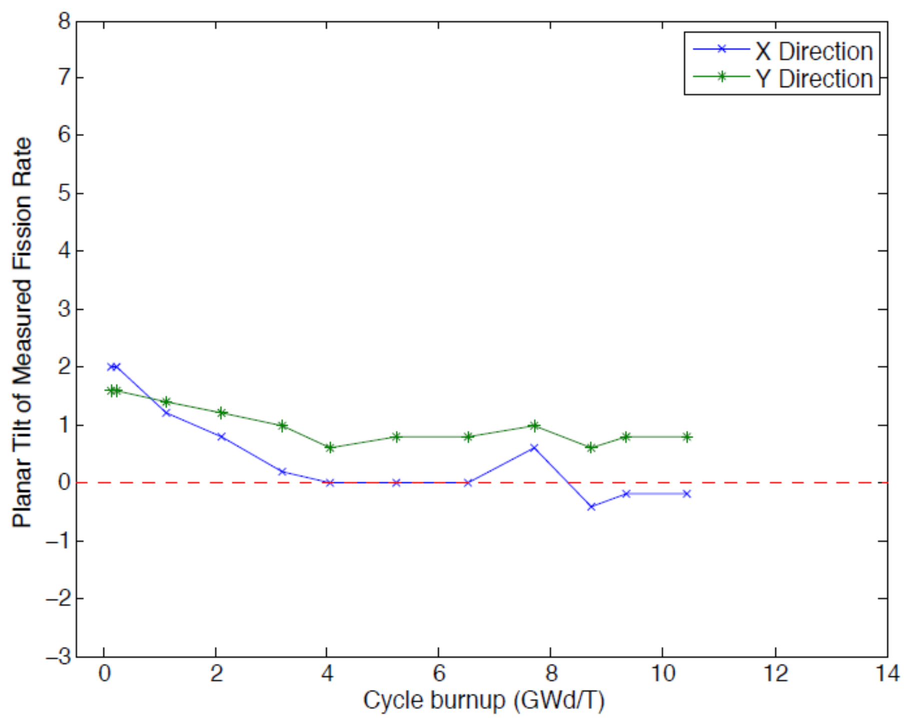


Figure 58: Planar tilt for cycle 2

### 3.3.3 Boron Letdown Curve

Also available is the boron letdown curve during Cycle 1 and Cycle 2 operation. Figure 59 and corresponding Table 24 presents the boron letdown data. Finally, the power history reference from Beginning of Cycle (BOC) for Cycle 1 operation is presented in Figure 60. Power history data is also available online at the MIT-CRPG website. In Figure 60, locations of where detector maps are available are also shown. Note, the powers shown in Figure 60 are 24-hr averages, whereas, in detector measurement files, powers reported are instantaneous at the time of measurement. In the plot they are shown to be coincident with the power history, however, in the files they may be slightly different. Similarly, Figure 61 shows the power history of Cycle 2.

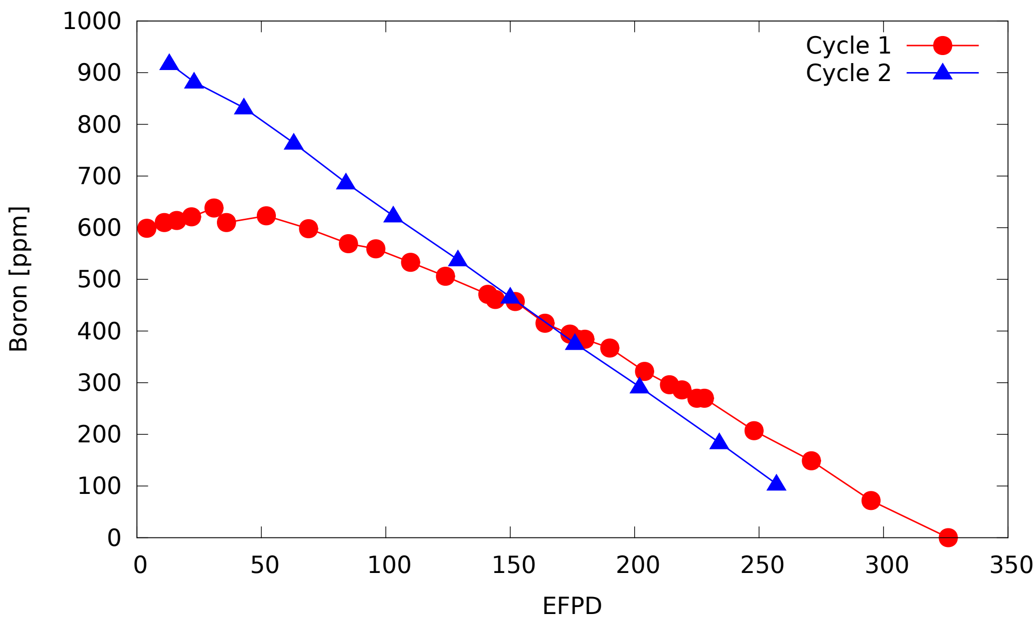


Figure 59: Measured boron letdown curves for two cycles of operation.

Table 24: Boron Letdown Curve Data for Cycles 1 and 2.

| Cycle 1 | | Cycle 2 | |
|---|---|---|---|
| EFPD | Boron [ppm] | EFPD | Boron [ppm] |
| 4 | 599 | 13 | 918 |
| 11 | 610 | 23 | 882 |
| 16 | 614 | 43 | 832 |
| 22 | 621 | 63 | 764 |
| 31 | 638 | 84 | 687 |
| 36 | 610 | 103 | 623 |
| 52 | 623 | 129 | 538 |
| 69 | 598 | 150 | 466 |
| 85 | 569 | 176 | 376 |
| 96 | 559 | 202 | 292 |
| 110 | 533 | 234 | 184 |
| 124 | 506 | 257 | 104 |
| 141 | 471 | | |
| 144 | 461 | | |
| 152 | 457 | | |
| 164 | 415 | | |
| 174 | 394 | | |
| 177 | 384 | | |
| 180 | 384 | | |
| 190 | 367 | | |
| 204 | 322 | | |
| 214 | 296 | | |
| 219 | 286 | | |
| 225 | 270 | | |
| 228 | 270 | | |
| 248 | 207 | | |
| 271 | 149 | | |
| 295 | 72 | | |
| 326 | 0 | | |

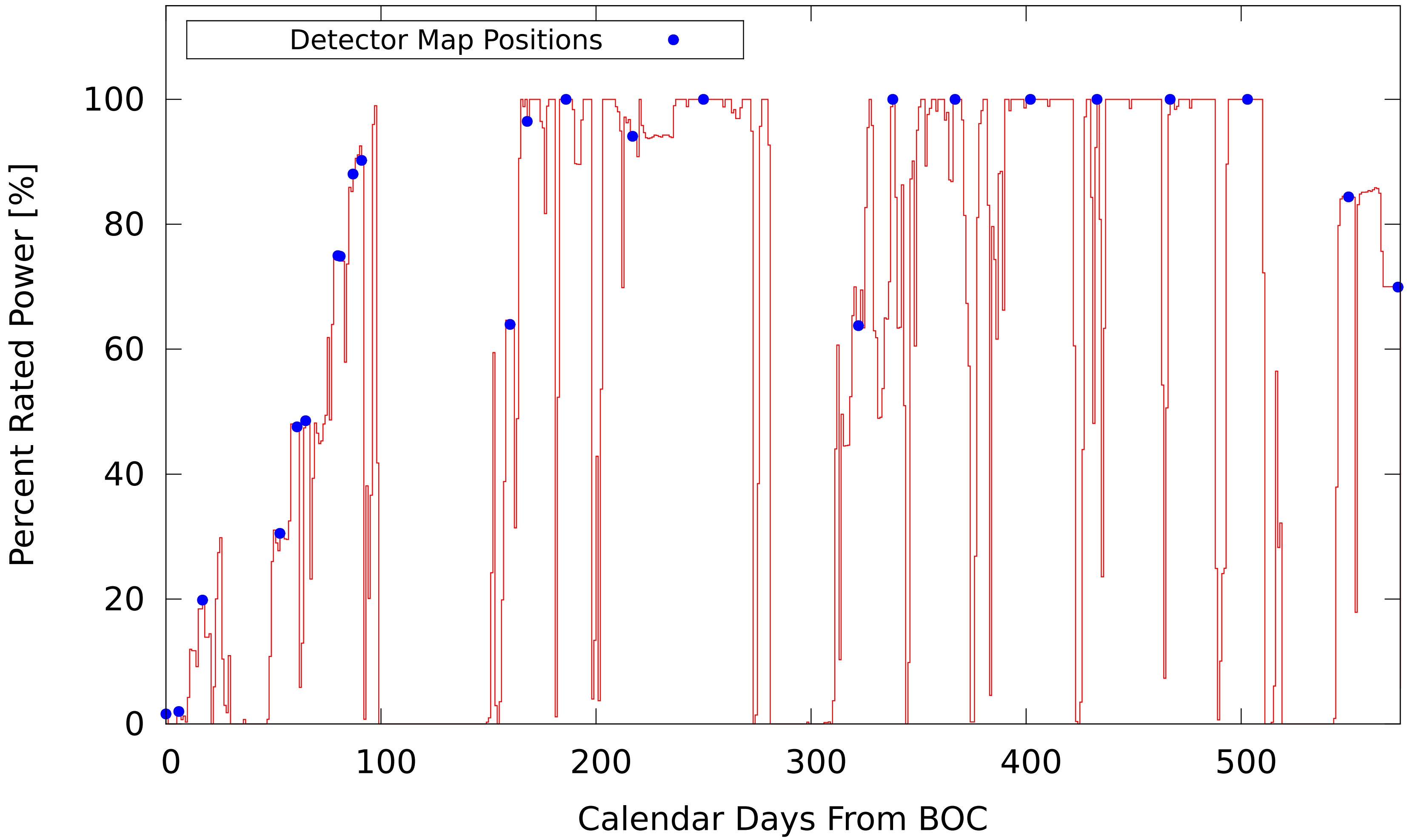


Figure 60: Power history of Cycle 1.

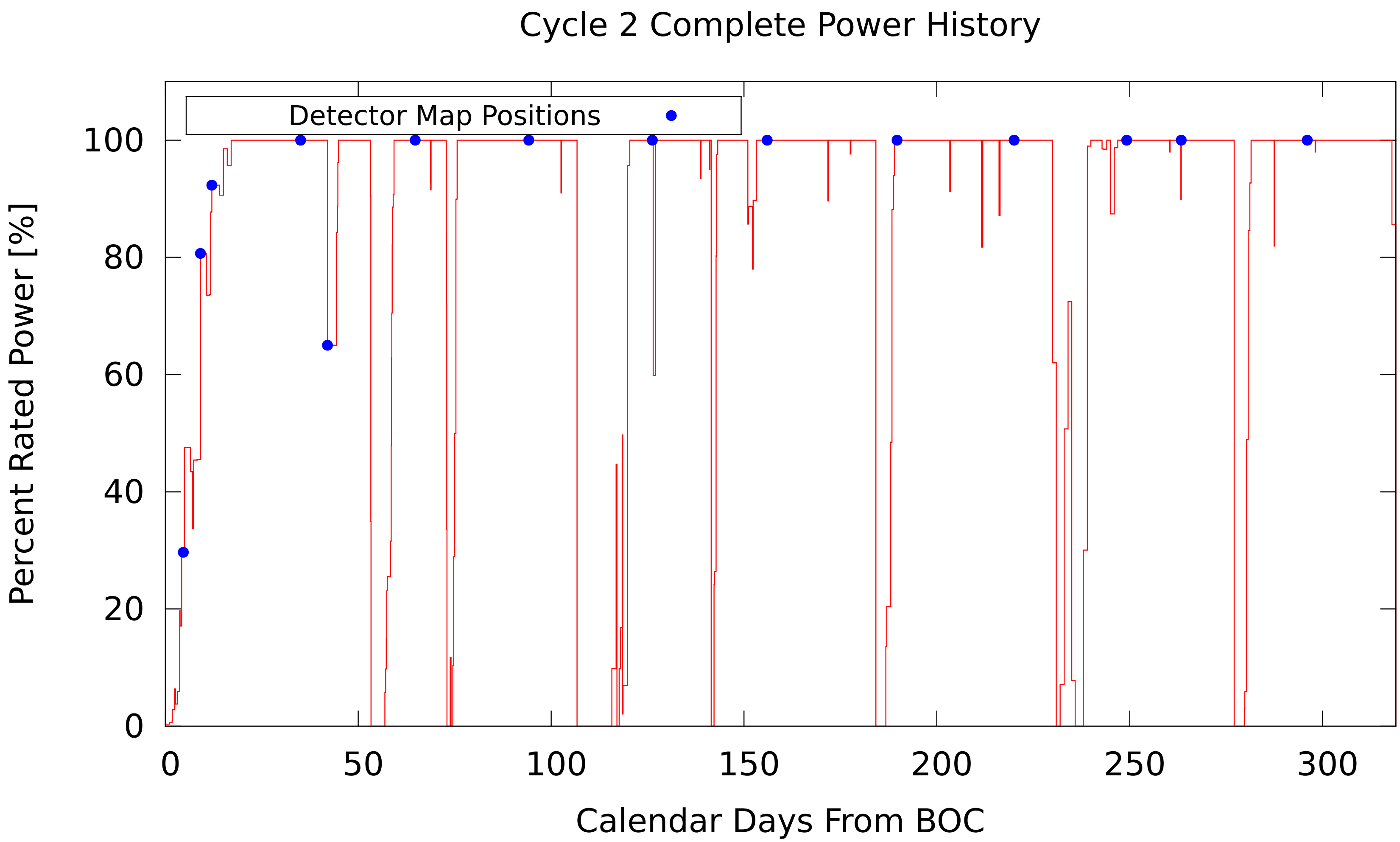


Figure 61: Power history of Cycle 2.

Table 25: Core operating data as a function of exposure

| Exporsure (EFPD) | Boron (ppm) | Inlet Temp. (F) | Bank D | % Power |
|---|---|---|---|---|
| .00 | 709 | 559.2 | 212 | 48.6 |
| 6.00 | 674 | 559.2 | 212 | 48.6 |
| 21.00 | 609 | 561.1 | 217 | 89.5 |
| 25.00 | 598 | 561.5 | 207 | 98.5 |
| 36.00 | 596 | 561.6 | 198 | 99.8 |
| 52.00 | 590 | 561.6 | 228 | 100.0 |
| 80.00 | 556 | 561.3 | 195 | 94.0 |
| 110.00 | 494 | 561.6 | 193 | 100.0 |
| 140.00 | 437 | 561.6 | 208 | 100.0 |
| 144.00 | 476 | 559.9 | 178 | 64.0 |
| 150.00 | 416 | 561.6 | 199 | 100.0 |
| 156.00 | 404 | 561.6 | 199 | 100.0 |
| 180.00 | 352 | 561.6 | 215 | 100.0 |
| 220.00 | 258 | 561.6 | 223 | 100.0 |
| 235.00 | 218 | 561.6 | 208 | 100.0 |
| 266.00 | 140 | 561.6 | 217 | 100.0 |
| 296.00 | 58 | 561.6 | 215 | 100.0 |
| 310.00 | 49 | 560.9 | 216 | 84.5 |
| 326.00 | 31 | 560.2 | 208 | 70.0 |
| 327.00 | 29 | 560.2 | 208 | 70.0 |

Additional data collected, listed in Table 25 shows how inlet temperature, critical boron concentration, bank D rod position and percent of full power as a function of exposure for cycle 1.

# References


[1] N. Horelik, B. Herman, B. Forget, and K. Smith. Benchmark for Evaluation and Validation of Reactor Simulations (BEAVRS), v1.0.1. *Proc. Int. Conf. Mathematics and Computational Methods Applied to Nuc. Sci. & Eng.*, 2013. Sun Valley, Idaho.

[2] K.S. Smith. Assembly homogenization techniques for light water reactor analysis. *Progress in Nuclear Energy*, 17(3):303 – 335, 1986.

[3] J. E. Hoogenboom and W. R. Martin. A Proposal for a Benchmark to Monitor the Performance of Detailed Monte Carlo Calculation of Power Densities in a Full Size Reactor Core. *Proc. Int. Conf. Mathematics, Computational Methods, and Reactor Physics*, 2009. Saratoga Springs, New York.

[4] D. Kelly, T. Sutton, T. Trumbull, and P. Dobreff. MC21 Monte Carlo Analysis of the Hoogenboom-Martin Full-Core PWR Benchmark Problem. *Proc. PHYSOR 2010, Adv. in Reac. Phys. to Power the Nuc. Renaissance, Pittsburgh, Pennsylvania, USA, May 9-14, on CD-ROM(2010)*, May 2010.

[5] D. Kelly, T. Sutton, and S. Wilson. MC21 Analysis of the Nuclear Energy Agency Monte Carlo Performance Benchmark Problem. *Proc. PHYSOR 2012, Adv. in Reac. Phys., Knoxville, Tennessee, USA April 15-20, on CD-ROM(2010)*, April 2012.

[6] K. Smith. Reactor Core Methods, 2003. Invited lecture at the M&C2003 International Conference, April 6-10, 2003, Gatlinburg, TN, USA (http://wwwtest.iri.tudelft.nl/j̃hoogenb).

[7] J. J. Jarrell, A. T. Godfrey, T. M. Evans, and G. G. Davidson. Full Core Reactor Analysis: Running Denovo on Jaguar. *Proc. PHYSOR 2012, Adv. in Reac. Phys., Knoxville, Tennessee, USA April 15-20, on CD-ROM(2010)*, April 2012.

[8] USDOE. Consortium for Advanced Simulation of Light Water Reactors (CASL), 2012. http://www.casl.gov/goals.shtml.

[9] USDOE. About CESAR | Center for Exascale Simulation of Advanced Reactors, 2012. http://cesar.mcs.anl.gov/content/about-cesar.

[10] OECD/NEA. International Reactor Physics Benchmark Experiments (IRPhE), May 2012. ISBN 978-92-64-99168-2.

[11] K.S. Smith, S. Tarves, T. Bahadir, and R. Ferrer. Benchmarks for Quantifying Fuel Reactivity Depletion Uncertainty. Technical Report 1022909, Electric Power Research Institute, 2011.

[12] Benchmark on Deterministic Transport Calculations Without Spatial Homogenisation. Technical Report NEA/NSC/DOC(2005)16, NEA No. 5420, 2005. ISBN 92-64-01069-6.

[13] S. Douglass, F. Rahnema, and J. Margulies. A stylized three dimensional PWR whole-core benchmark problem with Gadolinium. *Annals of Nuclear Energy*, 37(10):1384 – 1403, 2010.

[14] K. Smith. Personal communication on control rod sequence, May 2012.

[15] Civilian Radioactive Waste Management System Management & Operating Contractor. Summary Report of Commercial Reactor Criticality Data for Catawba Unit 1. Technical Report ML033530020, US Department of Energy, 1998.

[16] PWR Utility. Specifications and Measured Data from PWR Plant. 2012.

[17] Global Data. Power eTrack, Catawba 1 Nuclear Power Plant, 2013. http://www.poweretrack.com.libproxy.mit.edu/.

[18] Engineer at Utility. Additional PWR Plant Specifications, October 2012.

[19] K. J. Geelhood, W. G. Luscher, and C. E. Beyer. FRAPCON-3.4: Integral Assessment. Technical Report NUREG/CR-7022, Vol. 2; PNNL-19418, Vol. 2, Pacific Northwest National Laboratory; USNRC, March 2011. http://frapcon.labworks.org/.

[20] Tennessee Valley Authority. Watts Bar, Unit 2 - Amendment 98 to Final Safety Analysis Report, Section 4, Reactor. Technical Report ML101370397, USNRC, May 2010.

[21] PWR Utility. Data Measurements from PWR Plant for Cycles 1 and 2. 2012.

[22] Engineering Toolbox. Air Properties. Electronic, January 2013. http://www.engineeringtoolbox.com/air-properties-d_156.html.

[23] Studsvik Scandpower. *CASMO-4: A Fuel Assembly Burnup Program*, University edition, 2009.

[24] National Institute of Standards and Technology. Isothermal Properties for Helium. Electronic, January 2013.

[25] AK Steel. *304/304L Stainless Steel Product Data Sheet*, January 2013. UNS S30400.

[26] National Institute of Standards and Technology. Isothermal Properties for Water. Electronic, January 2013.

[27] American Society for Testing and Materials. *Standard Specification for Quenched and Tempered Vacuum-Treated Carbon and Alloy Steel Forgings for Pressure Vessels – A508* , June 2014.

[28] E. M. Baum, M. C. Ernesti, H. D. Knox, T. R. Miller, and A. M. Watson. *Nuclides and Isotopes*. Chart of the Nuclides. Knolls Atomic Power Laboratory, 17 edition, 2009.

[29] Juris Meija, Tyler B Coplen, Michael Berglund, Willi A Brand, Paul De Bièvre, Manfred Gröning, Norman E Holden, Johanna Irrgeher, Robert D Loss, Thomas Walczyk, et al. Isotopic compositions of the elements 2013 (iupac technical report). *Pure and Applied Chemistry*, 88(3):293–306, 2016.

## Source Details

### Source 1 — Core Arrangement of Fuel Assemblies

This information is reported on the Core Arrangement worksheet.

**References**

[16]

**Pages**

3, 27, 29, 31

## Source 2 — Cycle 2 Shuffling Pattern

This information is reported on the C2 Core Shuffle worksheet.

**References**

[16]

**Pages**

29

## Source 3 — Fuel Assembly Loading

This information is reported on the Assembly Loading worksheet.

**References**

[16]

**Pages**

3

## Source 4 — Fuel Lattice Specifications

This information is reported on the Fuel Lattice worksheet provided by the utility.

**References**

[16]

**Pages**

3, 13

## Source 5 — Active Core Height

This information is reported on the Fuel Lattice worksheet (Source 4). The active fuel length is

$$L_f = 144\,\text{in} \cdot 2.54\frac{\text{cm}}{\text{in}} = 365.76\,\text{cm}$$

**References**

[16]

**Value**

365.76

**Units**

cm

**Pages**

3, 34

## Source 6 — Nominal Core Power

Nominal Core Power is taken to be that for Catawba, which is available online from Power etrack.

**References**

[17]

**Value**

3411

**Units**

MWth

**Pages**

3

## Source 7 — Core Mass Flow Rate

From an email communication with the utility, the total pump flow rate is $61.5 \times 10^6$ kg/hr. Normally, about 5% of the flow goes into the bypass region, so 95% of flow is through the core area, and the flow in the guide tubes is very low. It is assumed that this has no impact on active cooling flow. It is common to take 5% for the flow fraction through the bypass region although it is not known precisely.

**References**

[18]

**Value**

$61.5 \times 10^6$

**Units**

kg/hr

**Pages**

3

## Source 8 — Fuel Pellet Radius

This information is reported on the Fuel Lattice worksheet (Source 4). The fuel pellet radius is calculated in the spreadsheet with the following forumla:

$$R_f = \frac{0.3088\,\text{in}}{2} \cdot 2.54\frac{\text{cm}}{\text{in}} = 0.39218\,\text{cm}$$

It can be inferred that the diameter of the fuel pellet that this radius was derived as was 0.3088 in.

**References**

[16]

**Value**

0.39218

**Units**

cm

**Pages**

5, 23, 24

## Source 9 — Fuel Cladding Inner Radius

This information is reported on the Fuel Lattice worksheet (Source 4). The fuel rod inner radius is calculated in the spreadsheet with the following forumla:

$$R_{IR} = \frac{0.36\,\text{in} - 0.0225\,\text{in} \cdot 2}{2} \cdot 2.54\frac{\text{cm}}{\text{in}} = 0.40005\,\text{cm}$$

It can be inferred that the cladding thickness is 0.0225 in.

**References**

[16]

**Value**

0.40005

**Units**

cm

**Pages**

5, 6, 23, 24

## Source 10 — Fuel Cladding Outer Radius

This information is reported on the Fuel Lattice worksheet (Source 4). The fuel rod outer radius given is calculated in the spreadsheet with the following forumla:

$$R_{OR} = \frac{0.36\,\text{in}}{2} \cdot 2.54\frac{\text{cm}}{\text{in}} = 0.45720\,\text{cm}$$

It can be inferred that the diameter of the fuel rod is 0.36 in.

**References**

[16]

**Value**

0.45720

**Units**

cm

**Pages**

5, 6, 23, 24

## Source 11 — Plenum Spring Radius

The radius for the mass of Inconel approximating the plenum spring is chosen to be the equivalent radius for the volume of an approximate helical spring. The spring wire diameter $d_{spgw}$ and number of turns $v_s$ for the helical spring are taken from the FRAPCON-3 Integral Assessment Document in the appendix regarding the Westinghouse BR-3 fuel rods, which are assumed to be similar to the fuel rods in this plant. The helix diameter $d_{spg}$ was chosen such that the ratio of the outer fuel rod cladding diameter $d_{co}$ to the helix diameter was the same.

$$\begin{aligned} v_s &= 8\,\text{turns} \\ d_{co,BR-3} &= 0.422\,\text{in} \\ d_{spg,BR-3} &= 0.37\,\text{in} \end{aligned}$$

$$d_{spg} = d_{co}\frac{d_{spg,BR-3}}{d_{co,BR-3}} = 0.3156\,\text{in}$$

From here volume of the helical spring is calculated as

$$\begin{aligned} V_{spring} &= v_s\pi\left(\frac{d_{spgw}}{2}\right)^2\pi\left(d_{dspg} - d_{spgw}\right) \\ V_{spring} &= 8\pi\left(\frac{0.055\,\text{in}}{2}\right)^2\pi(0.3156\,\text{in} - 0.055\,\text{in}) \\ V_{spring} &= 0.01556\,\text{in}^3 \end{aligned}$$

Finally, the equivalent radius $r_e$ is found with the plenum height $h_{pl} = 7.66\,\text{in}$ as

$$\begin{aligned} r_e &= \sqrt{\frac{V_{spring}}{\pi h_{pl}}} \\ r_e &= \sqrt{\frac{0.01556\,\text{in}^3}{\pi 7.66\,\text{in}}} \\ r_e &= 0.02543\,\text{in} \\ r_e &= 0.06459\,\text{cm} \end{aligned}$$

**References**

[19]

**Value**

0.06459

**Units**

cm

**Pages**

6

## Source 12 — RCCA Plenum Spring Radius

The plenum spring radius used in the control rod plenum was assumed to be the same as radius used for fuel pins. This makes no attempt to conform to the true volume of inconel in this region.

**Value**

0.06459

**Units**

cm

**Pages**

12

## Source 13 — Guide Tube Inner Radius

This information is reported on the Fuel Lattice worksheet (Source 4). The guide tube inner radius is calculated in the spreadsheet with the following forumla:

$$R_{IR} = \frac{0.442\,\text{in}}{2} \cdot 2.54\frac{\text{cm}}{\text{in}} = 0.56134\,\text{cm}$$

It can be inferred that the inner diameter of the guide tube is 0.442 in. Note that this dimension is also used for instrumentation tubes.

**References**

[16]

**Value**

0.56134

**Units**

cm

**Pages**

6, 7, 9, 11, 12

## Source 14 — Guide Tube Outer Radius

This information is reported on the Fuel Lattice worksheet (Source 4). The guide tube outer radius is calculated in the spreadsheet with the following forumla:

$$R_{OR} = \frac{0.474\,\text{in}}{2} \cdot 2.54\frac{\text{cm}}{\text{in}} = 0.60198\,\text{cm}$$

It can be inferred that the outer diameter of the guide tube is 0.474 in. Note that this dimension is also used for instrumentation tubes.

**References**

[16]

**Value**

0.60198

**Units**

cm

**Pages**

6, 7, 9, 11, 12

## Source 15 — Guide Tube Inner Radius at Dashpot

This information is reported on the Fuel Lattice worksheet (Source 4). The guide tube inner radius is calculated in the spreadsheet with the following forumla:

$$R_{IR} = \frac{0.397\,\text{in}}{2} \cdot 2.54\frac{\text{cm}}{\text{in}} = 0.50419\,\text{cm}$$

It can be inferred that the inner diameter of the guide tube is 0.397 in.

**References**

[16]

**Value**

0.50419

**Units**

cm

**Pages**

7, 10

## Source 16 — Guide Tube Outer Radius at Dashpot

This information is reported on the Fuel Lattice worksheet (Source 4). The guide tube outer radius is calculated in the spreadsheet with the following forumla:

$$R_{IR} = \frac{0.43\,\text{in}}{2} \cdot 2.54\frac{\text{cm}}{\text{in}} = 0.54610\,\text{cm}$$

It can be inferred that the outer diameter of the guide tube at dashpot is 0.43 in.

**References**

[16]

**Value**

0.54610

**Units**

cm

**Pages**

7, 10

## Source 17 — Instrumentation Tube Thimble Inner Radius

The instrumentation tube thimble inner radius was not reported in the spreadsheet. It is assumed that this dimension is the same as the burnable poison outer cladding inner radius (Source 23).

**References**

[16]

**Value**

0.43688

**Units**

cm

**Pages**

7, 8

## Source 18 — Instrumentation Tube Thimble Outer Radius

The instrumentation tube thimble outer radius is not reported in the spreadsheet. It is assumed that this dimension is the same as the burnable poison outer cladding inner radius (Source 24).

**References**

[16]

**Value**

0.48387

**Units**

cm

**Pages**

7, 8

## Source 19 — Inner Cladding Inner Radius of BP Pin

The dimensions of the Burnable Poison (BP) inner cladding inner radius is reported in the Fuel Lattice worksheet (Source 4). This number was calculated with the following formula:

$$R_{ICIR} = 0.08425\,\text{in} \cdot 2.54\frac{\text{cm}}{\text{in}} = 0.21400\,\text{cm}$$

**References**

[16]

**Value**

0.21400

**Units**

cm

**Pages**

9, 10

## Source 20 — Inner Cladding Outer Radius of BP Pin

The dimensions of BP the inner cladding outer radius is reported in the Fuel Lattice worksheet (Source 4). This number was calculated with the following formula:

$$R_{ICOR} = 0.1905\,\text{in} \cdot 2.54\frac{\text{cm}}{\text{in}} = 0.23051\,\text{cm}$$

**References**

[16]

**Value**

0.23051

**Units**

cm

**Pages**

9, 10

## Source 21 — Inner Radius of Poison of BP Pin

The dimensions of the poison inner radius is reported in the Fuel Lattice worksheet (Source 4). This number was calculated with the following formula:

$$R_{PIR} = 0.095\,\text{in} \cdot 2.54\frac{\text{cm}}{\text{in}} = 0.24130\,\text{cm}$$

**References**

[16]

**Value**

0.24130

**Units**

cm

**Pages**

9

## Source 22 — Outer Radius of Poison of BP Pin

The dimensions of the poison outer radius is reported in the Fuel Lattice worksheet (Source 4). This number was calculated with the following formula:

$$R_{POR} = 0.168\,\text{in} \cdot 2.54\frac{\text{cm}}{\text{in}} = 0.42672\,\text{cm}$$

**References**

[16]

**Value**

0.42672

**Units**

cm

**Pages**

9

## Source 23 — Outer Cladding Inner Radius of BP Pin

The dimensions of the BP outer cladding inner radius is reported in the Fuel Lattice worksheet (Source 4). This number was calculated with the following formula:

$$R_{OCIR} = 0.172\,\text{in} \cdot 2.54\frac{\text{cm}}{\text{in}} = 0.43688\,\text{cm}$$

**References**

[16]

**Value**

0.43688

**Units**

cm

**Pages**

9, 10, 93

## Source 24 — Outer Cladding Outer Radius of BP Pin

The dimensions of the BP outer cladding outer radius is reported in the Fuel Lattice worksheet (Source 4). This number was calculated with the following formula:

$$R_{OCOR} = 0.09075\,\text{in} \cdot 2.54\frac{\text{cm}}{\text{in}} = 0.48387\,\text{cm}$$

**References**

[16]

**Value**

0.48387

**Units**

cm

**Pages**

9, 10, 94

## Source 25 — Control Rod Thimble Inner Radius

The control rod thimble inner radius was taken from page 15 of [15].

**References**

[15]

**Value**

0.38608

**Units**

cm

**Pages**

11, 12

## Source 26 — Control Rod Thimble Outer Radius

The control rod thimble outer radius was taken from page 15 of [15].

**References**

[15]

**Value**

0.48387

**Units**

cm

**Pages**

11, 12

## Source 27 — Control Rod AIC Outer Radius

The control rod outer radius for the lower absorber region was taken from page 15 of [15].

**References**

[15]

**Value**

0.38227

**Units**

cm

**Pages**

11

## Source 28 — Control Rod B4C Outer Radius

The control rod outer radius for the upper absorber region was taken from page 15 of [15].

**References**

[15]

**Value**

0.37338

**Units**

cm

**Pages**

11

## Source 29 — Control Rod Spacer Outer Radius

The control rod outer radius for the spacer region was taken from page 15 of [15].

**References**

[15]

**Value**

0.37845

**Units**

cm

**Pages**

12

## Source 30 — Fuel Assembly Pitch

The fuel assembly pitch is taken from the Fuel Lattice worksheet (Source 4). The formula for calculating this parameter is

$$S_a = 8.466\,\text{in} \cdot 2.54\frac{\text{cm}}{\text{in}} = 21.50364\,\text{cm}$$

**References**

[16]

**Value**

21.50364

**Units**

cm

**Pages**

13, 24

## Source 31 — Fuel Pin Pitch

The fuel pin pitch is taken from the Fuel Lattice worksheet (Source 4). The formula for calculating this parameter is

$$S_p = 0.496\,\text{in} \cdot 2.54\frac{\text{cm}}{\text{in}} = 1.25984\,\text{cm}$$

**References**

[16]

**Value**

1.25984

**Units**

cm

**Pages**

13

## Source 32 — Inconel Grid Weight

Taken from email correspondence with an engineer at the utility. The weight of Inconel-718 for one end grid spacer is 332 lbs. The following formula is used to calculate the weight of Inconel per top/bottom grid:

$$W_{in} = 332\,\text{lb} \cdot 453.59237\frac{\text{g}}{\text{lb}} \cdot \frac{1}{193\,\text{assemblies}} = 780.273\,\text{g}.$$

**References**

[18]

**Value**

780.273

**Units**

g

**Pages**

13

## Source 33 — Zircaloy Grid Weight

Taken from email correspondence with an engineer at the utility. The weight of Zircaloy-4 for the grid spacers is 2985 lbs. The following formula is used to calculate the weight of Zircaloy-4 per intermediate grid:

$$W_{zr} = 2985\,\text{lb} \cdot 453.59237\frac{\text{g}}{\text{lb}} \cdot \frac{1}{193\,\text{assemblies}} \cdot \frac{1}{6\,\text{grids}} = 1,169.23\,\text{g}.$$

**References**

[18]

**Value**

1,169.23

**Units**

g

**Pages**

13

## Source 34 — Stainless Steel Grid Weight

Calculated from the volume of steel reported in Table 2-2 in [15] (11.3366$\text{cm}^3$) and the density of SS304 $\rho_{SS304}$ (8.03$g/\text{cm}^3$).

**References**

[15]

**Value**

91.0329

**Units**

g

**Pages**

13

## Source 35 — Burnable Poison Specifications

Taken from the data spreadsheet provided by the utility, on the sheet named BP Arrangement.

**References**

[16]

**Pages**

14, 15, 16, 17, 18, 19, 20, 21, 22

## Source 36 — Grid Spacers

The axial positioning of the grid centers was taken from the Fuel Lattice worksheet. Upper and lower planes for each grid were found using the grid heights specified in [15].

The masses for determining radial grid spacer dimensions are taken from Sources 32, 33, and 34.

**Top/Bottom Grid Sleeve**

As shown in Figure 25, the grid sleeve is a box shell defined by inner and outer square pitch parameters $P_i$ and $P_o$, where $P_i$ is found using the pin pitch as $17 \times S_p$. Using the density of SS304 $\rho_{SS304}$, the estimated mass for each grid $W_{SS304}$, and the height of the grid, the outer pitch is found as:

$$P_o = \sqrt{P_i^2 + \frac{W_{SS304}/\rho_{SS304}}{h_{tb}}} = \sqrt{(17 \times 1.25984\,\text{cm})^2 + \frac{91.0329\,\text{g}/8.03\,\frac{\text{g}}{\text{cm}^3}}{1.322\,\text{in} \times 2.54\frac{\text{cm}}{\text{in}}}}$$
$$= 21.4960\,\text{cm}$$

This fits between assemblies, as $P_o$ is less than the assembly pitch (21.50364 cm). The square radius reported in Figure 25 is half of $P_o$, or 10.73681 cm.

**Top/Bottom Egg-Crate**

As shown in Figure 23, the egg-crate is defined by a box shell defined by inner and outer square pitch parameters $p_i$ and $p_o$, where $p_o$ is simply the outer pincell pitch $S_p$. It is assumed that the entire mass of Inconel reported from Source 32 is uniformly distributed between all pincells in an assembly. Thus the mass of Inconel per pincell is $w_{in} = \frac{W_{in}}{17\times17} = 2.69990\,\text{g}$. Using this with the density of Inconel $\rho_{in}$ and the height of the grid, the inner pitch is found as:

$$p_i = \sqrt{p_o^2 - \frac{w_{in}/\rho_{in}}{h_{tb}}} = \sqrt{(1.25984\,\text{cm})^2 - \frac{2.69990\,\text{g}/8.2\,\frac{\text{g}}{\text{cm}^3}}{1.322\,\text{in} \times 2.54\frac{\text{cm}}{\text{in}}}}$$
$$= 1.22030\,\text{cm}$$

This fits between the pin and outer pincell pitch for all pincell types, as $p_i$ is greater than the guide tube diameter (1.20396 cm). The square radius reported in Figure 23 is half of $p_i$, or 0.62208 cm.

**Intermediate Grid Sleeve**

The dimensions for the intermediate grid sleeves are taken to be identical to those for the top/bottom grid sleeves.

**Intermediate Egg-Crate**

The intermediate grid egg-crate dimensions are found in the same way as the top/bottom grids, using the appropriate Zircaloy masses and densities. Here, the weight of Zircaloy $w_{zr,egg}$ used to calculate the egg-crate dimensions is the total grid weight of Zircaloy $W_{zr}$ from Source 33, less the weight of Zircaloy in the intermediate grid sleeve $w_{zr,sleeve}$, divided by the number of pincells. The weight in the sleeve is found using the density of Zircaloy and the volume of the sleeve from the intermediate grid height and the previosuly-calculated grid sleeve pitch parameters.

$$\begin{aligned} w_{zr,sleeve} &= \rho_{zr} h_{int} \left(P_o^2 - P_i^2\right) \\ &= 6.55 \frac{\text{g}}{\text{cm}^3} \times 2.25\,\text{in} \times 2.54 \frac{\text{cm}}{\text{in}} \left((21.4960\,\text{cm})^2 - (21.41728\,\text{cm})^2\right) \\ &= 126.455\,\text{g} \end{aligned}$$

$$\begin{aligned} w_{zr,egg} &= \frac{1}{17 \times 17} \left(W_{zr} - w_{zr,sleeve}\right) \\ w_{zr,egg} &= \frac{1}{17 \times 17} (1169.23\,\text{g} - 126.455\,\text{g}) \\ w_{zr,egg} &= 3.60850\,\text{g} \end{aligned}$$

$$\begin{aligned} p_i = \sqrt{p_o^2 - \frac{w_{zr,egg}/\rho_{zr}}{h_{int}}} &= \sqrt{(1.25984\,\text{cm})^2 - \frac{3.60850\,\text{g}/6.55\,\frac{\text{g}}{\text{cm}^3}}{2.25\,\text{in} \times 2.54\frac{\text{cm}}{\text{in}}}} \\ &= 1.22098\,\text{cm} \end{aligned}$$

This fits between the pin and outer pincell pitch for all pincell types, as $p_i$ is greater than the guide tube diameter (1.20396 cm). The square radius reported in Figure 24 is half of $p_i$, or 0.60978 cm.

**References**

[16] [15]

**Pages**

23, 24, 34, 35, 36, 37

## Source 37 — Core Baffle Thickness

Taken from email correspondence with an engineer at the utility. The core baffle is 7/8 inches thick. Converting this to centimeters:

$$T_{baf} = \frac{7}{8}\,\text{in} \cdot 2.54\frac{\text{cm}}{\text{in}} = 2.22250\,\text{cm}$$

**References**

[18]

**Value**

2.22250

**Units**

cm

**Pages**

26

## Source 38 — Core Barrel Inner Radius

Taken from email corresponding with an engineer at the utility. The inner diameter of the core barrel is 148.0 inches. The inner radius of the core barrel is calculated to be

$$R_{bar} = \frac{148.0\,\text{in}}{2} \cdot 2.54\frac{\text{cm}}{\text{in}} = 187.96\,\text{cm}$$

**References**

[18]

**Value**

187.96

**Units**

cm

**Pages**

26

## Source 39 — Core Barrel Outer Radius

Taken from email correspondence with an engineer at the utility. The outer diameter of the core barrel is 152.5 inches. The outer radius of the core barrel is calculated to be

$$R_{bar} = \frac{152.5\,\text{in}}{2} \cdot 2.54\frac{\text{cm}}{\text{in}} = 193.675\,\text{cm}$$

**References**

[18]

**Value**

193.675

**Units**

cm

**Pages**

26

## Source 40 — Core Barrel Material

From email correspondence with the utility, the core barrel is made out of Stainless Steel 304.

**References**

[18]

**Pages**

26

## Source 41 — RPV, Liner, and Shield Pannels

Core structural dimensions were taken from [15], with the exception of the baffle and core barrel dimensions that were provided by engineers at the utility. The water gap between fuel assemblies and the baffle was also taken from [15], which also indicates the material as Stainless Steel 304.

**References**

[15]

**Pages**

26

## Source 42 — Instrument Tube Axial Planes

The instrument tube thimble penetrates the bottom of the reactor vessel and extends to the end of guide tubes at the bottom of the upper nozzle. The source for these planes is described in Source 47.

**Pages**

36

## Source 43 — Burnable Absorber Axial Planes

Burnable absorbers are inserted from the top of assemblies with a spider assembly similar to those that hold control rods. The burnable absorber axial planes were set to be consistent with [15], Figure 2-9.

**References**

[15]

**Pages**

37

## Source 44 — Guide Tube Axial Planes

The guide tubes are the structural components of the assemblies, connecting the top of the lower nozzle to the bottom of the upper nozzle. The dashpot axial plane is placed at the control rod step 0 (see Source 45).

**Pages**

35, 37

## Source 45 — Control Rod Axial Planes

The control rod axial planes for full insertion were set to be consistent with [15], Figure 2-8. The step width of 1.582cm was caluclated by dividing the active absorbing height (142 in.) by 228.

**References**

[16] [15]

**Pages**

38, 121

## Source 46 — Assembly Nozzles

Upper nozzle and water gap axial spacings were estimated from the Watts Bar Unit 2 Safety Analysis Report, Section 4, Figure 4.2-2.

**References**

[20]

**Pages**

34, 35, 36, 37, 41

## Source 47 — Fuel Rod Axial Planes

Fuel rod axial planes were set to be consistent with [15], Figure 2-7.

**References**

[15]

**Pages**

26, 34, 119

## Source 48 — Location of Instrument Tubes

The locations of the instrumentation tubes were inferred from HZP detector measurement files. There are 58 locations in various locations around the core.

**References**

[21]

**Pages**

32

## Source 49 — 1.6% Enriched Fuel Composition

Provided in the spreadsheet sent by the utility the initial Uranium heavy metal mass and U-235 mass are detailed for each assembly under the worksheet, Assembly Loading. These allow us to calculate U-235 enrichments and fuel density. To limit the number of materials, the average values for the enrichments were calculated.

Using the detailed assembly loadings, the actual core-averaged enrichment for the cycle 1 low-enriched bundles is $\chi_{25} = 1.61006\%$ (see Source 70). It assumed that the enrichment of U-234 is 0.8% of this,

$$\chi_{24} = 0.008 \cdot 1.61006\% = 0.01288048\%.$$

The rest of the heavy metal in the initial fuel loading is made up of U-238 calculated as

$$\chi_{28} = 100\% - 1.61006\% + 0.01288048\% = 98.37705952\%.$$

The atomic mass of Uranium can be calculated from these weight percents of Uranium isotopes and the isotopic masses taken from Source 67:

$$M_U = \left[\frac{\chi_{24}}{M_{24}} + \frac{\chi_{25}}{M_{25}} + \frac{\chi_{28}}{M_{28}}\right]^{-1} = 238.001241436\,\text{amu}.$$

The weight fractions of Uranium in Uranium Dioxide and Oxygen in Uranium Dioxide can be determined by the following two expressions:

$$\omega_U = \frac{M_U}{M_U + 2 \cdot M_O} = 0.881485944114$$

and

$$\omega_O = 1 - \omega_U = 0.118514055886.$$

From the Uranium heavy metal weight percent, and detailed heavy metal loadings reported in the spreadsheet, the average density can be calculated. The total Uranium heavy metal mass for low enriched bundles is $m_f = 27.570971\,\text{MT}$ (see Source 70). If there are 65 low enriched bundles, the volume can be calculated with

$$V_f = \pi \cdot R_f^2 \cdot H \cdot N_{assy} \cdot N_{pins}$$

$$V_f = \pi \cdot 0.39218^2 \cdot 365.76 \cdot 65 \cdot 264 = 3032733.5050\,\text{cm}^3.$$

See Sources 8, 5 and Figures 14 and 27.

The fuel density can be calculated by computing the Uranium heavy metal density and dividing by its fractional weight

$$\rho_f = \frac{m_f}{V_f \cdot \omega_U} = 10.31341\,\frac{\mathrm{g}}{\mathrm{cm}^3}.$$

Isotopic number densities for Uranium are then calculated with

$$N = \frac{\widetilde{\rho} \cdot A}{M}.$$

The parameter $A$ is Avagadro's number $= 0.60221415 \cdot 10^{24}\,\frac{atom}{mol}$ and $\widetilde{\rho}$ is the isotopic mass density. The isotopic mass density is calculated by multiplying the weight fraction of the element by the weight fraction of the isotopic in that element $(\omega \cdot \chi)$ multiplied by the fuel mass density,

$$\widetilde{\rho} = \rho_f \cdot \omega \cdot \chi.$$

For oxygen, the total number density of oxygen is calculated with

$$N_O = \frac{\rho_f \cdot \omega_O \cdot A}{M_O}.$$

Isotopic number densities are then determined by multiplying by fractional abundances provided in Source 68.

**References**

[16]

**Pages**

43

## Source 50 — 2.4% Enriched Fuel Composition

Provided in the spreadsheet sent by the utility the initial Uranium heavy metal mass and U-235 mass are detailed for each assembly under the worksheet, Assembly Loading. These allow us to calculate U-235 enrichments and fuel density. To limit the number of materials, the average values for the enrichments were calculated.

Using the detailed assembly loadings, the actual core-averaged enrichment for the cycle 1 medium-enriched bundles is $\chi_{25} = 2.39993\%$ (see Source 70). It assumed that the enrichment of U-234 is 0.8% of this,

$$\chi_{24} = 0.008 \cdot 2.39993\% = 0.01919944\%.$$

The rest of the heavy metal in the initial fuel loading is made up of U-238 calculated as

$$\chi_{28} = 100\% - 2.39993\% + 0.01919944\% = 97.58087056\%.$$

The atomic mass of Uranium can be calculated from these weight percents of Uranium isotopes and the isotopic masses taken from Source 67:

$$M_U = \left[\frac{\chi_{24}}{M_{24}} + \frac{\chi_{25}}{M_{25}} + \frac{\chi_{28}}{M_{28}}\right]^{-1} = 237.976942215\,\text{amu}.$$

The weight fractions of Uranium in Uranium Dioxide and Oxygen in Uranium Dioxide can be determined by the following two expressions:

$$\omega_U = \frac{M_U}{M_U + 2 \cdot M_O} = 0.881475277232$$

and

$$\omega_O = 1 - \omega_U = 0.118524722768.$$

From the Uranium heavy metal weight percent, and detailed heavy metal loadings reported in the spreadsheet, the average density can be calculated. The total Uranium heavy metal mass for medium enriched bundles is $m_f = 27.104522\,\text{MT}$ (see Source 70). If there are 64 medium enriched bundles, the volume can be calculated with

$$V_f = \pi \cdot R_f^2 \cdot H \cdot N_{assy} \cdot N_{pins}$$

$$V_f = \pi \cdot 0.39218^2 \cdot 365.76 \cdot 64 \cdot 264 = 2986076.0665\,\text{cm}^3.$$

See Sources 8, 5 and Figures 14 and 27.

The fuel density can be calculated by computing the Uranium heavy metal density and dividing by its fractional weight

$$\rho_f = \frac{m_f}{V_f \cdot \omega_U} 10.29748 \, \frac{\text{g}}{\text{cm}^3}.$$

Isotopic number densities for Uranium are then calculated with

$$N = \frac{\widetilde{\rho} \cdot A}{M}.$$

The parameter $A$ is Avagadro's number $= 0.60221415 \cdot 10^{24} \, \frac{atom}{mol}$ and $\widetilde{\rho}$ is the isotopic mass density. The isotopic mass density is calculated by multiplying the weight fraction of the element by the weight fraction of the isotopic in that element ($\omega \cdot \chi$) multiplied by the fuel mass density,

$$\widetilde{\rho} = \rho_f \cdot \omega \cdot \chi.$$

For oxygen, the total number density of oxygen is calculated with

$$N_O = \frac{\rho_f \cdot \omega_O \cdot A}{M_O}.$$

Isotopic number densities are then determined by multiplying by fractional abundances provided in Source 68.

**References**

[16]

**Pages**

44

## Source 51 — 3.1% Enriched Fuel Composition

Provided in the spreadsheet sent by the utility the initial Uranium heavy metal mass and U-235 mass are detailed for each assembly under the worksheet, Assembly Loading. These allow us to calculate U-235 enrichments and fuel density. To limit the number of materials, the average values for the enrichments were calculated.

Using the detailed assembly loadings, the actual core-averaged enrichment for the cycle 1 high-enriched bundles is $\chi_{25} = 3.10221\%$ (see Source 70). It assumed that the enrichment of U-234 is 0.8% of this,

$$\chi_{24} = 0.008 \cdot 3.10221\% = 0.02481768\%.$$

The rest of the heavy metal in the initial fuel loading is made up of U-238 calculated as

$$\chi_{28} = 100\% - 3.10221\% + 0.02481768\% = 96.87297232\%.$$

The atomic mass of Uranium can be calculated from these weight percents of Uranium isotopes and the isotopic masses taken from Source 67:

$$M_U = \left[\frac{\chi_{24}}{M_{24}} + \frac{\chi_{25}}{M_{25}} + \frac{\chi_{28}}{M_{28}}\right]^{-1} = 237.955341741\,\text{amu}.$$

The weight fractions of Uranium in Uranium Dioxide and Oxygen in Uranium Dioxide can be determined by the following two expressions:

$$\omega_U = \frac{M_U}{M_U + 2 \cdot M_O} = 0.881464534041$$

and

$$\omega_O = 1 - \omega_U = 0.118535465959.$$

From the Uranium heavy metal weight percent, and detailed heavy metal loadings reported in the spreadsheet, the average density can be calculated. The total Uranium heavy metal mass for high enriched bundles is $m_f = 27.115256\,\text{MT}$ (see Source 70). If there are 64 high enriched bundles, the volume can be calculated with

$$V_f = \pi \cdot R_f^2 \cdot H \cdot N_{assy} \cdot N_{pins}$$

$$V_f = \pi \cdot 0.39218^2 \cdot 365.76 \cdot 64 \cdot 264 = 2986076.0665\,\text{cm}^3.$$

See Sources 8, 5 and Figures 14 and 27.

The fuel density can be calculated by computing the Uranium heavy metal density and dividing by its fractional weight

$$\rho_f = \frac{m_f}{V_f \cdot \omega_U} 10.30166 \, \frac{\text{g}}{\text{cm}^3}.$$

Isotopic number densities for Uranium are then calculated with

$$N = \frac{\widetilde{\rho} \cdot A}{M}.$$

The parameter $A$ is Avagadro's number $= 0.60221415 \cdot 10^{24} \, \frac{atom}{mol}$ and $\widetilde{\rho}$ is the isotopic mass density. The isotopic mass density is calculated by multiplying the weight fraction of the element by the weight fraction of the isotopic in that element $(\omega \cdot \chi)$ multiplied by the fuel mass density,

$$\widetilde{\rho} = \rho_f \cdot \omega \cdot \chi.$$

For oxygen, the total number density of oxygen is calculated with

$$N_O = \frac{\rho_f \cdot \omega_O \cdot A}{M_O}.$$

Isotopic number densities are then determined by multiplying by fractional abundances provided in Source 68.

**References**

[16]

**Pages**

44

## Source 52 — 3.2% Enriched Fuel Composition

Provided in the spreadsheet sent by the utility the initial Uranium heavy metal mass and U-235 mass are detailed for each assembly under the worksheet, Assembly Loading. These allow us to calculate U-235 enrichments and fuel density. To limit the number of materials, the average values for the enrichments were calculated.

Using the detailed assembly loadings, the actual average enrichment for these fresh assemblies is $\chi_{25} = 3.19547\%$ (see Source 71). It assumed that the enrichment of U-234 is 0.8% of this,

$$\chi_{24} = 0.008 \cdot 3.19547\% = 0.02556376\%.$$

The rest of the heavy metal in the initial fuel loading is made up of U-238 calculated as

$$\chi_{28} = 100\% - 3.19547\% + 0.02556376\% = 96.77896624\%.$$

The atomic mass of Uranium can be calculated from these weight percents of Uranium isotopes and the isotopic masses taken from Source 67:

$$M_U = \left[\frac{\chi_{24}}{M_{24}} + \frac{\chi_{25}}{M_{25}} + \frac{\chi_{28}}{M_{28}}\right]^{-1} = 237.952473579\,\text{amu}.$$

The weight fractions of Uranium in Uranium Dioxide and Oxygen in Uranium Dioxide can be determined by the following two expressions:

$$\omega_U = \frac{M_U}{M_U + 2 \cdot M_O} = 0.881465793436$$

and

$$\omega_O = 1 - \omega_U = 0.118535465959.$$

From the Uranium heavy metal weight percent, and detailed heavy metal loadings reported in the spreadsheet, the average density can be calculated. The total Uranium heavy metal mass for high enriched bundles is $m_f = 20.414365\,\text{MT}$ (see Source 71). If there are 48 bundles, the volume can be calculated with

$$V_f = \pi \cdot R_f^2 \cdot H \cdot N_{assy} \cdot N_{pins}$$

$$V_f = \pi \cdot 0.39218^2 \cdot 365.76 \cdot 48 \cdot 264 = 2239557.0499\,\text{cm}^3.$$

See Sources 8, 5 and Figures 14 and 27.

The fuel density can be calculated by computing the Uranium heavy metal density and dividing by its fractional weight

$$\rho_f = \frac{m_f}{V_f \cdot \omega_U} 10.34115 \, \frac{\text{g}}{\text{cm}^3}.$$

Isotopic number densities for Uranium are then calculated with

$$N = \frac{\widetilde{\rho} \cdot A}{M}.$$

The parameter $A$ is Avagadro's number $= 0.60221415 \cdot 10^{24} \frac{atom}{mol}$ and $\widetilde{\rho}$ is the isotopic mass density. The isotopic mass density is calculated by multiplying the weight fraction of the element by the weight fraction of the isotopic in that element $(\omega \cdot \chi)$ multiplied by the fuel mass density,

$$\widetilde{\rho} = \rho_f \cdot \omega \cdot \chi.$$

For oxygen, the total number density of oxygen is calculated with

$$N_O = \frac{\rho_f \cdot \omega_O \cdot A}{M_O}.$$

Isotopic number densities are then determined by multiplying by fractional abundances provided in Source 68.

**References**

[16]

**Pages**

iii, 45

## Source 53 — 3.4% Enriched Fuel Composition

Provided in the spreadsheet sent by the utility the initial Uranium heavy metal mass and U-235 mass are detailed for each assembly under the worksheet, Assembly Loading. These allow us to calculate U-235 enrichments and fuel density. To limit the number of materials, the average values for the enrichments were calculated.

Using the detailed assembly loadings, the actual core-averaged enrichment for these fresh assemblies is $\chi_{25} = 3.40585\%$ (see Source 71). It assumed that the enrichment of U-234 is 0.8% of this,

$$\chi_{24} = 0.008 \cdot 3.40585\% = 0.02724680\%.$$

The rest of the heavy metal in the initial fuel loading is made up of U-238 calculated as

$$\chi_{28} = 100\% - 3.40585\% + 0.02724680\% = 96.56690320\%.$$

The atomic mass of Uranium can be calculated from these weight percents of Uranium isotopes and the isotopic masses taken from Source 67:

$$M_U = \left[\frac{\chi_{24}}{M_{24}} + \frac{\chi_{25}}{M_{25}} + \frac{\chi_{28}}{M_{28}}\right]^{-1} = 237.946003706, \text{amu}.$$

The weight fractions of Uranium in Uranium Dioxide and Oxygen in Uranium Dioxide can be determined by the following two expressions:

$$\omega_U = \frac{M_U}{M_U + 2 \cdot M_O} = 0.881461693055$$

and

$$\omega_O = 1 - \omega_U = 0.118538306945.$$

From the Uranium heavy metal weight percent, and detailed heavy metal loadings reported in the spreadsheet, the average density can be calculated. The total Uranium heavy metal mass for high enriched bundles is $m_f = 6.816624\,\text{MT}$ (see Source 71). If there are 16 bundles, the volume can be calculated with

$$V_f = \pi \cdot R_f^2 \cdot H \cdot N_{assy} \cdot N_{pins}$$

$$V_f = \pi \cdot 0.39218^2 \cdot 365.76 \cdot 16 \cdot 264 = 746519.0166\,\text{cm}^3.$$

See Sources 8, 5 and Figures 14 and 27.

The fuel density can be calculated by computing the Uranium heavy metal density and dividing by its fractional weight

$$\rho_f = \frac{m_f}{V_f \cdot \omega_U} 10.35917 \, \frac{\text{g}}{\text{cm}^3}.$$

Isotopic number densities for Uranium are then calculated with

$$N = \frac{\widetilde{\rho} \cdot A}{M}.$$

The parameter $A$ is Avagadro's number $= 0.60221415 \cdot 10^{24} \frac{atom}{mol}$ and $\widetilde{\rho}$ is the isotopic mass density. The isotopic mass density is calculated by multiplying the weight fraction of the element by the weight fraction of the isotopic in that element $(\omega \cdot \chi)$ multiplied by the fuel mass density,

$$\widetilde{\rho} = \rho_f \cdot \omega \cdot \chi.$$

For oxygen, the total number density of oxygen is calculated with

$$N_O = \frac{\rho_f \cdot \omega_O \cdot A}{M_O}.$$

Isotopic number densities are then determined by multiplying by fractional abundances provided in Source 68.

**References**

[16]

**Pages**

iii, 45

# Source 54 — Composition of Air

The density of air was referenced from Engineering toolbox at 300 C to be $\rho_{air} = 0.000616$ g/cc. The composition of air included here contains Oxygen, Nitrogen, Argon and Carbon. Note that Hydrogen, Neon, Helium, Krypton and Xenon were all neglected as they contribute very little. Abundances were gathered from Engineering Toolbox and are listed below.

| Element | Fractional Abundance | Element | Fractional Abundance |
|---|---|---|---|
| O | 0.2095 | N | 0.7809 |
| Ar | 0.00933 | C | 0.00027† |

† Carbon adjusted slightly so sum is unity.

Using these abundances and elemental masses in Source 69, the mass of air can be calculated with

$$M_{air} = \sum_i \alpha_i M_i = 14.6657850715\,\text{amu},$$

where $\alpha$ represents the abundance fraction. The total number density of air can be calculated with

$$N_{air} = \frac{\rho_{air} \cdot A}{M_{air}} = 2.52945147219 \times 10^{-5} \frac{\text{atom}}{\text{barn} \cdot \text{cm}}.$$

The parameter $A$ is Avagadro's number $= 0.60221415 \cdot 10^{24} \frac{atom}{mol}$. Elemental number densities can be calculated by multiplying the number density of air by their respective abundances,

$$N_i = \alpha_i \cdot N_{air}.$$

Similarly, the isotopic number densities can be calculated by multiplying the elemental number densities by isotopic abundances reported in Source 68.

**References**

[22]

**Pages**

46

## Source 55 — Composition of Borosilicate Glass

The density of Borosilicate glass was referenced from the CASMO-4 manual to be $\rho_{bp} = 2.26$ g/cc. The composition, according to the manual is

| Element/Isotope | Weight Fraction | Element/Isotope | Weight Fraction |
|---|---|---|---|
| O | 0.5481 | Al | 0.0344 |
| Si | 0.3787 | B-10 | 0.0071 |
| B-11 | 0.0317 | | |

The relative weight fractions of B-10 and B-11 in Boron can be calculated using the absolute weight fractions above,

$$\chi_{50} = \frac{\omega_{50}}{\omega_{50} + \omega_{51}} \qquad \chi_{50} = \frac{\omega_{51}}{\omega_{50} + \omega_{51}}.$$

The elemental mass of Boron can be done using isotopic masses in Source 67,

$$M_B = \left[\frac{\chi_{50}}{M_{50}} + \frac{\chi_{51}}{M_{51}}\right]^{-1} = 10.812422457829642\,\text{amu}.$$

To compute the number densities of the elements/isotopes listed in the table above, the following formula can be used:

$$N_i = \frac{\omega_i \cdot \rho_{bp} \cdot A}{M_i}.$$

The parameter $A$ is Avagadro's number $= 0.60221415 \cdot 10^{24} \frac{atom}{mol}$. The isotopic number densities of the elements listed in the table can be calculated by multiplying the elemental number densities by isotopic abundances reported in Source 68.

**References**

[23]

**Pages**

46

# Source 56 — Composition of Ag-In-Cd Control Rods

The density of Ag-In-Cd control rods was referenced from the CASMO-4 manual to be $\rho_{cr} = 10.16$ g/cc. The composition, as given in the manual is 80% Ag, 15% In and 5% Cd.

Using these weight percents and elemental masses from Source 69, the number densities of each element can be calculated with.

$$N_i = \frac{\omega_i \cdot \rho_{cr} \cdot A}{M_i}.$$

The parameter $A$ is Avagadro's number $= 0.60221415 \cdot 10^{24} \frac{atom}{mol}$. The isotopic number densities of the elements listed in the table can be calculated by multiplying the elemental number densities by isotopic abundances reported in Source 68.

**References**

[23]

**Pages**

3, 47

## Source 57 — Composition of B4C Control Rods

The density of B4C control rods was referenced from the CASMO-4 manual to be $\rho_{cr} = 1.76$ g/cc. The composition, as given in the manual is 78.26% B and 21.74% C.

Using these weight percents and elemental masses from Source 69, the number densities of each element can be calculated with.

$$N_i = \frac{\omega_i \cdot \rho_{cr} \cdot A}{M_i}.$$

The parameter $A$ is Avagadro's number $= 0.60221415 \cdot 10^{24} \frac{atom}{mol}$. The isotopic number densities of the elements listed in the table can be calculated by multiplying the elemental number densities by isotopic abundances reported in Source 68.

**References**

[23]

**Pages**

3, 47

## Source 58 — Composition of Helium

The density of Helium gas was retrieved from NIST from a pressure of 2 MPa and temperature of 600 K. The density was given as $\rho_{He} = 0.0015981$ g/cc. The number density can be computed along with the element mass from Source 69,

$$N_{He} = \frac{\rho_{He} \cdot A}{M_{He}}.$$

The parameter $A$ is Avagadro's number $= 0.60221415 \cdot 10^{24} \, \frac{atom}{mol}$.

**References**

[24]

**Pages**

48

# Source 59 — Composition of Inconel

The density of Inconel-718 was referenced from the CASMO-4 manual to be $\rho_{in} = 8.2$ g/cc. The composition, according to the manual is

| Element/Isotope | Weight Fraction | Element/Isotope | Weight Fraction |
|---|---|---|---|
| Si | 0.0035 | Cr | 0.1896 |
| Mn | 0.0087 | Fe | 0.2863† |
| Ni | 0.5119 | | |

† weight fraction adjust such that sum is unity

To compute the number densities of the elements/isotopes listed in the table above, the following formula can be used:

$$N_i = \frac{\omega_i \cdot \rho_{in} \cdot A}{M_i}.$$

The parameter $A$ is Avagadro's number $= 0.60221415 \cdot 10^{24} \frac{atom}{mol}$. The isotopic number densities of the elements listed in the table can be calculated by multiplying the elemental number densities by isotopic abundances reported in Source 68.

**References**

[23]

**Pages**

48

## Source 60 — Composition of Stainless Steel

The density of Stainless Steel-304 was referenced from AK Steel Product Data Sheet to be $\rho_{ss} = 8.03$ g/cc. The composition, according to the data sheet is

| Element/Isotope | Weight Fraction | Element/Isotope | Weight Fraction |
|---|---|---|---|
| Si | 0.0060 | Cr | 0.1900 |
| Mn | 0.0200 | Fe | 0.6840$^{\dagger}$ |
| Ni | 0.1000 | | |

$^{\dagger}$ weight fraction adjust such that sum is unity

To compute the number densities of the elements/isotopes listed in the table above, the following formula can be used:

$$N_i = \frac{\omega_i \cdot \rho_{ss} \cdot A}{M_i}.$$

The parameter $A$ is Avagadro's number $= 0.60221415 \cdot 10^{24} \frac{atom}{mol}$. The isotopic number densities of the elements listed in the table can be calculated by multiplying the elemental number densities by isotopic abundances reported in Source 68.

**References**

[25]

**Pages**

49

## Source 61 — Composition of Zircaloy

The density of Zircaloy 4 was referenced from the CASMO-4 manual to be $\rho_{zr} = 6.55$ g/cc. The composition, according to the manual is

| Element/Isotope | Weight Fraction | Element/Isotope | Weight Fraction |
|---|---|---|---|
| O | 0.00125 | Cr | 0.0010 |
| Fe | 0.0021 | Zr | 0.98115$^{\dagger}$ |
| Sn | 0.0145 | | |

$^{\dagger}$ weight fraction adjust such that sum is unity

To compute the number densities of the elements/isotopes listed in the table above, the following formula can be used:

$$N_i = \frac{\omega_i \cdot \rho_{zr} \cdot A}{M_i}.$$

The parameter $A$ is Avagadro's number $= 0.60221415 \cdot 10^{24} \frac{atom}{mol}$. The isotopic number densities of the elements listed in the table can be calculated by multiplying the elemental number densities by isotopic abundances reported in Source 68.

**Pages**

50

## Source 62 — Composition of Borated Water

This source block describes how to compute the number density of isotopes in borated water. This block will show the necessary formulas, but the density and concentration of boron may change depending on cycle time. For a given reactor pressure and temperature, density of water is obtained from NIST. From the water density and boron weight percent, the density of borated water will be obtained.

For a given concentration of boron, the weight percent of boron in water is

$$\omega_B = C_B\,[\text{ppm}]^{-1} \times 10^{-6}.$$

The molecular mass of water can be determined from elemental masses in Source 69 as

$$M_{H_2O} = 2 \cdot M_H + M_O.$$

The number density of water can then be computed as

$$N_{H_2O} = \frac{\rho_{H_2O} \cdot A}{M_{H_2O}}.$$

The parameter $A$ is Avagadro's number $= 0.60221415 \cdot 10^{24}\,\frac{atom}{mol}$. The number density of hydrogen and oxygen are given as:

$$N_H = 2 \cdot N_{H_2O} \qquad N_O = N_{H_2O}.$$

The density of borated water can be computed from the density of water and the weight percent of boron,

$$\rho_{BW} = \frac{\rho_{H_2O}}{\omega_B}$$

To compute the number density of boron, the following expression is used:

$$N_B = \frac{\omega_B \cdot \rho_{BW} \cdot A}{M_B}.$$

The isotopic number densities of the elements can be calculated by multiplying the elemental number densities by isotopic abundances reported in Source 68.

**References**

[26]

**Pages**

51

## Source 63 — Composition of Borated Water in Nozzle and Support Plate Region

To conserve the mass of borated water in the nozzle and support plate region, the density of borated water is adjusted using formula:

$$\rho'_{water} = \frac{\rho_{water} \times V_{water}}{V'_{water}}$$

where $\rho_{water}$ and $V_{water}$ are the actual density and volume of water while $\rho'_{water}$ and $V'_{water}$ are the density and volume in the model.

According to Section 2.3.6.2, the volume of water in the nozzle and support plate region is

$$V'_{water} = S_a^2 - n_{pins} \times \pi \times R_{pin}^2 = 21.50364^2 - 264 \times \pi \times 0.45720^2 = 289.03961\,\text{cm}^3$$

From Reference [15], the volume fractions of water in the nozzle and support plate is 0.8280, so the actual volume of water should be:

$$V_{water} = S_a^2 \times 0.8280 = 382.87261\,\text{cm}^3$$

The adjusted density of borated water is:

$$\rho'_{water} = 0.740582067516 \times 382.87261/289.03961 = 0.9810025\,\text{g/cm}^3$$

The adjusted density can then be used to calculate number densities of nuclides in borated water described in Source 62.

**References**

[15]

**Pages**

51

## Source 64 — Composition of Stainless Steel in Nozzle and Support Plate Region

To conserve the mass of stainless steel in the nozzle and support plate region, the density of stainless steel is adjusted using formula:

$$\rho'_{ss} = \frac{\rho_{ss} \times V_{ss}}{V'_{ss}}$$

where $\rho_{ss}$ and $V_{ss}$ are the actual density and volume of stainless steel while $\rho'_{ss}$ and $V'_{ss}$ are the density and volume in the model.

According to Section 2.3.6.2, the volume of stainless steel in the nozzle and support plate region is

$$V'_{ss} = n_{pins} \times \pi \times R^2_{pin} = 264 \times \pi \times 0.45720^2 = 173.36692\,\text{cm}^3$$

From Reference [15], the volume fractions of stainless steel in the nozzle and support plate is 0.1720, so the actual volume of stainless steel should be:

$$V_{ss} = S^2_a \times 0.1720 = 79.533924\,\text{cm}^3$$

The adjusted density of stainless steel is:

$$\rho'_{ss} = 8.03 \times 79.533924/173.36692 = 3.683848\,\text{g/cm}^3$$

The adjusted density can then be used to calculate number densities of nuclides in stainless steel described in Source 60.

**References**

[15]

**Pages**

52

## Source 65 — Composition of Carbon Steel

The density of Carbon Steel was assumed to be $\rho_{zr} = 7.8$ g/cc. The composition, according to the ranges in an ASTM datasheet is

| Element/Isotope | Weight Fraction | Element/Isotope | Weight Fraction |
|---|---|---|---|
| C | 0.00270 | Mn | 0.00750 |
| P | 0.00025 | Si | 0.00400 |
| Mo | 0.00625 | Ni | 0.00750 |
| Fe | 0.96487 | S | 0.00025 |
| Cr | 0.00350 | V | 0.00050 |
| Nb | 0.00010 | Cu | 0.00200 |
| Ca | 0.00015 | B | 0.00003 |
| Ti | 0.00015 | Al | 0.00025 |

To compute the number densities of the elements/isotopes listed in the table above, the following formula can be used:

$$N_i = \frac{\omega_i \cdot \rho_{zr} \cdot A}{M_i}.$$

The parameter $A$ is Avagadro's number $= 0.60221415 \cdot 10^{24} \frac{atom}{mol}$. The isotopic number densities of the elements listed in the table can be calculated by multiplying the elemental number densities by isotopic abundances reported in Source 68.

### References

[27]

### Pages

53

## Source 66 — Missing Data

This reference box lists all of the values that were estimated:

- Lower support plate and nozzle heights were guessed

**Pages**

34, 35, 36, 37, 38

## Source 67 — Isotopic Masses

| Isotope | Mass [amu] | Isotope | Mass [amu] |
|---|---|---|---|
| H-1 | 1.0078250 | H-2 | 2.0141018 |
| He-4 | 4.0026032542 | B-10 | 10.0129370 |
| B-11 | 11.0093054 | C-12 | 12.0000000 |
| C-13 | 13.003354838 | O-16 | 15.9949146196 |
| O-17 | 16.9991317 | O-18 | 17.999161 |
| N-14 | 14.003074005 | N-15 | 15.000108898 |
| Si-28 | 27.976926532 | Si-29 | 28.97649470 |
| Si-30 | 29.97377017 | P-31 | 30.9737616 |
| Al-27 | 26.9815386 | Ar-36 | 35.96754511 |
| Ar-38 | 37.9627324 | Ar-40 | 39.962383123 |
| Cr-50 | 49.946044 | Cr-52 | 51.940507 |
| Cr-53 | 52.940649 | Cr-54 | 53.938880 |
| Mn-55 | 54.938045 | Fe-54 | 53.939611 |
| Fe-56 | 55.934937 | Fe-57 | 56.935394 |
| Fe-58 | 57.933276 | Ni-58 | 57.935343 |
| Ni-60 | 59.930786 | Ni-61 | 60.931056 |
| Ni-62 | 61.928345 | Ni-64 | 63.927966 |
| Zr-90 | 89.904704 | Zr-91 | 90.905646 |
| Zr-92 | 91.905041 | Zr-94 | 93.906315 |
| Zr-96 | 95.908273 | Mo-92 | 91.906811 |
| Mo-94 | 93.905088 | Mo-95 | 94.905842 |
| Mo-96 | 95.904679 | Mo-97 | 96.906021 |
| Mo-98 | 97.905408 | Mo-100 | 99.90748 |
| Ag-107 | 106.905097 | Ag-109 | 108.904752 |
| Cd-106 | 105.90646 | Cd-108 | 107.90418 |
| Cd-110 | 109.903002 | Cd-111 | 110.904178 |
| Cd-112 | 111.902758 | Cd-113 | 112.904402 |
| Cd-114 | 113.903359 | Cd-116 | 115.904756 |
| In-113 | 112.904058 | In-115 | 114.903878 |
| Sn-112 | 111.904818 | Sn-114 | 113.902779 |
| Sn-115 | 114.903342 | Sn-116 | 115.901741 |
| Sn-117 | 116.902952 | Sn-118 | 117.901603 |
| Sn-119 | 118.903308 | Sn-120 | 119.902195 |
| Sn-122 | 121.903439 | Sn-124 | 123.905274 |
| U-234 | 234.040952 | U-235 | 235.043930 |
| U-238 | 238.050788 | | |

**References**

[28]

**Pages**

126, 128, 130, 132, 134, 137

## Source 68 — Isotopic Natural Abundances

| Isotope | Fractional Abundance | Isotope | Fractional Abundance |
|---|---|---|---|
| Ag107 | 0.51839 | Ag109 | 0.48161 |
| Al27 | 1.0 | Ar36 | 0.003336 |
| Ar38 | 0.000629 | Ar40 | 0.996035 |
| B10 | 0.1982 | B11 | 0.8018 |
| C12 | 0.988922 | C13 | 0.011078 |
| Ca40 | 0.96941 | Ca42 | 0.00647 |
| Ca43 | 0.00135 | Ca44 | 0.02086 |
| Ca46 | 4e-05 | Ca48 | 0.00187 |
| Cd106 | 0.01245 | Cd108 | 0.00888 |
| Cd110 | 0.1247 | Cd111 | 0.12795 |
| Cd112 | 0.24109 | Cd113 | 0.12227 |
| Cd114 | 0.28754 | Cd116 | 0.07512 |
| Cr50 | 0.04345 | Cr52 | 0.83789 |
| Cr53 | 0.09501 | Cr54 | 0.02365 |
| Cu63 | 0.6915 | Cu65 | 0.3085 |
| Fe54 | 0.05845 | Fe56 | 0.91754 |
| Fe57 | 0.02119 | Fe58 | 0.00282 |
| H1 | 0.99984426 | H2 | 0.00015574 |
| He3 | 2e-06 | He4 | 0.999998 |
| In113 | 0.04281 | In115 | 0.95719 |
| Mn55 | 1.0 | Mo100 | 0.09744 |
| Mo92 | 0.14649 | Mo94 | 0.09187 |
| Mo95 | 0.15873 | Mo96 | 0.16673 |
| Mo97 | 0.09582 | Mo98 | 0.24292 |
| N14 | 0.996337 | N15 | 0.003663 |
| Nb93 | 1.0 | Ni58 | 0.680769 |
| Ni60 | 0.262231 | Ni61 | 0.011399 |
| Ni62 | 0.036345 | Ni64 | 0.009256 |
| O16 | 0.9976206 | O17 | 0.000379 |
| O18 | 0.0020004 | P31 | 1.0 |
| S32 | 0.9504074 | S33 | 0.0074869 |
| S34 | 0.0419599 | S36 | 0.0001458 |
| Si28 | 0.9222968 | Si29 | 0.0468316 |
| Si30 | 0.0308716 | Sn112 | 0.0097 |
| Sn114 | 0.0066 | Sn115 | 0.0034 |
| Sn116 | 0.1454 | Sn117 | 0.0768 |
| Sn118 | 0.2422 | Sn119 | 0.0859 |

| | | | |
|---|---|---|---|
| Sn120 | 0.3258 | Sn122 | 0.0463 |
| Sn124 | 0.0579 | Ti46 | 0.0825 |
| Ti47 | 0.0744 | Ti48 | 0.7372 |
| Ti49 | 0.0541 | Ti50 | 0.0518 |
| U234 | 5.4e-05 | U235 | 0.007204 |
| U238 | 0.992742 | V50 | 0.0025 |
| V51 | 0.9975 | Zr90 | 0.5145 |
| Zr91 | 0.1122 | Zr92 | 0.1715 |
| Zr94 | 0.1738 | Zr96 | 0.028 |

**References**

[29]

**Pages**

127, 129, 131, 133, 135, 136, 137, 138, 139, 141, 142, 143, 144, 148

## Source 69 — Elemental Masses

| Element | Mass [amu] | Element | Mass [amu] |
|---|---|---|---|
| Ag | 107.868150 | Al | 26.981539 |
| Ar | 39.947799 | B | 10.811825 |
| C | 12.011115 | Ca | 40.078023 |
| Cd | 112.413818 | Cr | 51.996132 |
| Cu | 63.546040 | Fe | 55.845144 |
| H | 1.007982 | He | 4.002601 |
| In | 114.818267 | Mn | 54.938044 |
| Mo | 95.948779 | N | 14.006726 |
| Nb | 92.906373 | Ni | 58.693351 |
| O | 15.999305 | P | 30.973762 |
| S | 32.063879 | Si | 28.085384 |
| Sn | 118.710113 | Ti | 47.866745 |
| U | 238.028910 | V | 50.941465 |
| Zr | 91.223642 | | |

**References**

[28]

**Pages**

136, 138, 139, 140, 144

## Source 70 — Cycle 1 Assembly Loadings

| Assembly ID | Uranium [g] | U-235 [g] | Enrichment [%] |
|---|---|---|---|
| A05 | 424944 | 13162 | 3.0973492978 |
| A06 | 420716 | 13030 | 3.0971011324 |
| A07 | 426067 | 13160 | 3.0887160939 |
| A08 | 424475 | 13142 | 3.0960598386 |
| A09 | 425874 | 13192 | 3.0976298154 |
| A10 | 425803 | 13186 | 3.0967372236 |
| A11 | 420801 | 13069 | 3.1057435700 |
| B03 | 424193 | 13136 | 3.0967036231 |
| B04 | 422216 | 13097 | 3.1019667658 |
| B05 | 420894 | 13253 | 3.1487738005 |
| B06 | 425287 | 6846 | 1.6097364838 |
| B07 | 425899 | 13198 | 3.0988567712 |
| B08 | 423432 | 6792 | 1.6040355949 |
| B09 | 425449 | 13182 | 3.0983737181 |
| B10 | 424324 | 6852 | 1.6148037820 |
| B11 | 424062 | 13129 | 3.0960095458 |
| B12 | 422104 | 13159 | 3.1174781570 |
| B13 | 423343 | 13140 | 3.1038661322 |
| C02 | 424937 | 13163 | 3.0976356495 |
| C03 | 424170 | 13119 | 3.0928637103 |
| C04 | 421871 | 10124 | 2.3997857165 |
| C05 | 424615 | 6829 | 1.6082804423 |
| C06 | 423086 | 10146 | 2.3980940045 |
| C07 | 422483 | 6783 | 1.6055083873 |
| C08 | 424345 | 10192 | 2.4018192744 |
| C09 | 424595 | 6849 | 1.6130665693 |
| C10 | 424891 | 10221 | 2.4055581314 |
| C11 | 424941 | 6844 | 1.6105765271 |
| C12 | 421583 | 10130 | 2.4028483122 |
| C13 | 423048 | 13127 | 3.1029575840 |
| C14 | 421975 | 13192 | 3.1262515552 |
| D02 | 424800 | 13159 | 3.0976930320 |
| D03 | 424180 | 10156 | 2.3942665849 |
| D04 | 424406 | 10169 | 2.3960547212 |
| D05 | 424911 | 10202 | 2.4009733803 |
| D06 | 424399 | 6848 | 1.6135759038 |
| D07 | 424181 | 10210 | 2.4069913551 |

| | | | |
|---|---|---|---|
| D08 | 425152 | 6833 | 1.6071898991 |
| D09 | 422222 | 10147 | 2.4032381070 |
| D10 | 424412 | 6847 | 1.6132908589 |
| D11 | 424304 | 10181 | 2.3994588785 |
| D12 | 423100 | 10150 | 2.3989600567 |
| D13 | 424783 | 10202 | 2.4016968664 |
| D14 | 424281 | 13124 | 3.0932330225 |
| E01 | 423404 | 13084 | 3.0901928182 |
| E02 | 420730 | 13039 | 3.0991372139 |
| E03 | 424543 | 6843 | 1.6118508608 |
| E04 | 421801 | 10123 | 2.3999468944 |
| E05 | 424255 | 6837 | 1.6115308011 |
| E06 | 423596 | 10170 | 2.4008725295 |
| E07 | 421655 | 6786 | 1.6093725913 |
| E08 | 423553 | 10191 | 2.4060743284 |
| E09 | 423530 | 6836 | 1.6140533138 |
| E10 | 423784 | 10167 | 2.3990995413 |
| E11 | 426061 | 6882 | 1.6152616644 |
| E12 | 420485 | 10097 | 2.4012747185 |
| E13 | 423910 | 6809 | 1.6062371730 |
| E14 | 424243 | 13137 | 3.0965743689 |
| E15 | 423782 | 13111 | 3.0938076653 |
| F01 | 421004 | 13280 | 3.1543643291 |
| F02 | 424776 | 6817 | 1.6048458482 |
| F03 | 423535 | 10162 | 2.3993294533 |
| F04 | 423810 | 6823 | 1.6099195394 |
| F05 | 423695 | 10149 | 2.3953551493 |
| F06 | 424865 | 6872 | 1.6174549563 |
| F07 | 421380 | 10157 | 2.4104134036 |
| F08 | 421443 | 6782 | 1.6092330398 |
| F09 | 423216 | 10180 | 2.4053911005 |
| F10 | 424117 | 6837 | 1.6120551640 |
| F11 | 424105 | 10174 | 2.3989342262 |
| F12 | 425283 | 6862 | 1.6135138249 |
| F13 | 421755 | 10118 | 2.3990231295 |
| F14 | 424904 | 6840 | 1.6097753846 |
| F15 | 424964 | 13164 | 3.0976741559 |
| G01 | 423798 | 13121 | 3.0960504769 |
| G02 | 425033 | 13158 | 3.0957596234 |
| G03 | 424241 | 6834 | 1.6108768365 |
| G04 | 423025 | 10162 | 2.4022220909 |
| G05 | 423622 | 6839 | 1.6144109607 |
| G06 | 424373 | 10207 | 2.4051954295 |
| G07 | 424759 | 6831 | 1.6082060651 |

| | | | |
|---|---|---|---|
| G08 | 423952 | 10177 | 2.4005076046 |
| G09 | 421474 | 6782 | 1.6091146785 |
| G10 | 423211 | 10156 | 2.3997485888 |
| G11 | 425181 | 6847 | 1.6103729941 |
| G12 | 424361 | 10148 | 2.3913601863 |
| G13 | 424788 | 6847 | 1.6118628586 |
| G14 | 426234 | 13199 | 3.0966558276 |
| G15 | 423030 | 13097 | 3.0959979198 |
| H01 | 424112 | 13134 | 3.0968234806 |
| H02 | 423343 | 6793 | 1.6046090286 |
| H03 | 423810 | 10136 | 2.3916377622 |
| H04 | 422511 | 6778 | 1.6042185884 |
| H05 | 423653 | 10164 | 2.3991332529 |
| H06 | 424642 | 6822 | 1.6065297356 |
| H07 | 421497 | 10187 | 2.4168618045 |
| H08 | 423849 | 6823 | 1.6097714044 |
| H09 | 422875 | 10143 | 2.3985811410 |
| H10 | 424615 | 6825 | 1.6073384124 |
| H11 | 424072 | 10157 | 2.3951121508 |
| H12 | 425265 | 6865 | 1.6142875619 |
| H13 | 422934 | 10150 | 2.3999016395 |
| H14 | 424688 | 6836 | 1.6096522624 |
| H15 | 425788 | 13194 | 3.0987251872 |
| J01 | 420911 | 13082 | 3.1080204604 |
| J02 | 425904 | 13192 | 3.0974116233 |
| J03 | 424409 | 6824 | 1.6078829620 |
| J04 | 424468 | 10163 | 2.3942912069 |
| J05 | 425512 | 6859 | 1.6119404388 |
| J06 | 424294 | 10208 | 2.4058789424 |
| J07 | 423432 | 6834 | 1.6139545429 |
| J08 | 423016 | 10153 | 2.4001456210 |
| J09 | 424375 | 6824 | 1.6080117820 |
| J10 | 424281 | 10221 | 2.4090166658 |
| J11 | 424993 | 6847 | 1.6110853591 |
| J12 | 424165 | 10176 | 2.3990664010 |
| J13 | 421347 | 6753 | 1.6027170005 |
| J14 | 424730 | 13157 | 3.0977326772 |
| J15 | 421853 | 13063 | 3.0965762955 |
| K01 | 422860 | 13118 | 3.1022087689 |
| K02 | 424618 | 6826 | 1.6075625621 |
| K03 | 421148 | 10132 | 2.4058050851 |
| K04 | 424555 | 6819 | 1.6061523242 |
| K05 | 421432 | 10140 | 2.4060821200 |
| K06 | 423746 | 6824 | 1.6103986822 |

| | | | |
|---|---|---|---|
| K07 | 424555 | 10169 | 2.3952138121 |
| K08 | 424044 | 6818 | 1.6078520154 |
| K09 | 422699 | 10153 | 2.4019455925 |
| K10 | 424649 | 6832 | 1.6088581393 |
| K11 | 423288 | 10149 | 2.3976583319 |
| K12 | 424956 | 6839 | 1.6093430849 |
| K13 | 423244 | 10138 | 2.3953086163 |
| K14 | 422255 | 6776 | 1.6047175285 |
| K15 | 424116 | 13121 | 3.0937290741 |
| L01 | 422352 | 13092 | 3.0997840664 |
| L02 | 420794 | 13073 | 3.1067458186 |
| L03 | 425338 | 6828 | 1.6053115405 |
| L04 | 424261 | 10159 | 2.3945165830 |
| L05 | 424742 | 6849 | 1.6125082992 |
| L06 | 424150 | 10166 | 2.3967935872 |
| L07 | 423764 | 6831 | 1.6119821410 |
| L08 | 424256 | 10154 | 2.3933662694 |
| L09 | 425410 | 6872 | 1.6153828072 |
| L10 | 424950 | 10200 | 2.4002823862 |
| L11 | 421625 | 6792 | 1.6109101690 |
| L12 | 423639 | 10192 | 2.4058219380 |
| L13 | 424023 | 6813 | 1.6067524639 |
| L14 | 424050 | 13133 | 3.0970404433 |
| L15 | 424459 | 13147 | 3.0973545148 |
| M02 | 425885 | 13193 | 3.0977846132 |
| M03 | 424014 | 10131 | 2.3893079002 |
| M04 | 421257 | 10112 | 2.4004348889 |
| M05 | 425262 | 10201 | 2.3987565313 |
| M06 | 423693 | 6822 | 1.6101280880 |
| M07 | 423907 | 10139 | 2.3917982010 |
| M08 | 424198 | 6854 | 1.6157549069 |
| M09 | 424072 | 10153 | 2.3941689147 |
| M10 | 425652 | 6843 | 1.6076513208 |
| M11 | 422201 | 10199 | 2.4156740510 |
| M12 | 424551 | 10155 | 2.3919387777 |
| M13 | 425089 | 10199 | 2.3992622721 |
| M14 | 425657 | 13183 | 3.0970946090 |
| N02 | 421693 | 13265 | 3.1456533545 |
| N03 | 422588 | 13124 | 3.1056253372 |
| N04 | 421881 | 10131 | 2.4013880691 |
| N05 | 423101 | 6785 | 1.6036360113 |
| N06 | 424140 | 10176 | 2.3992078087 |
| N07 | 425284 | 6870 | 1.6153911269 |
| N08 | 424883 | 10175 | 2.3947769151 |

| | | | |
|---|---|---|---|
| N09 | 425421 | 6872 | 1.6153410386 |
| N10 | 424268 | 10175 | 2.3982482770 |
| N11 | 424275 | 6852 | 1.6149902775 |
| N12 | 424620 | 10163 | 2.3934341293 |
| N13 | 422582 | 13101 | 3.1002267016 |
| N14 | 425319 | 13149 | 3.0915618630 |
| P03 | 424427 | 13146 | 3.0973524305 |
| P04 | 425671 | 13187 | 3.0979324408 |
| P05 | 422784 | 13107 | 3.1001646231 |
| P06 | 423297 | 6826 | 1.6125793474 |
| P07 | 425103 | 13163 | 3.0964260426 |
| P08 | 423857 | 6827 | 1.6106847357 |
| P09 | 420685 | 13284 | 3.1577070730 |
| P10 | 424630 | 6827 | 1.6077526317 |
| P11 | 423052 | 13116 | 3.1003280921 |
| P12 | 423471 | 13111 | 3.0960797788 |
| P13 | 422419 | 13108 | 3.1030801171 |
| R05 | 423062 | 13099 | 3.0962364854 |
| R06 | 422801 | 13119 | 3.1028781862 |
| R07 | 426100 | 13196 | 3.0969256043 |
| R08 | 424656 | 13155 | 3.0978015146 |
| R09 | 425240 | 13172 | 3.0975449158 |
| R10 | 422084 | 13071 | 3.0967769449 |
| R11 | 421775 | 13100 | 3.1059214036 |

To determine core-averaged enrichment for each enrichment type (1.6%, 2.4% and 3.1%), the Enrichment column was first separated by enrichment type. Then, all the enrichments for a given type were averaged. In order to compute densities, the total mass of Uranium is needed for each enrichment type. Both of these values are reported in the table below.

| Enrichment Type | Actual Core-averaged Enrichment | Total Heavy Metal [g] |
|---|---|---|
| 1.6% | 1.6100562050% | 27570971 |
| 2.4% | 2.3999267408% | 27104522 |
| 3.1% | 3.1022104528% | 27115256 |
| Core avg. enrichment | 2.366789812% | |
| Total Heavy Metal Mass | 81.79 MT | |

**References**

[16]

**Pages**

3, 126, 128, 130

## Source 71 — Cycle 2 Assembly Loadings

| Assembly ID | Uranium [g] | U-235 [g] | Enrichment [%] |
|---|---|---|---|
| A06 | 426378 | 14523 | 3.4061325866 |
| A07 | 425150 | 13582 | 3.1946371869 |
| A08 | 426115 | 14522 | 3.4080001877 |
| A09 | 425256 | 13588 | 3.1952518013 |
| A10 | 425004 | 14481 | 3.4072620493 |
| B04 | 424679 | 13568 | 3.1948836651 |
| B05 | 424804 | 13591 | 3.1993578215 |
| B11 | 425385 | 13581 | 3.1926372580 |
| B12 | 425013 | 13591 | 3.1977845384 |
| C03 | 426452 | 14523 | 3.4055415381 |
| C06 | 425896 | 13653 | 3.2057121926 |
| C10 | 425229 | 13600 | 3.1982766933 |
| C13 | 426588 | 14507 | 3.4007051300 |
| D02 | 425787 | 13600 | 3.1940853056 |
| D05 | 426941 | 13636 | 3.1938839324 |
| D11 | 425586 | 13580 | 3.1908944373 |
| D14 | 425027 | 13576 | 3.1941500187 |
| E02 | 424137 | 13537 | 3.1916574126 |
| E04 | 426071 | 13608 | 3.1938338915 |
| E06 | 423952 | 13485 | 3.1807846171 |
| E10 | 426192 | 13632 | 3.1985583962 |
| E12 | 424567 | 13551 | 3.1917223901 |
| E14 | 424969 | 13613 | 3.2032924755 |
| F01 | 426533 | 14524 | 3.4051292632 |
| F03 | 425176 | 13601 | 3.1989105688 |
| F05 | 425158 | 13594 | 3.1973995550 |
| F11 | 424465 | 13545 | 3.1910758249 |
| F13 | 424866 | 13596 | 3.2000677861 |
| F15 | 426756 | 14527 | 3.4040529014 |
| G01 | 424316 | 13554 | 3.1943174427 |
| G15 | 425838 | 13648 | 3.2049746617 |
| H01 | 424172 | 14448 | 3.4061654235 |
| H15 | 426814 | 14554 | 3.4099162633 |
| J01 | 426796 | 13635 | 3.1947347210 |
| J15 | 424420 | 13552 | 3.1930634749 |
| K01 | 424667 | 14464 | 3.4059627897 |
| K03 | 424774 | 13549 | 3.1896961678 |

| | | | |
|---|---|---|---|
| K05 | 425597 | 13596 | 3.1945713903 |
| K11 | 425570 | 13629 | 3.2025283737 |
| K13 | 424532 | 13566 | 3.1955188301 |
| K15 | 426322 | 14520 | 3.4058763095 |
| L02 | 425023 | 13605 | 3.2010032398 |
| L04 | 427865 | 13665 | 3.1937643883 |
| L06 | 425056 | 13597 | 3.1988726191 |
| L10 | 424429 | 13585 | 3.2007709181 |
| L12 | 424652 | 13520 | 3.1837834274 |
| L14 | 424696 | 13559 | 3.1926366154 |
| M02 | 425055 | 13586 | 3.1962922445 |
| M05 | 424994 | 13578 | 3.1948686334 |
| M11 | 424679 | 13566 | 3.1944127211 |
| M14 | 426884 | 13639 | 3.1950131652 |
| N03 | 427113 | 14526 | 3.4009735129 |
| N06 | 424710 | 13587 | 3.1991241082 |
| N10 | 425867 | 13611 | 3.1960682561 |
| N13 | 427170 | 14549 | 3.4059039727 |
| P04 | 425199 | 13588 | 3.1956801404 |
| P05 | 425430 | 13593 | 3.1951202313 |
| P11 | 426461 | 13632 | 3.1965408326 |
| P12 | 425352 | 13585 | 3.1938253494 |
| R06 | 425527 | 14493 | 3.4058943381 |
| R07 | 426122 | 13614 | 3.1948596881 |
| R08 | 426663 | 14554 | 3.4111230643 |
| R09 | 425742 | 13589 | 3.1918391890 |
| R10 | 424350 | 14449 | 3.4049723106 |

To determine core-averaged enrichment for each enrichment type (3.2% and 3.4%), the Enrichment column was first separated by enrichment type. Then, all the enrichments for a given type were averaged. In order to compute densities, the total mass of Uranium is needed for each enrichment type. Both of these values are reported in the table below.

| Enrichment Type | Actual Core-averaged Enrichment | Total Heavy Metal [g] |
|---|---|---|
| 3.2% | 3.1954737208% | 21066701 |
| 3.4% | 3.4058507275% | 7048788 |

**References**

[16]

**Pages**

iii, 3, 132, 134